University of Alberta

Statistical Data Analysis of Alberta Agroclimate and Global Surface Air Temperature

By

Huamei Yin 

A thesis submitted to the Faculty of Graduate Studies and Research in partial fulfillment of the requirements for the degree of Doctor of Philosophy

in

Applied Mathematics

Department of Mathematical & Statistical Sciences

Edmonton, Alberta

Spring 2006

Your file Votre référence
ISBN: 0-494-14067-4
Our file Notre référence
ISBN: 0-494-14067-4

University of Alberta

Library Release Form

Name of Author: Huamei Yin

Title of Thesis: Statistical Data Analysis of Alberta Agroclimate and Global Surface Air Temperature

Degree: Doctor of Philosophy

Year This Degree Granted: 2006

_____

Signature

22 10935-83 Street
Edmonton, Alberta
T5H 1M2
Canada

Dedication

This thesis is dedicated to my parents.

Abstract

This thesis discusses three topics related to climate change: agroclimatic change, error variance estimation of climate datasets, and drought monitoring. Agroclimatic change from 1901 to 2002 is assessed for the province of Alberta. The long-term temporal trends in the agroclimate of Alberta are examined and the spatial variations of the agroclimatic resources and the potential crop-growing area in Alberta are explored. The results imply that Alberta agriculture has benefited from the last century's climate change.

The error-assessment is made for the Global Historical Climatology Network data. The error variance of the surface air temperature data is computed for each $5^{o} \times 5^{o}$ grid box and for each month from January 1851 to December 2001. An error variance estimation method is developed based on three parameters: the number of stations, the spatial variance, and a correlation-factor determined by using a regression. The error variance is useful for the calculation of the global or regional average of the surface temperature and its associated uncertainties.

Drought assessment and monitoring discusses the statistical indices, definitions, calculations and their application to agriculture in Alberta. Four kinds of meteorological drought indices commonly used to monitor drought events are analyzed. The drought classification of the four indices is carried out by using a percentile approach, which is based on the probability of occurrence of the drought events. Furthermore, a new drought index, PPCI, is proposed to detect drought occurrence. It can reflect the spatial patterns of the variability of the precipitation field and thus can be used to quantitatively assess the drought risk over a region.

Acknowledgement

This thesis is a result of my five years of research work and supports from many people by various ways. Without them, this journey would be much more difficult and would not be ended within such a short-time frame. Now it is my pleasure to express my grateful thanks to all of them.

I am deeply indebted to my supervisor Professor Samuel S.P. Shen of the Department of Mathematical and Statistical Sciences at University of Alberta, who has inspired, encouraged and financially supported me during my research. I have benefited from his stimulating discussion, useful suggestions and patience in all the time of research for and writing of this thesis. His in-depth grasp and enthusiasm of research sets a good model for his students. My thanks to Dr. Shen will never be enough.

I would also like to express my gratitude to Dr. Hee-Seok Oh who have helped me understand many important statistical questions and applied statistical methods. I also want to thank my colleagues (Tingting Shu, Xiaodong Zheng and Aihui Wang) in the statistical climatology group for their inputs to the research through group meetings and discussions. A special thanks goes to Department of Mathematical and Statistical Sciences of University of Alberta for providing me an opportunity and research resources to pursue this degree.

Table of Contents

CHAPTER 1 INTRODUCTION 1
1.1 AGROCLIMATIC CHANGE 2
1.2 ERROR VARIANCE ESTIMATION 5
1.3 DROUGHT AND DROUGHT MONITORING 7
1.4 THESIS OUTLINE 10
CHAPTER 2 TEMPORAL AND SPATIAL CHANGES OF THE AGROCLIMATE IN ALBERTA 11
2.1 INTRODUCTION 11
2.2 DATA 14
2.3 INTERPOLATION OF THE MAY-AUGUST PRECIPITATION 18
2.4 AGROCLIMATIC PARAMETERS AND ANALYSIS METHOD 25
2.4.1 Summary of nine agroclimatic parameters 25
2.4.2 Methods for data analysis 28
2.5 RESULTS 31
2.6 SUMMARY AND DISCUSSION 48
CHAPTER 3 STATISTICAL ANALYSIS OF DROUGHT INDICES AND ALBERTA DROUGHT MONITORING 52
3.1 INTRODUCTION 52
3.2 DATA 55
3.3 SOME OF THE EXISTING DROUGHT INDICES 56
(1) Standardized Precipitation Index (SPI) 56
(2) Rainfall Anomaly Index (RAI) 60
(3) Rainfall Decile Index (RDI) 61
(4) Standardized Anomaly Index (SAI) 63
3.4 WHEAT DROUGHT IN CANADA'S PALLISER TRIANGLE 64
3.5 INTERPRETING DROUGHT BY PROBABILITY OF OCCURRENCE 68
3.6 PROBABILITY TRANSITION OF DROUGHT CONDITIONS 75
3.7 SUMMARY AND DISCUSSION 80
CHAPTER 4 PPCI AS A DROUGHT INDICATOR 83
4.1 INTRODUCTION 83
4.2 PRINCIPAL COMPONENT INDEX (PCI) 85

4.3 PCI AND ITS CORRELATION WITH THE AVERAGE PRECIPITATION 86
4.4 EOF PATTERNS AND THE PCI OF THE ALBERTA AGRICULTURAL REGION 91
4.5 PROBABILISTIC PRINCIPAL COMPONENT INDEX 103
4.6 SUMMARY AND DISCUSSION 107
CHAPTER 5 AN ESTIMATE OF THE ERROR VARIANCE OF THE GHCN MONTHLY SURFACE AIR TEMPERATURE DATA 108
5.1 INTRODUCTION 108
5.2 DATA 111
5.3 METHOD 116
5.3.1 Basic formulas 116
5.3.2 Computation of anomalies and estimation of σ_s^2 121
5.3.3 Validation of the regression error model 125
5.3.4 Interpolation of α_S and σ_S^2 135
5.4 RESULTS 13636
5.4.1 Global results of the error variance on each grid box 136
5.4.2 Comparison with J97's data 144
5.5 SUMMARY AND DISCUSSION 148
CHAPTER 6 SUMMARY AND DISCUSSION 151
BIBLIOGRAPHY 155

List of Tables

Table 2.1. Acronyms of agroclimatic parameters, polygons, and ecoregions 15

Table 2.2. Correlation coefficients (r) between the annual agroclimatic parameters and time from 1901 to 2002, and slopes (s) of the trend for the nine annual agroclimatic parameters 33

Table 2.3. The total changes (t) and the percentage changes (p) from 1901 to 2002 of the nine annual agroclimatic parameters (the percentage change is with respect to the linear fitted value in 1901) 34

Table 3.1. SPI probability for drought interpretation 71

Table 3.2. Original SPI classification used by McKee 71

Table 3.3. The threshold values of drought classification for the growing season in the entire Alberta agricultural region 72

Table 3.4. The threshold values of drought classification for the growing season in the Mixed Grassland region 72

Table 3.5. The threshold values of different RAIs for the growing season in the entire Alberta agricultural region 74

Table 3.6. The threshold values of different RAIs for the growing season in the Mixed Grassland region 74

Table 4.1. The correlations of the May-August precipitation with SPI, RAI, SAI and PCI in the Mixed Grassland region. 98

Table 4.2. PPCI probability for drought interpretation 106

Table 5.1. A sample data set of climate anomalies for the Little Falls Mill ST station (ID 4257448004) of the United States. Unites is [°C], –9999 stands for missing data, and –8888 indicates the existence of station data whose anomaly cannot be calculated 122

Table 5.2. Sensitivity test for the values of spatial variance $\hat{\sigma}_s^2$ and the correlation factor α_s over the grid boxes (70°-75°W, 40°- 45°N) and (120°-125°W, 45°-50°N) when the sub-sample size n= 30, 20, 10, 9, 8, 7, 6, 5, and 4. The results are for the year 1975 131

Table 5.3. Comparison between the results from the formula (5.10) and J97's formula. The comparison is done for the year 1975. The 29-year MTW results are in round brackets, and the other results are from the 5-year MTW. The MSE(1) is the "true" MSE computed from the mean of the 1000 random 1-station samplings 146

List of Figures

Figure 2.1. The province of Alberta and the six ecoregions with extensive agriculture. 122

Figure 2.2. The monthly number of Alberta stations used in the data interpolation. The smoothed curves are obtained from the 12-point moving averages. 19

Figure 2.3. Distributions of the Alberta precipitation stations in the periods of 1901-1912, 1913-1942, 1943-1972, and 1973-2002. 20

Figure 2.4. Distribution of the Alberta precipitation stations whose 1961-1990 May-August precipitation normals were computed. 23

Figure 2.5. The difference of the interpolated May-August precipitation between the two methods (the one using the improved method minus the one using the original method) in the periods of 1901-1912 and 1973-2002 (units: mm). 24

Figure 2.6. Annual time series (thin curve with dots), 11-year running mean (thick curve), and linear regression line (straight line). (a) May-August precipitation [units: mm], (b) LSF [units: day], (c) FFF [units: day], (d) FFP [units: day], (e) accumulated GDD in the growing season, and (f) ACHU. 35

Figure 2.7. Spatial distribution of the temporal trends from linear regression. (a) May-August precipitation (units: mm/102yr), (b) FFP (units: day/102yr). The shaded regions are where significant trends exist at the 5% significance level. The Rocky Mountain areas are blacked out because of insufficient station data and large gradients of trends, and hence possibly very large errors. 36

Figure 2.8. The difference of the recent 30-year normal (1973-2002) minus the 1913-1942 normal for six agroclimatic parameters. (a) May-August precipitation [units: mm], (b) SGS [units: day], (c) EGS [units: day], (d) LSF [units: day], (e) FFF [units: day], and (f) ACHU. The Rocky Mountain areas are blacked out due to insufficient data. 42

Figure 2.9. The difference of the recent 30-year normal (1973-2002) minus the 1943-1972 normal for four agroclimatic parameters. (a) SGS [units: day], (b) EGS [units: day], (c) GDD, and (d) ACHU. The Rocky Mountain areas are blacked out due to insufficient data. 46
Figure 2.10. The areas with ACHU ≥ 2,000 for the 1913-1942 normal, 1943-1972 normal and 1973-2002 normal. 47
Figure 3.1. Alberta ecoregions 56
Figure 3.2. Schematic diagram of an equiprobability transformation from a fitted gamma distribution to the standard normal distribution (from Lloyd-Hughes and Saunder, 2002) 59
Figure 3.3. Historic Prairie wheat drought areas (from PFRA, 1998) 65
Figure 3.4. May to August precipitation from 1901 to 2002 and corresponding RAI over the Mixed Grassland region 66
Figure 3.5. May to August precipitation from 1901 to 2002 and corresponding SAI over the Mixed Grassland region 66
Figure 3.6. May to August precipitation from 1901 to 2002 and corresponding SPI over the Mixed Grassland region 67
Figure 3.7. Rainfall Decile Index and precipitation (the black curve represents precipitation, and the gray straight lines represent deciles) 67
Figure 3.8. The illustration of the probability of the transition of weekly precipitation. 75
Figure 3.9. The wet-to-dry probability transition for Mixed Grassland 77
Figure 3.10. The dry-to-wet probability transition for the Mixed Grassland region 78
Figure 3.11. The 20% to 100% percentiles for five of the ecoregions. 79
Figure 4.1. The (a) EOF1 and (b) EOF2 modes of the May-August precipitation for the Alberta agricultural region 93
Figure 4.2. The (a) first and (b) second homogeneous correlation maps of the May-August precipitation for the Alberta agricultural region 95
Figure 4.3. The (a) EOF1 and (b) EOF2 modes of the May-August precipitation for four townships 99

Figure 4.4. The PC1 and the May-August precipitation in (a) the agricultural region and (b) the Mixed Grassland region 101
Figure 4.5. The dimensionless PC1 and the May-August precipitation in (a) the agricultural region and (b) the Mixed Grassland region 102
Figure 4.6. The transformation of the PCI to PPCI for the Mixed Grassland region. 104
Figure 4.7. The PPCI and the May-August precipitation in (a) the agricultural region and (b) the Mixed Grassland region 105
Figure 5.1. History of the number of stations in the GHCN network from January 1835 to February 2004 112
Figure 5.2. Spatial distribution of stations 113
Figure 5.3. Grid boxes in the contiguous United States and southern Canada, total number of stations in a box in the GHCN history, and two error-validation boxes in the United States: (120°-125°W, 45°-50°N) with 55 stations and (70°-75°W, 40°-45°N) with 68 stations 115
Figure 5.4. Time series and their 5-year MTW smoothed series of the spatial variances over a validation box (120°-125°W, 45°-50°N). The January results are computed from 41 stations with complete records and the July results from 35 stations with complete records. Units: $[°C]^2$ 123
Figure 5.5. The "true" MSE of January 1961 computed from the 1,000 random samplings and the exhausted samplings, respectively, for the grid box (120°-125°W, 45°-50°N). Twenty seven stations in the grid box are used 128
Figure 5.6. The ratio of the 5-year MTW smoothed "true" MSE $\hat{E}_n^2$ to the 5-year MTW smoothed spatial variance $\hat{\sigma}_s^2$ as a function of the number of sample stations for the grid box (70°-75°W, 40°- 45°N) in the eastern United States when the total number of stations is N= 30, 20, 10, 9, 8, 7, 6, 5, and 4 stations: (a) January 1975, and (b) July 1975 132

Figure 5.7. The regression parameter α_s, and error variance E^2 as a function of the month for the two grid boxes in the US. The units for the error variance is $[°C]^2$ 133
Figure 5.8. The 1961-1990 30-year mean of the "true" MSE (solid line) and the 1961-1990 30-year mean of the estimated MSE (dashed line) for the grid boxes (120°-125°W, 45°-50°N) and (70°-75°W, 40°-45°N). The bars on each side of the mean are the one-standard deviations of the 30 "true" MSE values. Units: $[°C]^2$ 134
Figure 5.9. Maps of the estimated error variances of the grid boxes with data for four selected months. Units: $[°C]^2$ 138
Figure 5.10. Monthly time series of the estimated MSE for the grid box (120°-125°W, 45°-50°N) from December 1849 to December 2001. Units: $[°C]^2$ 140
Figure 5.11. Time series of the spatial average of the estimated MSE (solid line, units: $[°C]^2$) and the time series of the station-covered areas (dashed line, units: $[km]^2$) from January 1837 to December 2001 141
Figure 5.12. The ratio of the number of boxes with at least four stations to the number of boxes with data..... 143
Figure 5.13. History of the number of grid boxes with the calculated values of spatial variance and correlation factor (solid line) and the total number of grid boxes with at least one station (dashed line) 149

Chapter 1

Introduction

Climate change became a serious issue during the last century and continues to be a major concern for scientists and the public. The warming climate is having a great influence on agriculture, forestry, water resources, and many other environmental and socio-economic sectors. Nearly every Canadian and every sector of the Canadian economy is involved in activities that are sensitive to changes in climate. Therefore, appropriate detection and assessment of the existing changes in the climate system is important for decision makers wanting to develop and implement adaptation strategies.

This thesis focuses on three topics related to climate change: agroclimatic change, error variance estimation of climate datasets, and drought monitoring. Agroclimatic change from 1901 to 2002 is assessed for the province of Alberta and emphasizes the changes of the climate elements relevant to agriculture, such as the length of growing season, the frost-free period, the growing degree days, and the corn heat units. The error-assessment is made for the Global Historical Climatology Network data and is useful for the calculation of the global or regional average of the surface temperature and its associated uncertainties. Drought assessment and monitoring discusses the statistical indices, definitions, calculations and their application to agriculture in Alberta.

1.1 Agroclimatic change

Climate plays a crucial role in agricultural production by affecting the soil, the water, land use, and agricultural potential. Higher temperatures, changes of annual and seasonal precipitation and soil moisture, and variations of extreme weather events such as drought will have extensive influence on the world food system (Parry, 1990). Global warming will result in the extension of the length of the potential growing season, earlier planting of crops in the spring, and earlier maturation and harvesting. In countries such as Canada and Russia, which are in higher latitudes, the crop-producing areas may expand toward the north, while in lower latitudes countries, the net growth and yield might drop when temperatures exceed the optimal for biological processes. Climate change will modify rainfall, evaporation, runoff, and soil moisture storage, thus affecting the crop growth. The changes in the frequency of extreme climatic events such as spells of high temperature, heavy storms, or droughts will also affect crop production (Parry, 1990; Rosenzweig and Hillel, 1995). For example, wheat production in the Canadian prairies is constrained mainly by the first fall frost occurrence before the crops mature. Thus, the possible changes in the climate variability are perhaps more significant to agriculture than those in climate means. By increasing scientific knowledge of climate change and its effects on global agriculture, we can help decision makers formulate better adaptation policies. In order for agricultural production to meet the demands of the ever-growing human

population, the impact of the climate must be understood and integrated into any future planning (Bazzaz and Sombroek, 1996).

While scientists agree that the global mean temperature has changed by 0.6 ± 0.2°C since the late 19th century (IPCC, 2001), the regional changes of climate are not uniform, and the warming is faster in some regions than in others (Karl et al., 1997; Environment Canada, 1995). The agricultural economy in a given region depends largely on the interplay of many dynamic factors specific to each region.

In Canada, about 5% of the land area is suitable for farming, in two main zones – the Prairies and the mixed Wood Plains of the St. Lawrence River and Great Lakes regions, while the rest of the land area is forested (Motha and Baier, 2005). Understanding climate change in the prairie region is critical since this area accounts for 82% of the cultivated land in Canada and is an important supplier of food for the global community (Parry, 1990; McGinn et al., 2001). Recent studies indicate an increase of the annual mean temperature by 0.5 °C to 1.5 °C and an increase of annual precipitation by 5% to 35% in southern Canada during the period 1900-1998, with the greatest warming occurring in the west (Zhang et al., 2000). Decadal variability was found to be a dominant feature of both the frequency and intensity of annual precipitation (Bonsal et al., 1999; Zhang et al., 2001). In the Canadian prairies, it was found that the number of rainfall events and the rainfall amounts had significantly increased, with the largest increase occurring in spring (January to April) and no significant increase occurring during autumn (September to December). As well, the increase was due mainly to the increase in the number of low-intensity events (Akinremi et al., 1999 and 2001; Cutforth, 2000). The annual mean temperature in the

Prairie provinces has increased by about 1.2°C over the last 50 years; winter temperature has warmed by about 3.0°C and summer temperature has warmed by about 0.2°C (Pollution Probe, 2004). The higher air temperatures will increase the rate of evaporation and enhance the tendency for the climate to become drier even though the precipitation increases (Bootsma, 1997).

Besides the changes in temperature and precipitation, the changes of other parameters that contain agroclimatic properties such as frost dates, growing degree days, and corn heat units are also important to agriculture. Studies of selected stations in Canada showed a significant increase in the number of growing degree days, earlier last spring frost dates, and longer frost-free period (Bonsal et al., 2001; Bootsma, 1994; Cutforth et al., 2004).

This thesis studies the agriclimatic change of Alberta in the period of 1901-2002. The results of the agroclimatic change included are from the main conclusions of a study in collaboration with Alberta Agriculture, Food and Rural Development (AAFRD) and are important to AAFRD's climate-adaptation strategies. Our study focuses on the agroclimatic change of Alberta by analyzing the long-term trends in the agroclimatic parameters and the spatial distribution of the changes to provide quantitative information to the decision makers in Alberta's agriculture sector to help them optimally manage the land usage for crops and livestock. This study uses a complete coverage and variance-retained interpolated daily climate dataset over ecodistrict polygons, in contrast to other studies based on data at unevenly distributed stations.

1.2 Error variance estimation

Understanding and quantifying the error variance, also known as the "uncertainty", will help decision-makers to quantitatively assess the potential risks from climate change and to plan adaptation to it. Uncertainties can come from natural variability, coarseness of the spatial and temporal resolution of climate data or errors in data observation. Examples of errors include rough errors resulting from coding mistakes or transmission problems, systematic errors resulting from inhomogeneities (e.g., the urbanization effect) and instrumental change, and random errors that inherent in all data. While some of the errors can be reduced through data quality control, other subtle errors (e.g., random error) cannot be eliminated.

The error estimation addressed in this thesis is another kind of error appearing in the assessment of the change in the global (regional) average temperature. This error, called "sampling error", results from the spatial sampling from insufficiently covered data observations. The estimate of the global (regional) average temperature, by using either optimal averaging or simple averaging methods, needs to use the discrete observational station data. Madden et al. (1993) used a model-derived time series to investigate the effects of imperfect spatial and temporal sampling on the estimation of the global average surface temperature. Karl et al. (1994) examined the effect of the spatial sampling errors on the estimate of global and hemispheric trends in temperature and found that the uncertainty in calculating historical temperature trends is dependent upon the pattern of temperature change, the method of treating the effect of nonrandom spatial sampling, and the time and length over which the trend is calculated. In a study of the sampling error's effect on the detection of anthropogenic

climate change, Hegerl et al. (2001) concluded that including the effect of the sampling error will increase the uncertainty in estimates of the greenhouse gas–plus–sulfate aerosol signal from observations by 2% to 8% for trend patterns.

Shen et al. (1998) provided a procedure, "reduced space optimal averaging", for computing the regional average of climate data by using the covariance function expressed in terms of empirical orthogonal functions. This method can not only minimize the mean square error but also explicitly estimate the error. Folland et al. (2001) used this method to estimate the global temperature change and its uncertainties. Both Shen et al. (1998) and Folland et al. (2001) need data errors, which were first systematically estimated by Jones et al. (1997). Jones et al. (1997)'s standard error estimate was based on the number of stations, the average correlation between each pair of stations, and the temporal variability of the temperature in each grid box. The authors provided the estimates of the sampling error in 5° by 5° grid boxes on interannual and interdecadal timescales as well as the sampling errors of the global mean temperature.

In our study, a new method is developed to estimate the error variances of the $5^{\circ} \times 5^{\circ}$ Global Historical Climatological Network (GHCN) monthly surface air temperature data. Our error estimation is determined by three parameters: the number of stations, the spatial variance, and a correlation-factor determined by using a regression. The advantage of this error estimation is its tolerance of the inhomogeneity of the temperature field in a grid box, and the spatial inhomogeneity is taken into account mainly by the spatial variance.

1.3 Drought and drought monitoring

Drought is a recurrent natural disaster often resulting in tremendous economic, social, and environmental costs and thus has great impact on society. The definition of "drought" is both spatially variant and context dependent. Generally speaking, drought is an extended period of time with precipitation deficiency from expected or normal (Wilhite, 2000; Heim, 2002). Conventional scientific literature recognizes four types of droughts: meteorological, hydrological, agricultural and socioeconomic drought (American Meteorological Society, 1997; Wilhite, 2000, Wilhite and Glantz 1985).

Drought research usually address (1) the drought characteristics and severity, (2) the causes and mechanism of drought, (3) the impacts of drought, or (4) the adaptation to drought (Byun and Wilhite, 1999). The first category's research involves the quantification of the intensity, duration, and spatial coverage of drought. Drought index is a major tool. Since the beginning of the last century, numerous drought indices have been proposed to quantitatively assess drought severity. Some of the indices such as the Rainfall Anomaly Index (van Rooy, 1965), the Bhalme-Mooley Index (Bhalme and Mooley, 1980), and the Standardized Anomaly Index (Katz and Glantz, 1986) use only precipitation as input. Some others take into consideration more elements like precipitation, potential evapotranspiration, soil moisture, runoff, and reservoir storage. These indices include the Palmer Drought Severity Index (PDSI), the Palmer Moisture Anomaly Index (Z index) (Palmer, 1965), the Crop Moisture index (Palmer, 1968), and the Surface Water Supply Index (Shafer and Dezman, 1982). Some of the indices such as the Rainfall Deciles (Gibbs and Maher,

1967; Kininmonth et al., 2000) and the Standardized Precipitation Index (SPI) (Mckee et al., 1993, 1995) are probability-based whereas others are not. Some indices address drought in general while others consider specific crop responses to the drought events (the Crop-specific Drought Index, Meyer et al., 1993; Meyer and Hubbard, 1995). Among all of the indices, the PDSI is the mostly widely recognized index and has been used for decades. In recent years, the SPI has increased in popularity and has been used in many countries including Canada. Heim (2002) thoroughly reviewed thirteen drought indices used in the United States. Each of the indices was developed specifically for a region or application, and each has its own merits and limitations (Alley, 1984; Guttman, 1991 and 1998; Heim, 2002; Wu et al., 2005). Thus, comparative studies of the indices became necessary (Akinremi and McGinn 1996; Byun and Wilhite, 1999; Guttman, 1999; Keyantash and Dracup, 2002; Oladipo, 1985; Quiring and Paparkryiakou 2003).

The second category of drought studies goes into two directions. One emphasizes the anthropogenic factors and the feedback between the atmospheric circulation and the land surface processes (Charney, 1975; Taylor et al., 2002). The other believes that changes in the global sea surface temperature triggered the large-scale atmospheric circulation changes and, hence, are associated with drought occurrence (Bonsal and Lawford, 1999; Giannini, et al., 2003; Hoerling and Kumar, 2003; Lau, et al., 2005; Schubert et al., 2004; Shabbar and Skinner, 2004). Zeng (2003) suggested that drought very likely results from the synergistic action of sea surface temperature change, natural vegetation processes, and land-use changes.

The third category of studies focuses on the costs and losses associated with droughts. The fourth category of studies focuses on adaptation and mitigation strategies for drought-impact reduction. The studies on the impacts of drought and adaptation strategies for the Canadian prairies include Herrington et al. (1997), Wheaton (2000), Wheaton et al. (2005), and Gan (2000).

The drought analysis included in this thesis is from the results of a project in collaboration with Alberta Agriculture, Food and Rural Development (AAFRD) and is an integral part of the Alberta agriculture drought risk management plan. Alberta, especially southern Alberta, is a drought-prone region in Canada. Alberta's agriculture industry usually is the first sector to suffer serious impacts from the recurring droughts. Thus, a drought risk management plan was launched in 2002 in order to provide well-coordinated, immediate response during a drought crisis and to reduce droughts impacts in both the short and long terms (Agriculture and Agri-Food Canada, 2002). In our study, various types of drought indices are analyzed to provide quantitative information on the severity of drought conditions from meteorological perspectives. The analyzed information will be integrated into an operational system that can monitor the Alberta agricultural drought. In particular, a new drought index, the Probabilistic Principal Component Index (PPCI), will be proposed. The PPCI can reflect not only the fundamental dynamical behavior of the stochastic precipitation field through the EOF (empirical orthogonal functions) patterns, but also the probabilistic properties of the drought conditions over a large area.

1.4 Thesis outline

This thesis is structured as follows. Chapter 2 presents the results of the agroclimatic change in Alberta. The long-term (1901-2002) temporal trends in the agroclimate of Alberta are analyzed, and the spatial variations of the agroclimatic resources and the potential crop-growing area in Alberta are explored by investigating nine agroclimatic parameters.

In Chapter 3, four kinds of meteorological drought indices are analyzed for the detection of wheat droughts in southern Alberta. The classification of the drought categories is discussed.

Chapter 4 proposes a new drought index: the PPCI. The calculation procedure is provided. The results of the PPCI's application to Alberta's agricultural regions are presented.

Chapter 5 addresses the estimation of the standard errors (sampling errors) of the $5^{\circ} \times 5^{\circ}$ Global Historical Climatological Network (GHCN) monthly surface air temperature data. The method is described, and the results are compared with those of Jones et al. (1997).

This thesis's conclusions and major results are summarized in Chapter 6. Some future possible improvements are listed.

Chapter 2

Temporal and Spatial Changes of the Agroclimate in Alberta

2.1 Introduction

Located where the Rocky Mountains meet the prairie, Alberta has a varied landscape with mountains in the west and plains in the north, center and south (Fig. 2.1). Climate change has a crucial impact on the sustainability of agriculture and agriculture production in the region. As one of the three prairie-provinces in Canada, Alberta has an area of 0.662 million square km, more than a third of which is farmland. The agricultural industry is one of the most important industries in Alberta's economy. In 2003, Alberta's agriculture and food industries contributed 3.5 per cent to the province's Gross Domestic Product (GDP) (Alberta Agriculture, Food and Rural Development, 2005). The sustainable development of agriculture and the agricultural industry is of crucial importance for the long-term economy of Alberta. Adaptation strategies must be in place to cope with the climate change. Therefore, the study of agroclimatic change is important to the decision makers from the agriculture sector in Alberta to optimally manage the land usage for crops and livestock.

Environment Canada (1995) reported that Alberta's surface air temperature had gone up and Alberta's winter had become milder. In the period 1895 to 1991, Alberta's daily minimum surface air temperature increased about 1.3-2.1°C. The warming climate has been perceived to benefit Alberta agriculture, including the

growth of both crops and livestock. Despite these observational results and perceptions, Alberta Agriculture, Food and Rural Development (AAFRD), an Alberta

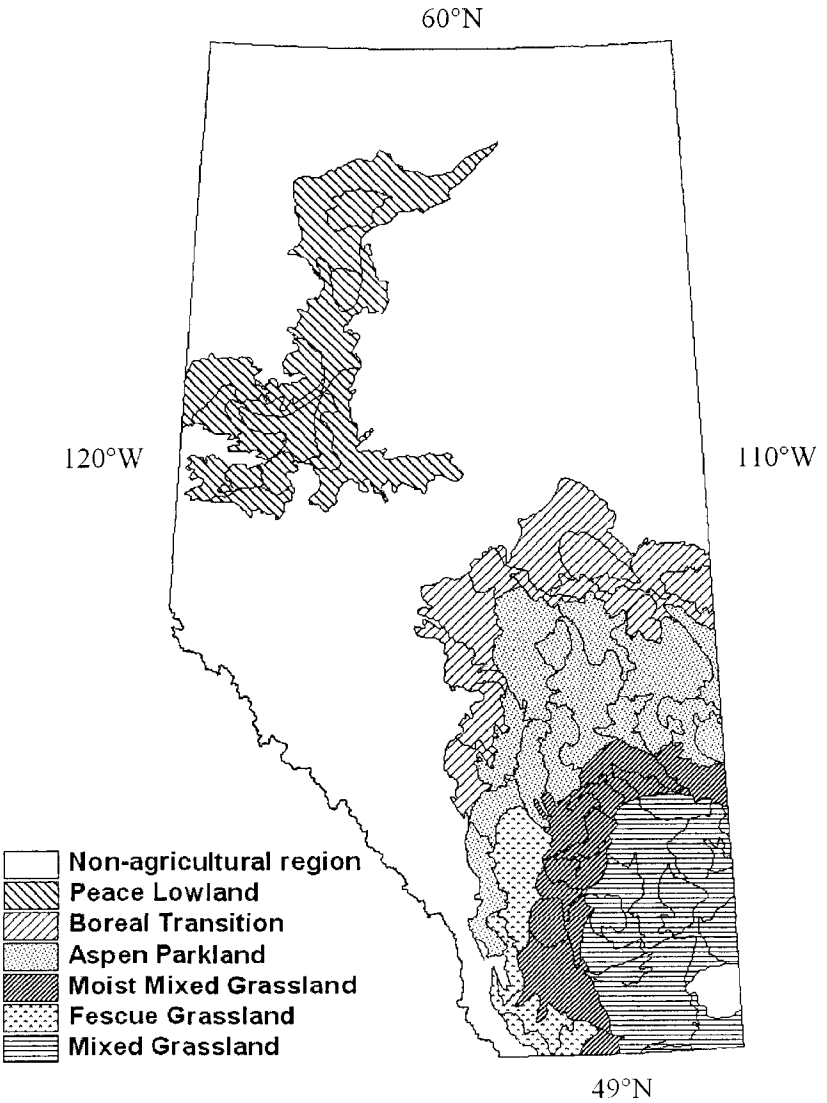

Figure 2.1. The province of Alberta and the six ecoregions with extensive agriculture.

provincial governmental ministry, still needs a quantitative and systematic analysis of the agroclimatic changes in terms of both time and space. The results included in this chapter are from the main conclusions of AAFRD's research on agroclimatic change and are important to AAFRD's climate adaptation strategies. Other innovative aspects of this study are on the analysis approaches: (a) the variance-retained interpolated daily climate data over ecodistrict polygons were used, in contrast to the data at unevenly distributed stations used in other studies (Akinremi et al., 1999; Bootsma 1994; Bootsma et al., 2001; Bonsal et al., 2001), and (b) the area weight was used to calculate the agroclimatic parameters of each ecoregion before regression analysis.

This study uses the master dataset produced by AAFRD by using an optimal hybrid interpolation method (Griffith, 2002; Shen et al., 2000a, b, 2001). When this research project started, the time span of the dataset was from January 1, 1901 to December 31, 2002. Thus, the results in this chapter are for the agroclimatic change during this period.

The agricultural regions in Alberta, as shown in Fig. 2.1, are the southeast prairie land and the western Peace Lowland and have an area of 0.256 million square km. The rest of Alberta is either covered with forest or its elevation is too high for crop cultivation. Currently, the major Alberta crops are spring wheat, barley, canola and alfalfa. The most important livestock are beef-cattle. The agroclimatic changes in this study are investigated according to six ecoregions with extensive agriculture, Alberta as a whole, and nine agroclimatic parameters. (The Agroclimatic Atlas of Alberta by Chetner et al. (2003) and its associated website include the information on the ecoregions and agroclimatic parameters.) The nine parameters are the May-August

precipitation (PCPN), the start of growing season (SGS), the end of growing season (EGS), the length of growing season (LGS), the date of the last spring frost (LSF), the date of first fall frost (FFF), the length of frost-free period (FFP), the growing degree days (GDD), and the corn heat units (CHU). (The acronyms are summarized in Table 2.1.) The research on these agroclimate parameters has provided important information to AAFRD, and this study will present scientific evidence that the last century's climate change has been beneficial to Alberta agriculture.

This study focuses on the change of Alberta's agroclimate and does not intend to review the changes in the usual climatic parameters, such as maximum daily temperature and monthly precipitation. The latter have been addressed in many studies, such as those by Bonsal et al., (2001), Environment Canada (1995), Gan (1995), Gullet and Skinner (1992), Zhang et al. (2000), Zhang et al. (2001), and the references therein. However, the parameters under the present investigation are related to those climatic parameters, and, hence, our results are compared with the existing results from climate-change studies when applicable.

2.2 Data

Some soil-quality models, such as the Erosion/Productivity Impact Calculator, need continuous daily climate data at a given resolution as their input. Irregular and often discontinuous observations of weather make it necessary to interpolate the point-based weather station data onto a regular grid or over polygons. Realistic simulations crucially depend not only on the climate mean but also on the climate variations. The latter are more important, but are often ignored in many spatial

interpolation schemes derived from the best fit to the mean. The problem is particularly serious for

Table 2.1. Acronyms of agroclimatic parameters, polygons, and ecoregions

Acronym	Meaning	Unit
ACHU	Accumulated corn heat unit	Dimensionless
AP	Aspen Parkland	Ecoregion
AR	Agricultural Region	Region
BT	Boreal Transition	Ecoregion
CHU	Corn heat unit	Dimensionless
EDP	Ecodistrict polygon	Polygon ID
EGS	End of growing season	Calendar day
FFF	First fall frost	Calendar day
FFP	Frost free period	Days
FG	Fescue Grassland	Ecoregion
GDD	Growing degree day	Degree Centigrade
GSP	Growing season precipitation	Millimeter/day
LGS	Length of growing season	Days
LSF	Last spring frost	Calendar day
MG	Mixed Grassland	Ecoregion
MMG	Moist Mixed Grassland	Ecoregion
PL	Peace Lowland	Ecoregion
SGS	Start of growing season	Calendar day
SLC	Soil landscapes of Canada	Polygon ID

precipitation because the daily precipitation, such as that in the convective summer storms over the Canadian Prairies, can be spatially localized, while an interpolation method often makes the field spatially spread out and smooth. Precipitation frequency is another problem since most interpolation methods yield too many wet days in a month but too little precipitation in a day so that the results do not retain enough temporal variation and hence are temporally too smooth. Shen et al. (2001) overcame the problem and developed a hybrid interpolation scheme that uses a reference station to preserve the variance of the interpolated field and still maintain the monthly mean. Using this method and the raw point-based observed weather station data provided by Environment Canada, the U.S. National Climatic Data Center, and Agriculture and Agri-Food Canada, AAFRD produced a master set of daily climate data with different resolutions: (1) 10 km by 10 km regular grid, (2) 6,900 townships, (3) 894 soil landscapes of Canada (SLC) polygons, and (4) 149 ecodistrict polygons (EDP) (Griffith, 2002; Shen et al., 2000a, b, 2001). At these resolutions, every grid or polygon has a uniquely defined value for a climate parameter on each day. An updated AAFRD master dataset includes the daily data from January 1, 1901 to December 31, 2002. This study uses not only the data over EDP and SLC polygons to derive the main results, but also the station data for result-checking. The Canadian station data are also checked by comparing with the data from the US National Climatic Data Center's Global Daily Climatology Network dataset.

All the agroclimatic parameters, except the May-August precipitation, analyzed in this study are derived from the daily maximum temperature, and daily minimum temperature in the EDP and SLC master dataset. This dataset has several

advantages. (1) It is the most complete long-term daily dataset for Alberta. (2) It reflects the daily weather variability well; this capability is important when calculating the agoclimatic elements (such as the SGS and LSF) that are sensitive to the daily climate change. (3) The EDPs are exactly embedded into ecoregions divided according to distinctive regional ecological characteristics including climate, physiography, vegetation, soil, water and fauna. Each ecoregion consists of a number of EDPs, ranging from 4 to 38. Thus, using the EDP data is convenient to calculate the agroclimatic properties for each ecoregion.

Therefore, this study features the use of the daily interpolated data with complete coverage, compared to the data used in either the station-based studies or the studies based on interpolated data with too little variance. Of course, caution is always required when using the interpolated data in the data sparse regions due to possibly large errors.

The accuracy of the master dataset was investigated when the interpolation was made. Five stations at Lethbridge, Lacombe, Edmonton, Beaverlodge, and High Level, ranging from southern to northern Alberta, were selected for cross-validation to assess the interpolation errors (Griffith, 2002; Shen et al., 2001). The root mean square errors, which measure the difference between the interpolated and the true observed values, are in the following range (for the 1961-1997 data): daily maximum temperature 1.4 to 3.2°C, daily minimum temperature 1.8 to 3.2°C, and daily precipitation 1.8 to 2.8 mm. Many more cross-validation experiments were made and showed that, for daily temperature and precipitation, the hybrid method had smaller errors than the interpolation methods of simple nearest-station assignment, inverse-

distance-square weighting, and kriging. Fortunately, the errors are not biased toward one side (see Table 2 of Shen et al. (2001)), but the size of the precipitation error still needs attention, particularly for the northern regions during the first half of the last century.

2.3 Interpolation of the May-August Precipitation

From the initial calculation of the long-term trend in May-August precipitation, an unusually large precipitation trend over the northern Alberta was found by using this dataset that were interpolated directly from the daily station records.

After an investigation, it was found this falsely large trend was due to the sparse stations in the early years of last century and large elevation variations in the northern part of Alberta. In the early period of the last century, weather stations were usually constructed in flat and low elevation land areas. In mountain and lake areas, the weather data cannot be collected. Therefore, if we spatially interpolate the weather data directly by the daily station records, we would use the weather in low-elevation land areas to represent the weather in high-elevation mountain areas. This will obviously lead to bias, especially for topographical precipitation.

Figure 2.2 shows the monthly series of the total number of temperature and precipitation stations in Alberta from January 1901 to December 2002. The seasonal fluctuations are due to the fact that some stations were operating only in growing season. Fig. 2.3 shows the distribution of the precipitation stations in four periods: 1901-1912, 1913-1942, 1943-1972, and 1973-2002. Only four stations (Fort

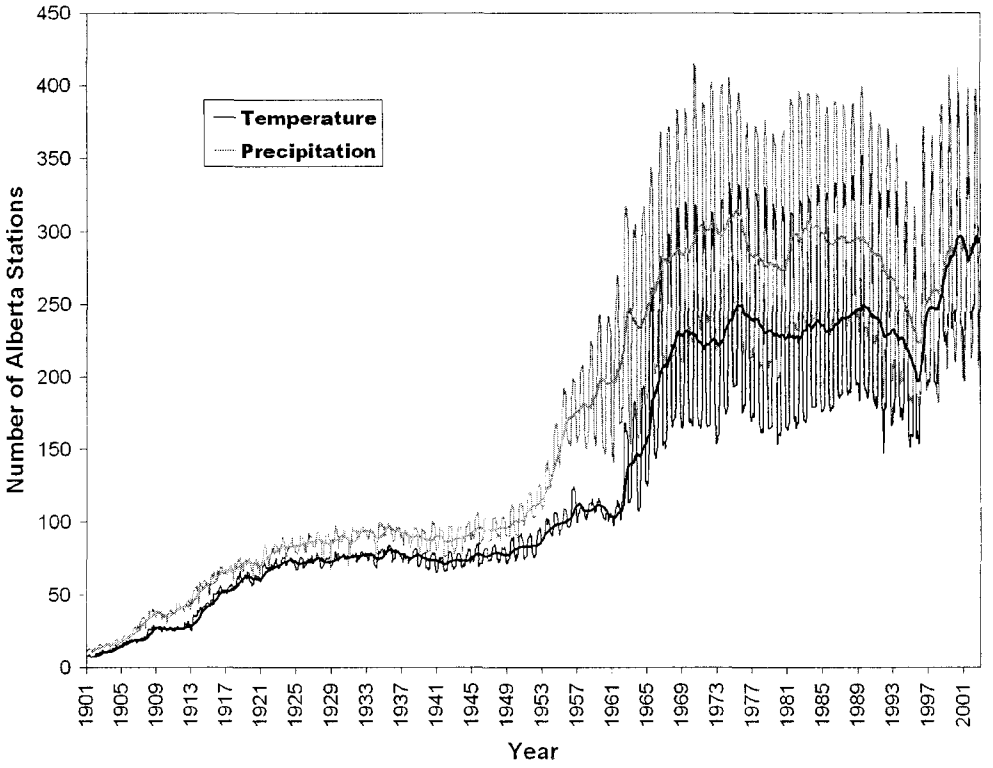

Figure 2.2. The monthly number of Alberta stations used in the data interpolation. The smoothed curves are obtained from the 12-point moving averages.

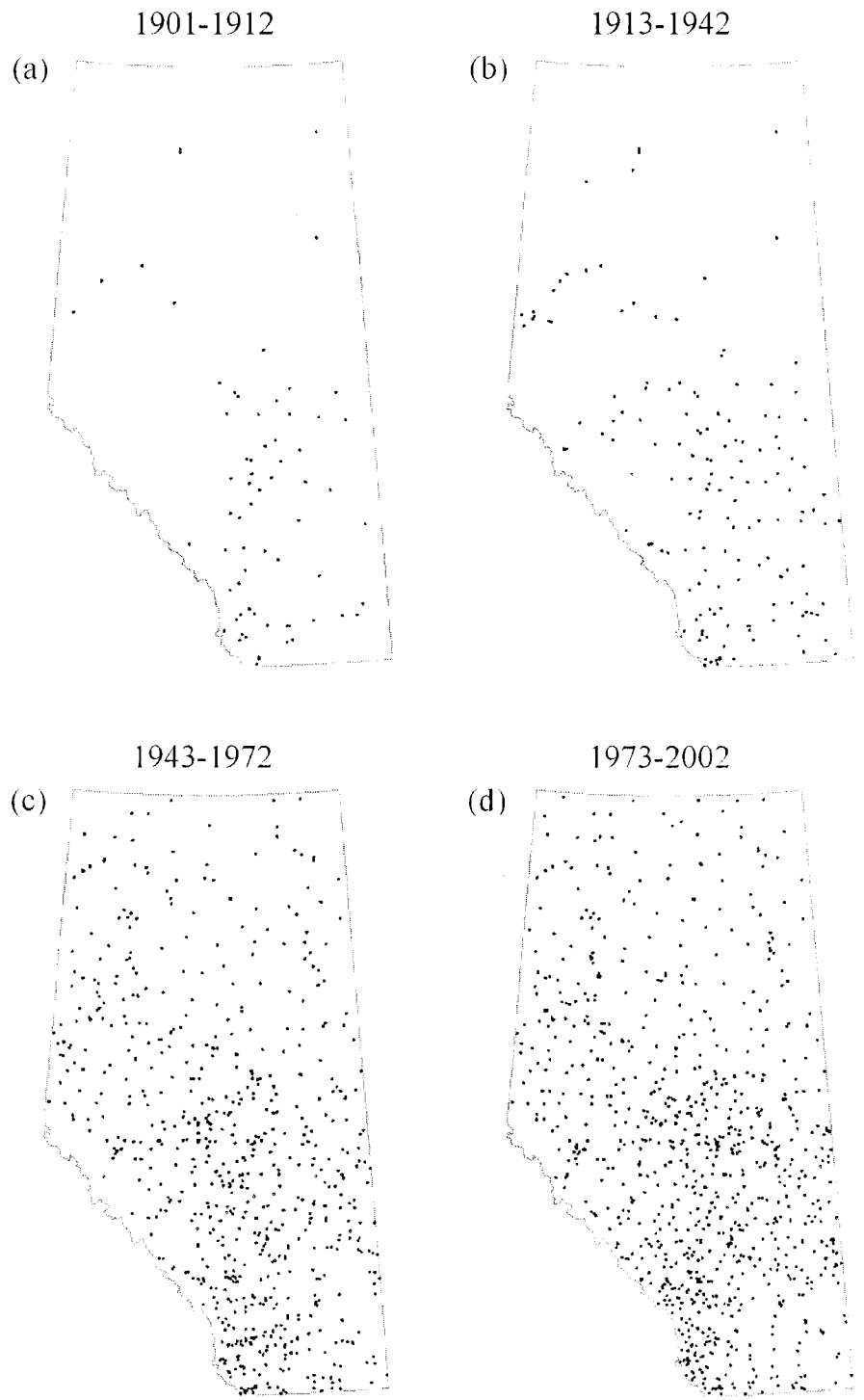

Figure 2.3. Distributions of the Alberta precipitation stations in the periods of 1901-1912, 1913-1942, 1943-1972, and 1973-2002.

Chipewyan, two stations in Fort Vermillion, and Fort McMurray) were north of 56°N before 1912, and they had low elevations and hence did not measure the topographic precipitation over the mountain regions (i.e., Caribou Mountains, Buffalo Hills, Clear Hills, Birch Mountains) and the lake regions (i.e., Lake Athabasca and Lake Claire). The mountain and lake areas should have higher monthly precipitation than the low-elevation, dry areas. But they were not measured until the late 1960s when stations were placed in these mountain and lake areas. Thus, the original 1901-2002 master dataset has a low precipitation bias in the first part of the last century in northern Alberta. The high precipitation of these areas were replaced by the low precipitations measured by the long-term stations in low-elevation and dry areas and hence would lead to an unrealistically large trend for the May-August precipitation over the mountain and lake areas.

To overcome this particular problem and to accurately access the May-August precipitation trend in northern Alberta, the 1961-1990 May-August precipitation normals and the daily precipitation anomalies were interpolated separately. At first, stations were selected to compute the 1901-1990 normals. Those stations selected satisfy the following two conditions:

(1) Having data for at least 98 days among the 123 days (from May 1 to August 31).

(2) Having at least 21 years that satisfy Condition (1).

Two hundred and eighteen (218) stations in Alberta during 1961-1990 satisfied the above two conditions, and their distribution is shown in Fig. 2.4. These stations covered Alberta reasonably well, except in some areas in the Canadian Rockies, and,

particularly, they covered the mountain and lake regions in the north. The May-August precipitation normals were interpolated onto all the stations by using the nearest-station-assignment method. The daily station anomalies were computed according to these interpolated normals. Then, normals and anomalies were interpolated onto the 10-by-10 km grid by the nearest-station-assignment method and the inverse-distance method, respectively. On each grid, the normal and the daily anomalies were added together, and these sums were further added together for the period from May 1 to August 31. Furthermore, the grid data were used to calculate the precipitation for ecodistrict polygons (EDP) and the polygons of the soil landscapes of Canada (SLC). The EDP May-August precipitation was assigned the average of the values of the grid points inside the polygon.

Figure 2.5 shows the difference of the interpolated May-August precipitation by the improved method (Method1) mentioned above and the original direct interpolation method (Method2) in the periods of 1901-1912 and 1973-2002. The values in the figure are calculated by the precipitation from method1 minus the precipitation from method2. The difference is relatively large in the period 1901-1912 when the number of stations is small in the northern Alberta. There was a 50-100 mm difference of the precipitation in most of the northern parts, which means the interpolated precipitation is larger when both the normal and anomaly in the mountain and lake areas are counted. As mentioned previously, the interpolated precipitation by using direct interpolation was lower than reality. Therefore, the new method corrected the error. In contrast, the difference is small in the southern

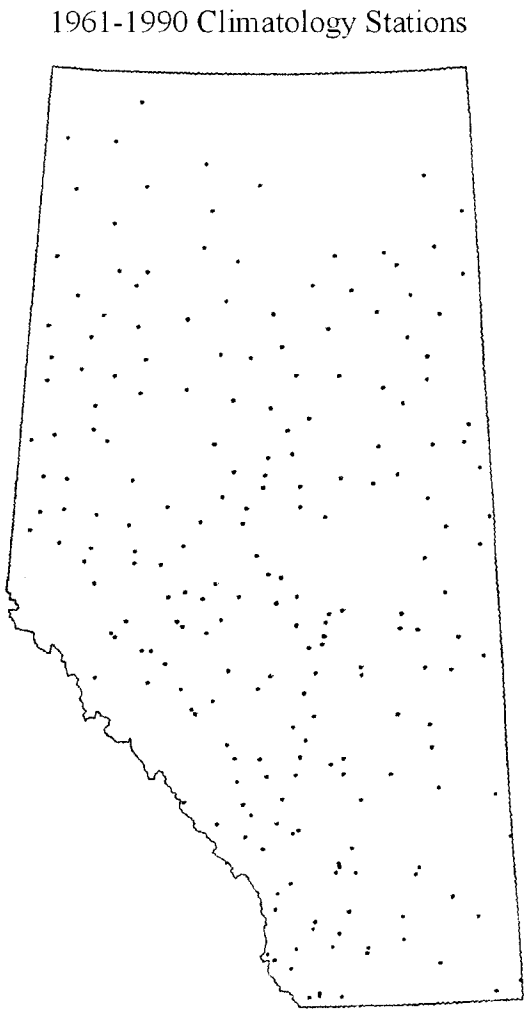

Figure 2.4. Distribution of the Alberta precipitation stations whose 1961-1990 May-August precipitation normals were computed.

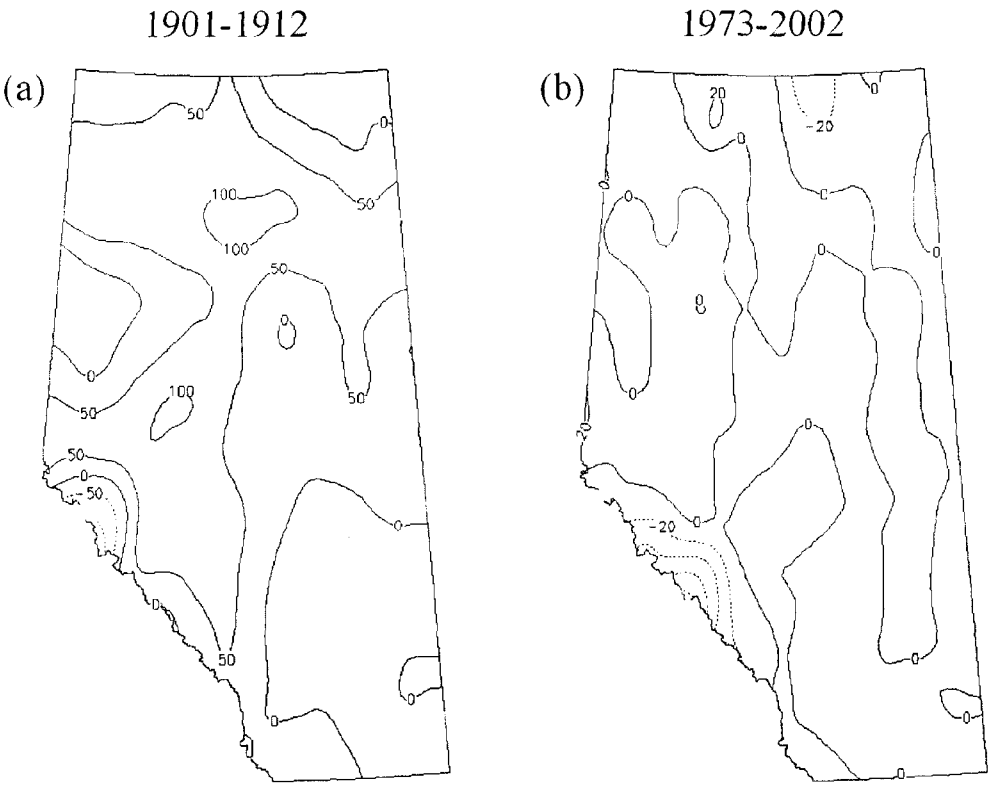

Figure 2.5. The difference of the interpolated May-August precipitation between the two methods (the one using the improved method minus the one using the original method) in the periods of 1901-1912 and 1973-2002 (units: mm).

parts of Alberta (near zero) in the same period (1901-1912) since the stations are relatively dense (Fig. 2.3a). It is not surprising to see that the difference is nearly zero almost everywhere in the period 1973-2002 (Fig. 2.5b) since the number of stations has largely increased.

The daily data produced from the above interpolation, although good for the May-August precipitation, have much smaller-than-realistic variance and are not suitable for studies of climate extremes such as precipitation intensity.

2.4 Agroclimatic parameters and analysis method

Although most materials contained in this section are available in the literature (e.g., Bootsma et al., 2001; Chetner et al., 2003; and Dzikowski and Heywood, 1989), they are briefly summarized here to facilitate a systematic study of Alberta's agroclimatic changes.

2.4.1 Summary of nine agroclimatic parameters

Alberta is divided into ten ecoregions, but only six have extensive agriculture: Peace Lowland (PL), Boreal Transition (BT), Aspen Parkland (AP), Moist Mixed Grassland (MMG), Fescue Grassland (FG) and Mixed Grassland (MG) (Fig. 2.1). The analyses of the temporal trends in the agroclimatic parameters are conducted mainly on these six ecoregions. The analyzed agroclimatic parameters are summarized as follows.

(1) GROWING SEASON

The SGS (start of growing season) is the first day of a year when five consecutive days have a mean temperature above 5°C. The EGS (end of growing

season) is the first day in the fall on which the mean temperature is below 5°C. Both SGS and EGS are sensitive to weather outliers in spring and fall, as are the crops. For example, in 1910, an abnormally warm week at the end of March started the growing season about a month earlier than normal, but a cold event occurred at the beginning of June and put the LSF later than normal. The LGS (length of growing season) is the number of days between the SGS and the EGS:

$$LGS = EGS - SGS + 1.$$

The means (standard deviations) of the SGS, EGS, and LGS for the Alberta AR region in 1961-1990 are 108 (9.78) [calendar day of a year, i.e., April 18 if not a leap year], 263 (10.80) [calendar day of a year, i.e., September 20 if not a leap year], and 156 (14.99) [days], respectively.

(2) FROST-FREE PERIOD

The LSF (last spring frost) day is defined as the last date in a year on or before July 15 when the daily minimum temperature $T_{min} \leq 0°C$. The FFF (first fall frost) day is defined as the first date in a year on or after July 16 when $T_{min} \leq 0°C$. Similar to SGS and EGS, LSF and FFF are also sensitive to weather outliers, particularly the cold outliers, in late spring and early fall and are good indicators for crops' frost damage. The FFP (frost-free period) is the number of days between the LSF and the FFF:

$$FFP = FFF - LSF + 1.$$

The means (standard deviations) of the LSF, FFF, and FFP for the Alberta AR region in 1961-1990 are 140 (7.36) [calendar day of a year, i.e., May 20 if not a leap year], 257 (8.66) [calendar day of a year, i.e., September 14 if not a leap year], and 118

(11.39) [days], respectively. The LGS is in general longer than the FFP. For genetically improved seeds, the growing season may be even longer and can start on the first calendar date of the five consecutive days with a mean temperature above 0°C, rather than 5°C.

(3) GROWING DEGREE DAYS

Most of the natural crop species can grow when the daily mean temperature is above 5°C, although the genetic-engineered species can sustain lower temperature and grow even when the daily mean temperature is between 0°C and 5°C. Some people now use values based on 0°C for the growing degree day (GDD). However, because our purpose is to assess the agroclimatic change since 1901, our values for the GDD are still based on 5°C and computed from the mean daily air temperature (T_{mean}) by using the formula

$$\text{Daily GDD} = \begin{cases} T_{mean} - 5.0, & \text{if } T_{mean} > 5.0, \\ 0 \quad , & \text{otherwise,} \end{cases}$$

where $T_{mean} = (T_{\max} + T_{\min})/2.0$. The GDD is accumulated from the SGS to the EGS.

(4) CORN HEAT UNIT

The growth of warm-season crops like corn and soybeans depends on the daily minimum and maximum temperatures in a more refined way than GDD and is normally indicated by the corn heat unit (CHU). Corn growth is slow at a low temperature and increases as the temperature rises until it reaches a threshold temperature beyond which the growth again becomes slow. The daily CHU is computed from the daily maximum and minimum temperatures. The CHU calculations are treated separately for daytime and nighttime. As well, these

calculations assume that no growth occurs at night when the temperature is below 4.4°C or during the day when the temperature is below 10°C. Moreover, these calculations use 30°C as the threshold temperature of the daytime because warm-season crops develop fastest at 30°C. The night does not have a threshold temperature since the nighttime temperature seldom exceeds 25°C. The daily CHU is the average of the nighttime CHU and the daytime CHU, calculated by the formulas below:

$$CHU = (CHU_X + CHU_Y)/2,$$

where the nighttime CHU is

$$CHU_X = 1.8(T_{\min} - 4.4),$$

and the daytime CHU is

$$CHU_Y = 3.33(T_{\max} - 10) - 0.084(T_{\max} - 10)^2.$$

In the above, $CHU_X = 0$ if $T_{\min} < 4.4^{\circ}C$ and $CHU_Y = 0$ if $T_{\max} < 10.0^{\circ}C$. The accumulated CHU (i.e., ACHU) is the accumulation of the daily CHU from the last day of three consecutive days in the spring with mean daily air temperatures greater or equal to 12.8°C, to the first day after July 16, with a minimum temperature less than or equal to -2°C (Bootsma and Brown, 1995). The critical temperature 12.8°C is the value that corresponds closely with the average seeding date for grain corn and also corresponds to the time when sufficient heat has been received to raise the soil temperature to 10°C, which ensures corn germination.

2.4.2 Methods for data analysis

(1) Area-weighted average of the agroclimatic parameters

The above eight temperature-related and other precipitation-related agroclimatic parameters are computed by using the daily temperature and precipitation data for every EDP. The calculated agroclimatic parameters for the EDPs are then averaged for the ecoregions and the entire province of Alberta. Since both the EDPs and the ecoregions are irregular polygons, and their areas vary, the use of a simple average is inappropriate. Instead, the area-weighted average is used. For an ecoregion with N EDPs, the area-weighted parameter $\overline{R}(t)$ can be calculated by using

$$\overline{R}(t) = \frac{1}{\sum_{i=1}^{N} A_i} \sum_{i=1}^{N} A_i R_i(t),$$

where A_i is the area of the ith EDP, and R_i is the value of the parameter R for this polygon. The ecoregion-averaged data are then employed to create the annual time series of the agroclimatic parameters for the six agricultural ecoregions, the agricultural regions as a whole (i.e., the union of the six ecoregions with extensive agriculture), and the entire province.

(2) Trend analysis and the temporal change of the agroclimate

After the preparation of the regionally averaged annual time series, the temporal trends of the nine agroclimatic parameters are studied by using the linear regression method. The linear correlation coefficients and significance levels are computed for each agroclimatic parameter to detect if significant linear temporal trends exist. Kendall's Tau significance is used to examine the hypothesis that the correlation is different from zero. This non-parametric method does not require the

normality assumption of the slope as the t-test does and has been used in climate research for trend detection (Daniel, 1990; Zhang et al., 2000). Let (X_i, Y_i) and (X_j, Y_j) be a pair of observations. If the difference between X_i and X_j is in the same direction as the difference between Y_i and Y_j (in other words, the differences have the same sign), the two pairs are called *concordant*. If the differences are in reverse direction, the two pairs are called *discordant*. Let the sample size be n, then the total number of possible data pairs is $n(n-1)/2$. The Kendall's Tau correlation is defined as follows

$$\hat{\tau} = \frac{C - D}{n(n-1)/2},$$

where C is the number of concordant pairs and D is the number of discordant pairs. If all the pairs are concordant, the $\hat{\tau}$ equals 1. If all the pairs are discordant, the $\hat{\tau}$ equals -1.

In the situations when ties occur, the $\hat{\tau}$ statistic is adjusted as

$$\hat{\tau} = \frac{C - D}{\sqrt{\frac{1}{2}n(n-1) - T_x}\sqrt{\frac{1}{2}n(n-1) - T_y}},$$

where $T_x = \frac{1}{2}\sum t_x(t_x - 1)$, $T_y = \frac{1}{2}\sum t_y(t_y - 1)$; and $t_x(t_y)$ is the number of $X(Y)$ observations that are tied at a given rank. The assumptions for Kendall's Tau statistics are as follows: (a) The data consist of a random sample of n observation pairs (X_i, Y_i) of numeric or nonnumeric observations, and each pair of observations represents two measurements taken on the same unit of association; and (b) The data

are measured on at least an ordinal scale, so that we can rank the observations (Daniel, 1990). Although the Kendall's Tau is a measure of correlation, it is frequently used as tests for trend. To test for trend in time series data, we may denote X as time variable and Y as time-dependent variable. If the sample data exhibit a positive (negative) trend, the Y values tend to increase (decrease) over time. In our study, X represents year; Y represents annual agroclimatic variable, which can be ranked. Thus, the assumptions above are applicable to our analysis.

(3) Spatial change of the agroclimate

To analyze the spatial changes of the agroclimate, the spatial distributions of three 30-year mean conditions for the agroclimatic parameters in Alberta are plotted. The 30-year periods are 1913-1942, 1943-1972, and 1973-2002. Their differences are analyzed to show the changes among the three periods. Also, the spatial distribution of the 102-year trend is studied. The changing and shifting of the agricultural climatic resources and the potential crop-growing areas are analyzed.

2.5 Results

Table 2.2 contains the r and s values for nine different agroclimate parameters and six ecoregions with extensive agriculture, the agricultural region as a whole, and the Alberta region as a whole, where r is the correlation coefficient between each agroclimatic parameter and time (units: year), and s is the slope of the temporal trend of each agroclimatic parameter. The agricultural ecoregions are denoted by PL (Peace Lowland), BT (Boreal Transition), AP (Aspen Parkland), MMG (Moist Mixed Grassland), FG (Fescue Grassland), and MG (Mixed Grassland) and are ordered according to their locations from the northwest to the southeast of Alberta. (See Fig.

2.1 for the locations of the ecoregions and Table 2.1 for acronyms.) AR stands for the agricultural region as the union of the six ecoregions, and AB stands for Alberta as the union of the ten ecoregions. When the slope s is found to be significant by using Kendall's Tau statistic at the significance level of 10%, then both the r and s values are shown in bold face in Table 2.2; otherwise, the r and s values are in plain text. With different P-values, the significant correlation coefficients are marked by double asterisks when $P \leq 0.01$, by a single asterisk when $0.01 < P \leq 0.05$, and a dagger when $0.05 < P \leq 0.10$.

The results show that the precipitation from May to August, usually included in the growing season defined in Section 2.4.1(1), increased 8% (18 mm) during the period 1901 to 2002 (Fig. 2.6a) over the Alberta agricultural region (AR), and that this increase is significant at the 10% significance level (Tables 2.2 and 2.3). However, the increment is non-uniform and appears to have a pattern: the increment is the largest in the north and the northwest of Alberta; then the increment diminishes in central and southern Alberta (i.e., the AP and MMG regions); finally, the increment becomes prominent again in the southeast corner of the province (Fig. 2.7a). This pattern transition seems to follow that of the 30-year normals, except in the northeast and the northwest of Alberta (Chetner et al., 2003; Dzikowski and Heywood, 1989). Two small areas in central and southern Alberta even experienced a decrease of 30 mm. The PL region's May-August precipitation increased 26% (53 mm) over the period 1901 to 2002, and the increment is significant at the 5% significance level. The MMG region experienced zero increment. Thus, the May-August precipitation increase over the agricultural region is attributed to the increase over the northwest and southeast

Table 2.2. Correlation coefficients (*r*, dimensionless) between the annual agroclimatic parameters and time from 1901 to 2002, and slopes (*s, units: climate units per 102 years*) of the trend for the nine annual agroclimatic parameters

Region		PCPN (May-August)	SGS	EGS	LGS	LSF	FFF	FFP	GDD	ACHU
PL	*r*	**0.15***	-0.09	-0.05	0.01	**-0.38****	**0.36****	**0.46****	-0.04	**0.12†**
	s	**0.52**	-0.04	-0.03	0.01	**-0.20**	**0.20**	**0.40**	-0.28	**1.47**
BT	*r*	0.06	0.03	-0.01	-0.01	**-0.24****	**0.35****	**0.38****	**0.18****	**0.25****
	s	0.13	0.01	0.00	-0.01	**-0.12**	**0.17**	**0.29**	**1.09**	**3.03**
AP	*r*	0.05	0.02	-0.01	-0.03	**-0.23****	**0.32****	**0.37****	**0.23****	**0.26****
	s	0.04	0.02	0.00	-0.02	**-0.11**	**0.16**	**0.27**	**1.49**	**2.99**
MMG	*r*	0.06	0.00	0.00	0.02	**-0.14***	**0.19****	**0.22****	**0.19****	**0.20****
	s	0.00	-0.02	-0.01	0.01	**-0.07**	**0.08**	**0.15**	**1.56**	**2.53**
FG	*r*	0.07	0.03	-0.07	-0.08	-0.03	0.02	0.06	-0.07	-0.06
	s	0.09	0.01	-0.05	-0.06	-0.02	0.00	0.02	-0.51	-0.20
MG	*r*	0.09	-0.02	-0.02	-0.02	-0.04	0.09	0.10	0.09	0.05
	s	0.11	-0.02	-0.03	-0.01	-0.02	0.04	0.06	0.75	0.97
AR	*r*	**0.12†**	0.00	-0.02	0.00	**-0.25****	**0.33****	**0.36****	**0.11†**	**0.18****
	s	**0.18**	-0.01	-0.01	0.00	**-0.10**	**0.13**	**0.23**	**0.76**	**2.02**
AB	*r*	**0.18****	-0.02	-0.11	-0.06	**-0.31****	**0.37****	**0.43****	-0.09	0.06
	s	**0.32**	-0.01	-0.05	-0.04	**-0.13**	**0.16**	**0.29**	-0.40	0.62

** Significance level : $0.00<P\leq0.01$
* Significance level : $0.01<P\leq0.05$
† Significance level : $0.05<P\leq0.10$

Table 2.3. The total changes (*t*) and the percentage changes (*p*) from 1901 to 2002 of the nine annual agroclimatic parameters (the percentage change is with respect to the linear fitted value in 1901)

Region		PCPN (May-August)	SGS	EGS	LGS	LSF	FFF	FFP	GDD	ACHU
PL	*t*	**53.0**	-4.1	-3.1	1.0	**-20.4**	**20.4**	**40.8**	-28.6	**149.9**
	p (%)	**25.5**	-3.5	-1.2	0.7	**-13.1**	**8.5**	**48.8**	-2.5	**9.1**
BT	*t*	13.3	1.0	0.0	-1.0	**-12.2**	**17.3**	**29.6**	**111.2**	**309.1**
	p (%)	4.8	0.9	0.0	-0.6	**-8.0**	**7.1**	**32.3**	**9.7**	**18.5**
AP	*t*	4.1	2.0	0.0	-2.0	**-11.2**	**16.3**	**27.6**	**152.0**	**305.0**
	p (%)	1.6	1.9	0.0	-1.3	**-7.5**	**6.6**	**28.4**	**12.8**	**17.3**
MMG	*t*	0.0	-2.0	-1.0	1.0	**-7.1**	**8.2**	**15.3**	**159.1**	**258.1**
	p (%)	0.0	-1.9	-0.4	0.6	**-4.9**	**3.2**	**13.7**	**12.1**	**13.1**
FG	*t*	9.2	1.0	-5.1	-6.1	-2.0	0.0	2.0	-52.0	-20.4
	p (%)	3.7	1.0	-1.9	-3.6	-1.4	0.0	1.8	-4.0	-1.1
MG	*t*	11.2	-2.0	-3.1	-1.1	-2.0	4.1	6.1	76.5	98.9
	p (%)	6.3	-2.0	-1.1	-0.6	-1.4	1.6	5.0	5.0	4.3
AR	*t*	**18.4**	-1.0	-1.0	0.0	**-10.2**	**13.3**	**23.5**	**77.5**	**206.0**
	p (%)	**8.0**	-0.9	-0.4	0.0	**-6.9**	**5.4**	**23.4**	**6.2**	**11.1**
AB	*t*	**32.6**	-1.0	-5.1	-4.1	**-13.3**	**16.3**	**29.6**	-40.8	63.2
	p (%)	**13.6**	-0.9	-1.9	-2.7	**-8.6**	**6.7**	**33.5**	-3.5	3.7

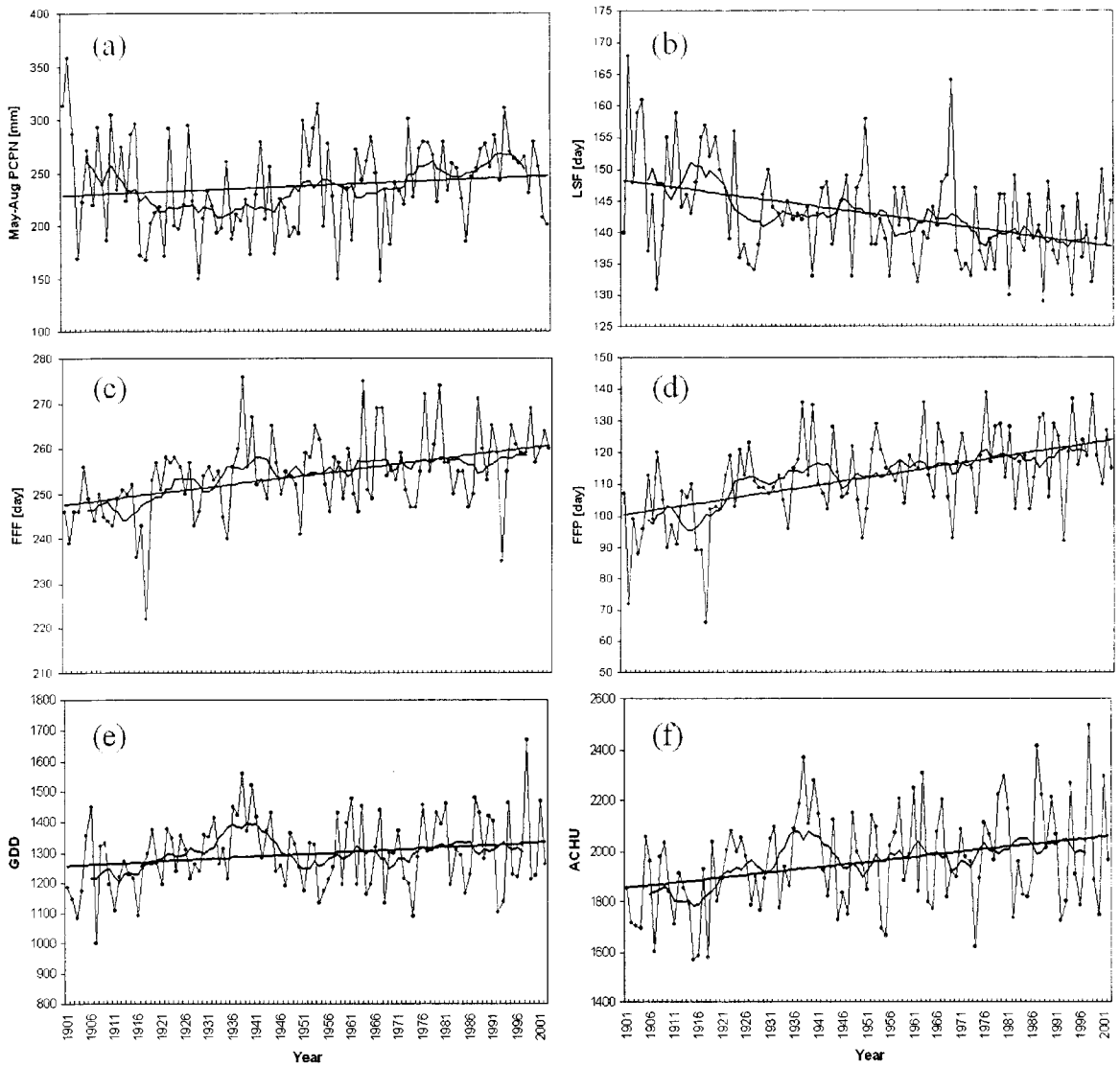

Figure 2.6. Annual time series (thin curve with dots), 11-year running mean (thick curve), and linear regression line (straight line). (a) May-August precipitation [units: mm], (b) LSF [units: day], (c) FFF [units: day], (d) FFP [units: day], (e) accumulated GDD in the growing season, and (f) ACHU.

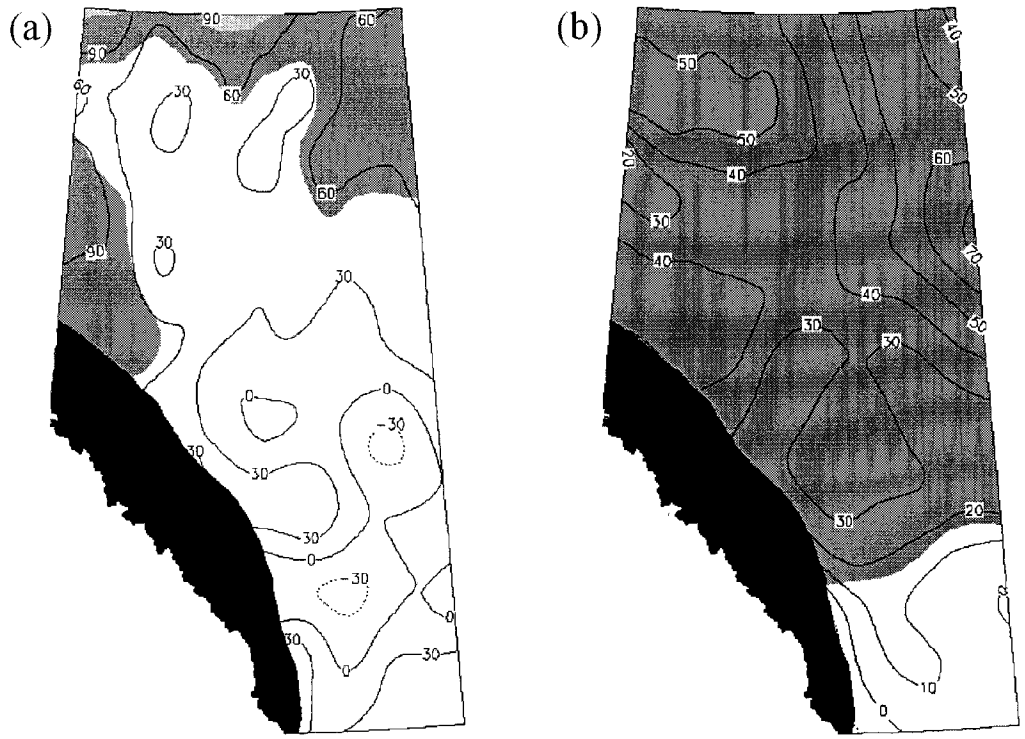

Figure 2.7. Spatial distribution of the temporal trends from linear regression. (a) May-August precipitation (units: mm/102yr), (b) FFP (units: day/102yr). The shaded regions are where significant trends exist at the 5% significance level. The Rocky Mountain areas are blacked out because of insufficient station data and large gradients of trends, and hence possibly very large errors.

areas. Similar analysis of Fig. 2.7a implies that the significant increment of the May-August precipitation over the entire province is mainly attributable to the non-agricultural regions in the north and west and the ecoregion PL. The precipitation results in Tables 2.2 and 2.3 agree with the findings of Zhang et al. (2000), who identified the positive precipitation trend in eastern Canada and in the western-most province, British Columbia, and found no significant trends in the Canadian Prairies, especially in southern Alberta and the eastern neighboring province, Saskatchewan. The increase of the May-August precipitation is attributable mainly to the increasing number of events of low-intensity precipitation, as Akinremi et al. (1999), Zhang et al. (2001) and Kunkel (2003) concluded. Our percentile analysis also shows no significant increase of the events of the 90^{th}, 95^{th} and 99^{th} percentile precipitation from 1901 to 2002 over both the agricultural region (AR) and the entire province (AB). The Alberta drought records show no discernible increase signal of drought events or intensity in the 20^{th} century (Shen et al., 2003). Karl and Knight (1998) identified an increase in the 20^{th}-century precipitation over the United States and attributed the increase to high-intensity events. Thus, the available results from others support our finding of different patterns of climate change in terms of precipitation in the United States and Canada during the last century.

The above conclusions were first derived from the daily precipitation data on EDPs. To further verify these results, the same calculation was made by using finer resolution data, the data on SLC polygons. The May-August precipitation trend from 1901 to 2002 for every SLC polygon was computed and tested for significance. Fig. 2.7a depicts the contour plot of the trend.

The values of SGS, EGS, and LGS do not show significant changes from 1901 to 2002, possibly because the climate warming is caused mainly by the higher minimum temperature, particularly in the winter, and the increase of the mean temperature in the spring and fall is small. For this reason, one may infer that the agroclimatic parameters crucially depending on daily minimum temperature should have changed significantly. Our data analysis supports this inference. Our numerical results have demonstrated a significantly earlier LSF, a later FFF, and a longer FFP in the four northern agricultural regions: PL, BT, AP and MMG. The linear regression slopes become smaller from the north to the south, indicating a larger change in the north and a smaller change in the south, as is clearly shown in Fig. 2.7b. This figure shows that the FFP has increased over the entire province from 1901 to 2002. According to the linear regression from 1901 to 2002, the LSF in the ecoregion PL was 20 days earlier in 2002 compared to that in 1901, 12 days earlier in the ecoregion BT, 11 days earlier in the ecoregion AP, 7 days earlier in the ecoregion MMG, 10 days earlier in the entire agricultural region AR, and 13 days earlier in the entire province AB. The FFF was 20 days later in PL, 17 days later in BT, 16 days later in AP, 8 days later in MMG, 13 days later in AR, and 16 days later in AB. This trend of an earlier LSF and later FFF resulted in an increase in the FFP of 41, 30, 28, 14 days in the PL, BT, AP, MMG, respectively, 24 days in the entire agricultural region, and 30 days in the entire Alberta (the spatial distribution of the trends is shown in Fig. 2.7b). The earlier LSF implies that consecutive warm days in the spring occur earlier and hence allow spring melts to occur earlier too. These conditions raise soil temperature earlier for seed germination and thus reduce the frost risk for spring

crops. The delay of consecutive cold days in the fall improves the chances for crops to mature to a higher quality yield. The percentage change of the FFF from 1901 to 2002 is the largest over PL (8.5%) (Table 2.3). The absolute value of the FFF slope is comparable to that of the LSF for most ecoregions. However, our provincial average suggests a slightly larger FFF increment than a LSF decrease, and the difference between the FFF increase and the LSF decrease is 3 days (see Tables 2.2 and 2.3). It was noticed that Bonsal et al. (2001) found a slightly larger decrease of LSF than the increase of FFF for most of Canada, based upon an analysis of data from 210 high-quality stations in the periods of 1900-1998 and 1951-1998. Due to the spatial inhomogeneity of the LSF and FFF changes discerned in Table 2.3, the difference between the conclusions of Bonsal et al. (2001) and our research is insignificant considering the noise level of the current data. Nonetheless, this difference will be worth investigating further when more accurate data sets become available.

The GDD and ACHU are two types of easy-to-use energy terms in agroclimatology that relate plant growth to temperature. The more energy available, the more likely the plant will be to reach maturity, and the more hybrids of the plant can be grown in an area. Table 2.2 shows significant positive trends (at the 1% significance level) in the GDD and ACHU in three ecoregions (BT, AP and MMG), and the increments over the period 1901 to 2002 are around or greater than 10%. The largest percentage change in the GDD is over AP (13%), and in the CHU is over BT (19%). These increases are consistent with the increment of the plant hardiness subzone index for most of Alberta and make growing more varieties of crop species possible (McKenney et al., 2001).

Figure 2.6 shows the annual time series of the six agroclimatic parameters with significant linear trends in the entire agricultural area AR. The 11-year running means are also shown. The positive trend of the May-August precipitation is a result of the steady increase of precipitation after the 1920s. The variance of the temporal precipitation change over time decreased during 1973-2002. To check the moisture supply due to precipitation for the entire crop-growing period, the total growing season precipitation (GSP) in units of [mm/day] was calculated. The GSP follows a similar trend as the May-August precipitation, and their correlation is 0.90. The shift of the LSF to an earlier date before the 1940s and between the1970s and 1980s, together with the shift of the FFF to a later date in the same periods, cause the increase of the FFP in the corresponding period. This increase indicates lower risks for frost damage to crops in Alberta, if crops are planted at the normal time. This result is consistent with the findings of Zhang et al. (2000), who showed that a mean temperature warming of 0.9°C in southern Canada (south of 60°N) resulted from the increases in temperature prior to the 1940s and after the 1970s. This result also agrees with that of Folland et al. (2001), who found that most of the increase of the temperature occurred in two periods, from about 1910 to 1945 and since 1976. This warming trend is also manifested in Alberta by a rapid increase of the GDD and ACHU from 1901 to the1940s, but the increase rate is smaller after the 1970s. This is because the increase of temperature after 1970s mainly occurred in winter while winter temperature normally dose not affect the GDD computation. The LSF usually occurred in May during the decade of the 1960s. However, in 1969, the minimum temperature fell below zero almost all over the province on around June 13, and this

resulted in an exceptionally late LSF in that year (see Fig. 2.6b). Another exceptional case involves the FFF in 1918. Observations from the northern and central part of Alberta indicated a below-zero minimum temperature on around July 24, which was almost one month earlier than usual and caused the earlier FFF in that year. From July 21 to 23 in 1992 (see Fig. 2.6c), the minimum temperature decreased to below zero over most of the province, resulting in a small value of FFF in 1992. Other extremes were also checked and compared with the station observations. Most of these extremes were due to the natural variance, while the results before the1910s may be inaccurate because of too few observations.

Alberta has relatively large geographical variability across the province. From the Subarctic region in the north to the Prairie Grassland in the south, from the high elevation mountains in the west to the flat areas in the east, the Alberta climate varies considerably from region to region. The climate change over time in Alberta also differs from place to place. Fig. 2.8 shows the difference between the recent 30-year normal (1973-2002) and the 30-year normal of 60 years earlier (1913-1942) for six agroclimatic parameters. The results in this figure are based on the data over the SLC polygons. The information given in the plots over the northmost areas of Alberta is not as reliable as that for the agricultural regions because of very sparse station observations. Fig. 2.8a indicates an increase in the May-August precipitation of 40-60 mm over PL and BT. The change over other agriculture areas is about 20-60 mm. In general, the western part of the province had a larger increase in precipitation than the eastern part, which is typically drier. The black area over the Canadian Rockies indicates an inaccurate-conclusion area due to insufficient data coverage.

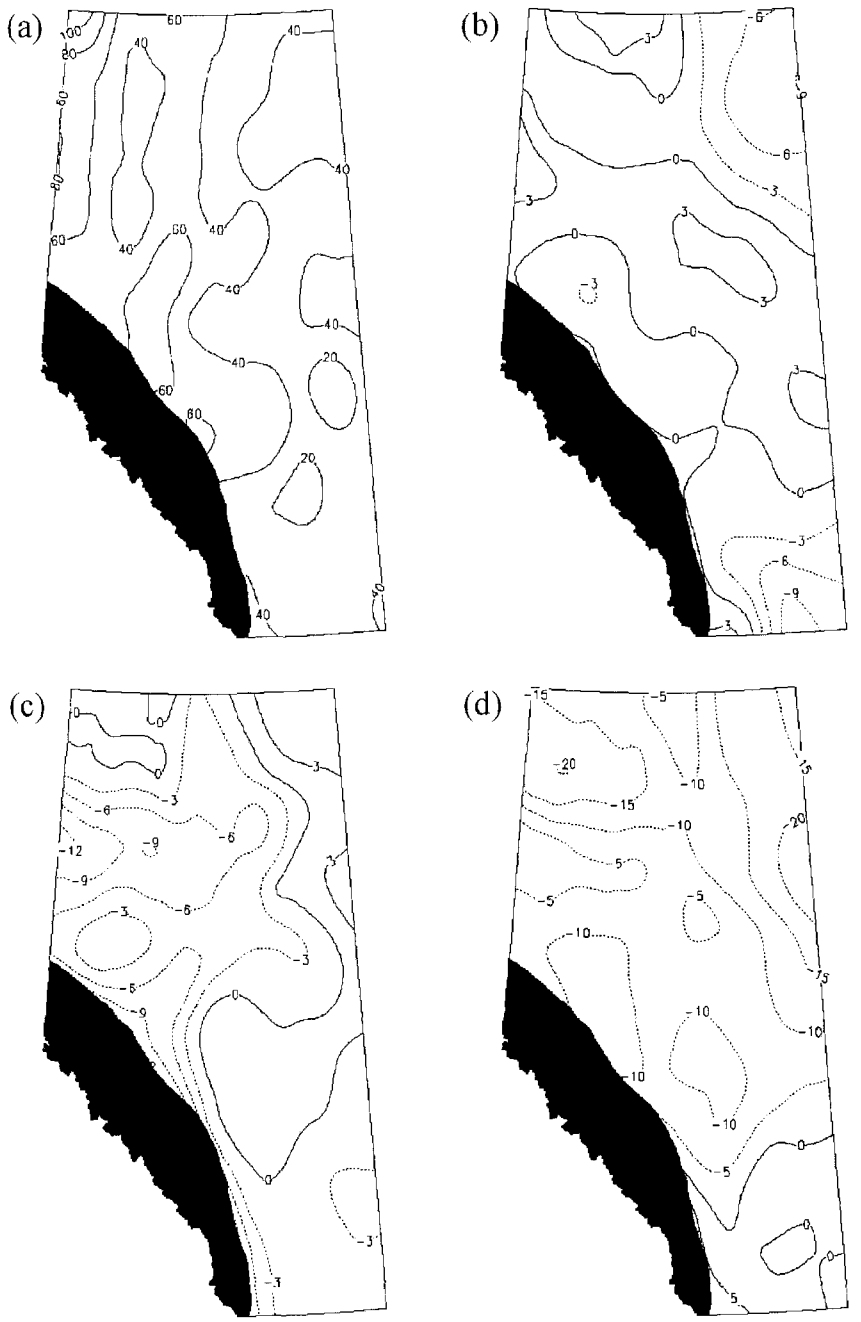

Figure 2.8. The difference of the recent 30-year normal (1973-2002) minus the 1913-1942 normal for six agroclimatic parameters. (a) May-August precipitation [units: mm], (b) SGS [units: day], (c) EGS [units: day], (d) LSF [units: day], (e) FFF [units: day], and (f) ACHU. The Rocky Mountain areas are blacked out due to insufficient data.

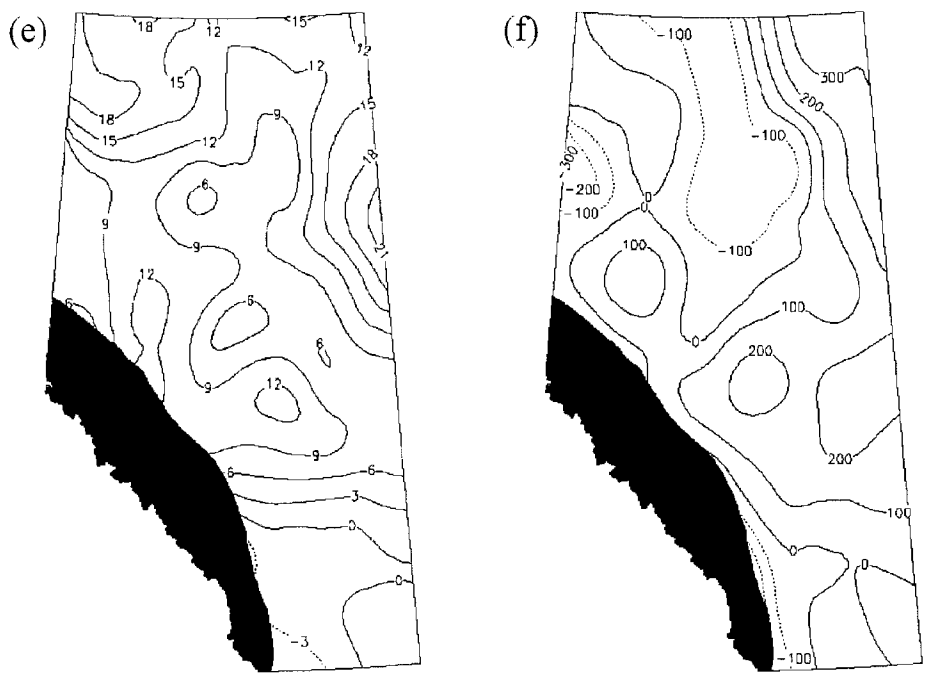

Figure 2.8. Continued.

The changes in the SGS, EGS, and LGS were also non-uniform. Fig. 2.8b shows the change in the SGS and appears to support a northwest-southeast-oriented pattern. The most remarkable change occurred over the southeast corner of Alberta where the SGS is 3-9 days earlier now than it was 60 years ago. The EGS in the PL region (Fig. 2.8c) was noticeably earlier (3-9 days) than it was 60 years ago. The southeast corner also has an earlier EGS, but the difference is small. As a result, the LGS (not shown in the figure) became 3-9 days longer than it was 60 years ago in the southeast corner of the province and 0-3 days longer in part of the BT and AP, while in the PL region, the LGS was shorter by 3-12 days. Although the SGS, EGS and LGS do not have a long-term linear trend from 1901 to 2002, Alberta's climate experienced some changes during the last 60 years. An earlier LSF (Fig. 2.8d), a later FFF (Fig. 2.8e) and a longer FFP (not shown in the figure) occurred in most of Alberta excluding the southeast corner. The change shows a north-south gradient pattern. In the northern agricultural regions, the LSF was earlier by 10-15 days, and the FFF was later by about 10 days from 1973-2002 compared to that of 60 years ago. As a result, the FFP was longer by about 20 days in most of the agricultural regions, but in the southeast corner, the FFP did not significantly change. The ACHU (Fig. 2.8f) increased most over the BT and AP ecoregions by an amount of 100-200 units, yet almost no increase occurred in southern Alberta, and a decrease occurred in part of the PL ecoregion. The GDD's 30-year normal (not shown in the figure) has a similar spatial pattern to that of the ACHU.

The 1973-2002 normals and the 1943-1972 normals are compared in Fig. 2.9. The difference in the May-August precipitation (not shown) has a similar pattern

to that shown in Fig. 2.8a, but the magnitude is smaller. The SGS (Fig. 2.9a) was earlier by 3-6 days in almost the entire province, with the greatest difference in the southeast corner and in part of the PL region. On average, the EGS (Fig. 2.9b) occurred 0-6 days later in the Alberta agriculture region. The EGS was late by 6 days in part of the PL region. The earlier SGS and later EGS resulted in a longer LGS (not shown) in all the agricultural regions in Alberta by 5-10 days. The LSF, FFF and FFP (not shown) have a similar pattern to those in Fig. 2.8 but with smaller magnitudes. A larger area of increased ACHU (Fig. 2.9d) has been found comparable to that shown in Fig. 2.8f.

The increase in GDD and ACHU over the agricultural regions is an important climatic development for farmers, who have more options to select crop hybrids based on factors such as agronomic parameters for a given farmland. For instance, corn hybrids grown for silage on the Prairies usually require 2,000 to 2,100 ACHU, while grain hybrids require 2200 to 2400 ACHU to mature. Knowing where ACHUs are above these thresholds is important to the corn and feed industry. Fig. 2.10 shows the regions of the ACHU greater than or equal to 2,000 for the 1913-1942 normal, 1943-1972 normal, and 1973-2002 normal. The area suitable for planting corn according to the 1973-2002 normal has extended to the north by about 200-300km compared to the1913-1942 normal, and by about 50-100 km compared to the 1943-1972 normal. This finding indicates that with the increasing heat units in growing season, the potential growing areas for some warm-season crops such as corn have increased.

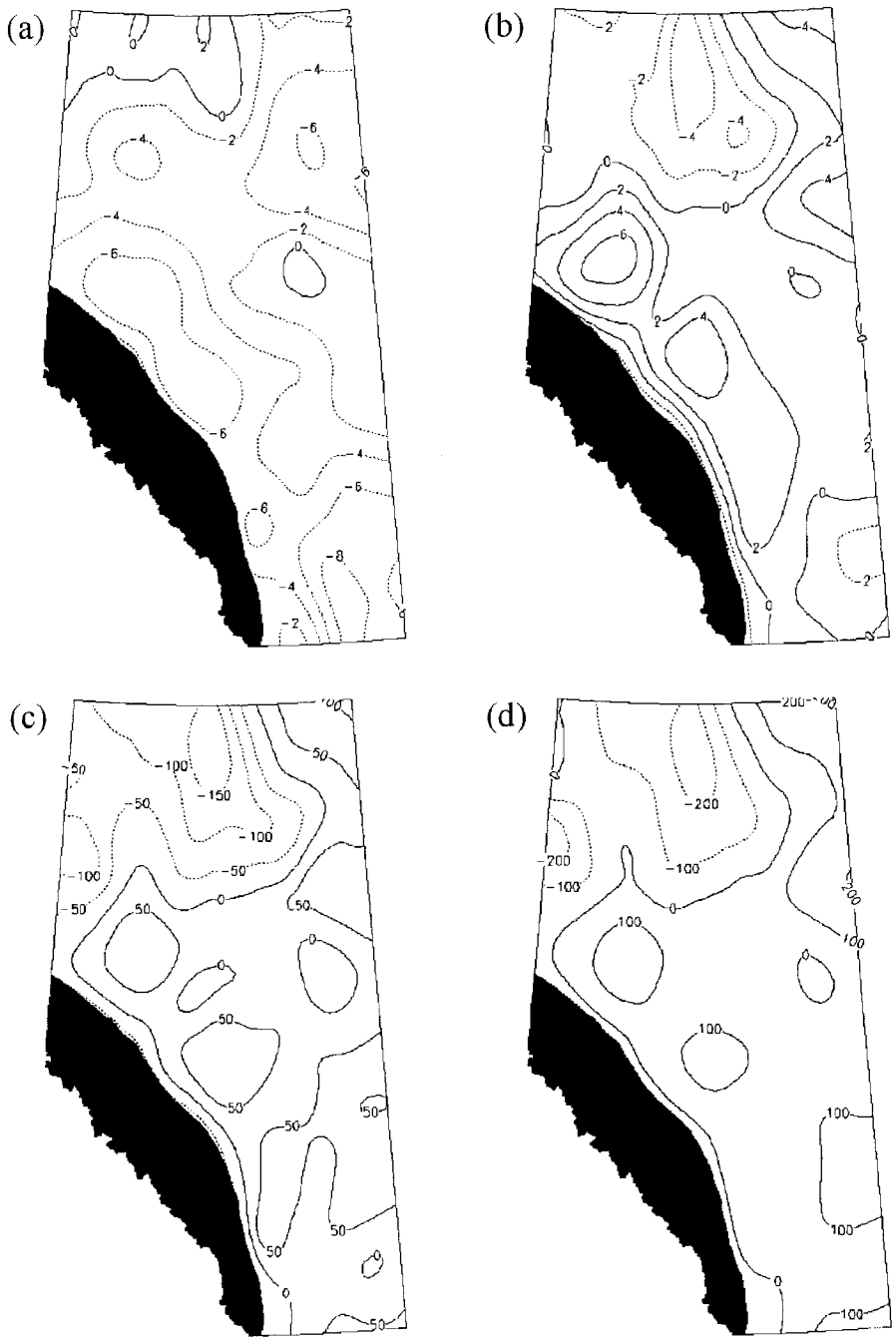

Figure 2.9. The difference of the recent 30-year normal (1973-2002) minus the 1943-1972 normal for four agroclimatic parameters. (a) SGS [units: day], (b) EGS [units: day], (c) GDD, and (d) ACHU. The Rocky Mountain areas are blacked out due to insufficient data.

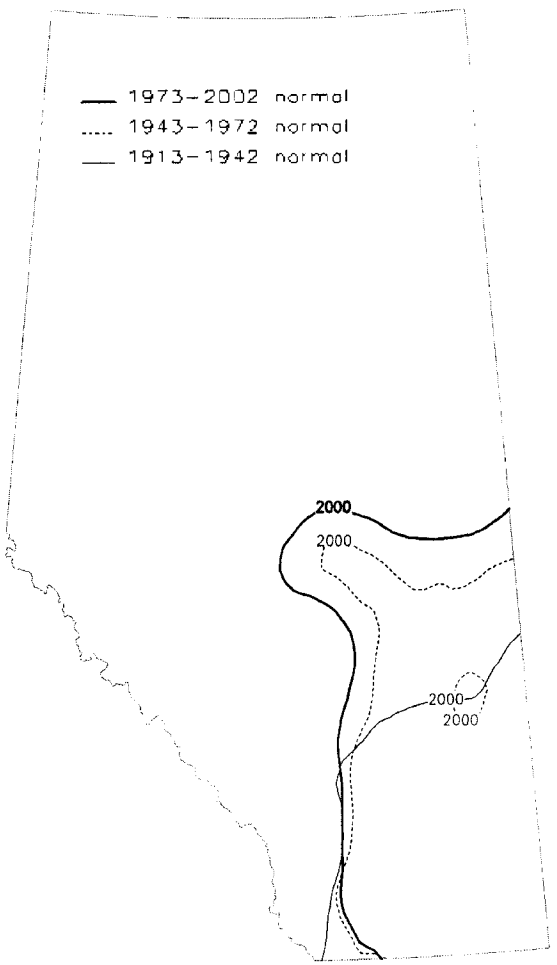

Figure 2.10. The areas with ACHU ≥ 2,000 (areas below the contours) for the 1913-1942 normal, 1943-1972 normal and 1973-2002 normal.

2.6 Summary and discussion

By using the interpolated data of daily maximum temperature, daily minimum temperature, and daily precipitation over the EDP and SLC polygons and using area-weighted averages and linear regression, the temporal and spatial changes of nine agroclimatic parameters in Alberta during the period 1901- 2002 have been analyzed. The temporal changes are represented by linear trends. The significance levels of the linear trends are determined by Kendall's Tau method. The spatial changes are represented by the climate differences during the three time periods (1913-1942, 1943-1972 and 1973-2002). Our numerical results support the following conclusions. The May-August precipitation had increased over Alberta from 1901 to 2002, but the increase is non-uniform. The largest and significant increment (at the 5% significance level) was in northern and northwestern Alberta, ranging from 30 to 90 mm. The increment was not significant in other areas of Alberta. The increment diminished to zero or was even negative in central and southern Alberta, and it became large again (reaching 30 mm) in Alberta's southeast corner. This spatial pattern of precipitation change and the increase of the surface air temperature made central and southern Alberta vulnerable to the impact of drought toward the end of the last century (and the years to come if the pattern and trend continue). In deriving the above conclusions on precipitation, the errors attributed to the changes of rain gauges and coding practices were not considered. The wind undercatch and wetting loss before 1970s may

contribute to 2-4% of underestimation of the precipitation in the earlier part of the last century (Zhang et al., 2000, and Zhang et al., 2001).

An earlier LSF, a later FFF and a longer FFP now occur in most of Alberta. Significant long-term trends in these parameters exist in almost the entire province except in the southeastern tip of Alberta. The significant extension of FFP over 30 days in northern and central Alberta can greatly reduce the frost risks to crops and bring economic benefits to Alberta agricultural producers. The FFP extension occurred in concurrence with the rise of the plant hardiness index, which depends on minimum temperature, by one or two zones over Alberta (McKenney et al., 2001). However, no significant long-term trends have been found for the SGS, EGS, and LGS based on the definition of the daily mean temperature greater than 5°C for 5 consecutive days. The conclusion may vary if the definition is changed to the daily mean greater than 0°C or changed to the daily minimum temperature, according to some new types of seeds, or new types of crops. Nonetheless, by comparing the 1973-2002 and 1943-1972 normals, an earlier SGS, a later EGS and a longer LGS over the Alberta agricultural region were detected with the magnitudes of 3-6 days, 0-6 days, and 5-10 days, respectively. The LGS extension can benefit both crop yield and quality, and other agricultural production activities on a farm.

The warming trend in Alberta's climate has been demonstrated by the increase of the GDD and ACHU in most of the agricultural regions in Alberta. The area with sufficient ACHU for corn production has extended to the north by about 200-300km since the 1910s, and by about 50-100 km since the 1940s. This extension implies that

Alberta farmers now have a larger variety of crops to choose from than were available previously.

A warming trend exists in Alberta, and this trend will affect crop-management decisions such as those involving the seeding date and crop-variety choices. The warming trend varies spatially. The analysis of regional or local changes of climate is important for decision-making by the agricultural sector. Of course, the possible impact of climate change on agriculture is far more complicated than what the nine agroclimatic parameters can address here. For example, in addition to the change in the mean conditions of the climate, extreme weather events and the processes of moisture variation on the land-surface can also cause significant damage to agriculture. Our own and other's percentile analyses on daily precipitation have indicated that the increase of annual and growing season precipitation in Alberta is attributed to low-intensity events. Therefore, although there exists no hesitation for us to conclude that the warming climate and increased precipitation benefit agriculture in Alberta, more quantitative studies of the agroclimatic parameters based on many important factors, such as soil moisture, relative humidity and evapotranspiration, should be made in the future.

In addition, the data analysis method needs to be further improved. The errors in both the station data and the interpolated data need to be assessed more carefully despite the initial estimate of the interpolation errors by cross validation (Shen et al., 2001). Due to the over-smoothness of the interpolation results, the method used here that interpolates the climate normals and climate anomalies separately for the May-August precipitation total cannot be applied to either precipitation intensity studies or

frost conditions. An interpolation method needs to be developed to take care of both topographic elevation and climatic variance for temperature and precipitation.

Finally, the linear trend analysis can be subjected to further scrutiny. Although trends of increase or decrease are clearly demonstrated in Figs. 2.6b, c, d, and f, and less clear trends in Figs. 2.6a and 2.6e, the small correlations shown in Table 2.2 imply a small portion of the variance is explained by the linear regression. Regression with higher order polynomials or a finite Fourier series may be more meaningful in climate change analysis (Vinnikov et al., 2002). It is also worth exploring the application of the trend detection method that was developed to analyze the data from nonlinear and non-stationary processes.

Chapter 3

Statistical Analysis of Drought Indices and Alberta Drought Monitoring

3.1 Introduction

Recurring droughts in Alberta can seriously decrease crop yields and affect the whole Alberta agriculture industry. As a result of the drought events in Alberta such as those of the 1930s (so-called Dirty Thirties), the 1980s, 1990s, and 2000-2002, the Alberta government has implemented some soil-conservation and water-management programs to reduce the drought impact. Despite these existing irrigation programs, Alberta crops, particularly the spring wheat, are vulnerable to drought conditions. The 2001 drought made the Alberta yield lower than that of each of the 10 proceeding years, with the 2001 yield only 84% of the ten-year mean (Source: Agriculture Division, Statistics Canada). The 2000-2002 successive droughts in Alberta resulted in payments of over $1 billion Canadian dollars for farm assistance from the Alberta government and also in an Agriculture Drought Risk Management Plan for Alberta in 2002 (Source: Alberta Premier's web site). Hence, the proper assessment and prediction of drought severity and duration would be very helpful for reducing the effects of droughts on the Alberta agriculture industry. An effective drought-monitoring system and a reliable drought-monitoring scheme are urgently needed in

order to properly assess the drought severity and to predict future drought events and the duration of current droughts.

Hall et al. (2003) studied the history of agricultural droughts in Alberta. Their report includes records and anecdotes involving drought on the prairies during the 20th century. Although these data are valuable, if correct, for validating a drought-monitoring model, they do not provide a systematic assessment of the drought severity. Using dimensionless indices to classify drought conditions is still the most effective way to monitor moisture deficiency and the duration and intensity of a drought over an entire region. Many indices have been proposed. From the earlier indices that directly measure the rainfall deficiency to the more complicated Palmer Drought Severity Index, Surface Water Supply Index and Standardized Precipitation Index, drought indices have evolved slowly over the past several decades (Heim, 2002; Keyantash and Dracup, 2002). Although various drought indices exist, their applicability is specific for both purposes and regions. For example, the Palmer Index was designed specifically for semiarid and dry subhumid climates and did not take into account the contributions of snowmelt to surface water. (Snowmelt is common in Alberta.) Usually, meteorological drought-monitoring programs use the stations' observation data, but the non-uniform distribution of the stations makes the reliability questionable. It is advantageous to develop the drought indices according to the land areas with similar ecological and/or soil properties. This consideration motivated us to use the interpolated precipitation data of the Ecodistrict Polygons (EDP) for drought index-computing and monitoring. Shen et al. (2001) developed a hybrid method that interpolates the daily station precipitation data onto the EDPs. The interpolation

retains both the spatial and temporal variances of the original precipitation field. Specifically, it retains the precipitation frequency of a region over a given period, say, a month. This data set of daily EDP precipitation allows one to study the precipitation indices and the probability of a change from one drought condition to another at different time scales, ranging from a week to 36 months.

The work presented here is an integral part of the Alberta agriculture drought risk- management plan. The analysis of various types of drought indices will provide quantitative information on the severity of the drought conditions from a meteorological perspective. The analyzed information will be integrated into an operational system that monitors Alberta's agricultural drought. The system will help with the optimal management of the drought risks for Alberta agriculture.

In this research, we will analyze four kinds of meteorological drought indices commonly used to monitor the drought events, particularly the wheat drought, in Alberta: the standardized precipitation index (SPI), the rainfall anomaly index (RAI), the standardized anomaly index (SAI), and the rainfall decile index (RDI). The wheat-drought events in southern Alberta, ranked according to their strength in descending order, occurred in 2002, 2001, 2000, 1984, 1936, 1977, 1985, 1961, 1937, 1943, and 1931. The drought events of the "Dirty Thirties," the 1980s, and the consecutive three years from 2000 to 2002 are used to validate the applicability of the drought indices for drought assessment.

Furthermore, the drought classification of the four indices is carried out by using a percentile approach. This classification is based on the probability of

occurrence of the drought events and thus brings probabilistic features to the non-probabilistic indices.

The information about the transition of the drought conditions can help the farmers and decision-makers to be better prepared than they are currently. In addition to the real-time monitoring of the precipitation and soil moisture deficiency, incorporating into the drought monitoring system the probabilities of the transition from the historical data will also contribute to the performance of the monitoring system. To do so, this study analyzes the 1901-2000 weekly precipitation and calculates the probabilities of the transition of the drought condition from one week to another (e.g., from drought to normal).

3.2 Data

The data for 102 years of daily precipitation data from January 1, 1901 to December 31, 2002 are used for this study. The stations' observation data are interpolated onto 149 Alberta ecodistrict polygons (EDP). The interpolation method used is a hybrid of the methods of inverse-distance-weight and nearest-station-assignment developed by Shen et al. (2001). The interpolated daily data fit not only the climate mean but also the climate variability, in particular, the number of days with precipitation per month. This method also can reliably calculate the precipitation amount for a day over an EDP. For more details and accuracy of the dataset, the reader could refer to Section 2.2 in Chapter 2.

Alberta is divided into 10 ecoregions (Fig. 3.1) according to distinctive regional ecological characteristics including climate, physiography, vegetation, soil,

water and fauna. Each ecoregion contains a number of EDPs. Our indices analysis is conducted on the ecoregions and focuses especially on the southwest corner of Alberta.

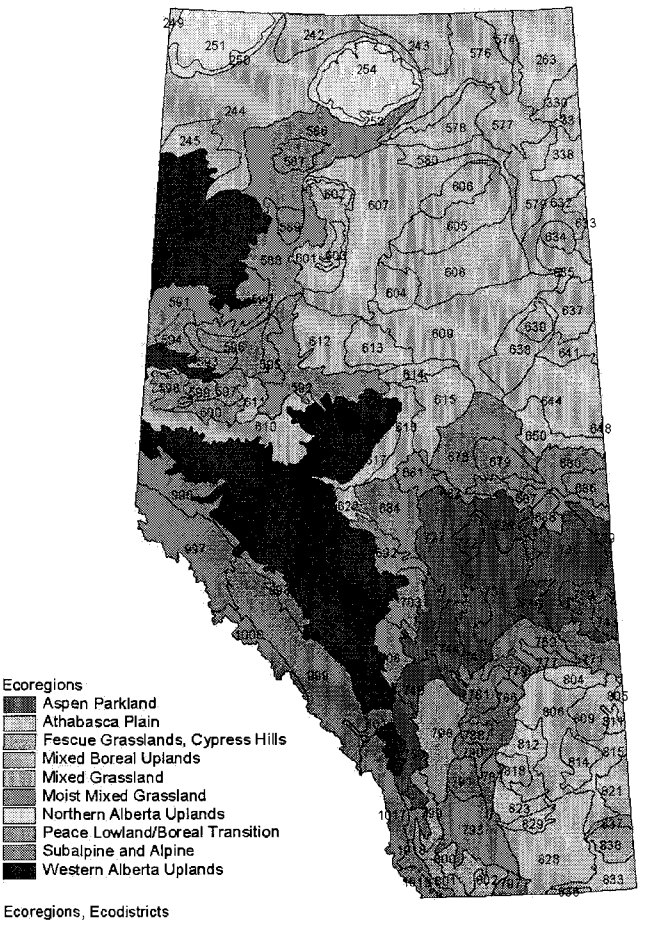

Figure 3.1. Alberta's ten ecoregions.

3.3 Some of the existing drought indices

(1) Standardized Precipitation Index (SPI)

Calculation of the SPI for any location is based on the long-term precipitation record for an objective period (3 months, 6 months, etc.). This long-term record is

fitted to a probability distribution, which is then transformed into a normal distribution so that the mean SPI for the location and desired period is zero.

The precipitation field is usually not a normal distribution, particularly for a short time scale. Various types of precipitation distributions have been used for different spatial regions and different time scales. The SPI is defined as the equivalence value of the accumulative probability in normal distribution (McKee et al., 1993)(Fig. 3.2). The computational procedure follows three steps. First, the precipitation time series data are fitted to a 2-parameter gamma distribution, whose two parameters are estimated by using the maximum likelihood method (Thom, 1958). The probability density function of the gamma distribution is

$$f(X \mid a,b) = \frac{1}{b^a \Gamma(a)} x^{a-1} e^{-\frac{x}{b}},$$

where $a(>0)$ is a shape parameter, $\beta(>0)$ is a scale parameter, and

$$\Gamma(a) = \int_0^\infty y^{a-1} e^{-y} dy$$

is the gamma function.

Second, after the estimation of the parameters, the probability of each precipitation observation can be calculated from the gamma distribution with the two parameters by using the gamma cumulative distribution function. The cumulative probability is given by

$$F(X \mid a,b) = \int_0^x f(t)dt = \frac{1}{b^a \Gamma(a)} \int_0^x t^{a-1} e^{-\frac{t}{b}} dt.$$

Because the precipitation total could be zero for some time scales, and the gamma function is undefined when $x = 0$, the cumulative probability could be revised as

$$H(x) = q + (1 - q)F(x),$$

where q is the probability of a zero. It can be estimated by $\frac{m}{n}$, where m is the number of zeros in the time series, and n is the total number of observations.

Finally, the inverse of the normal cumulative distribution function with mean $\mu = 0$ and variance $\sigma = 1$ at the corresponding probability can be calculated for each observation. These resulting values are the SPI's.

An important feature of this equi-probability transformation from one distribution to another distribution is that the probability of being less than a given value of a variate is the same as the probability of being less than the corresponding value of the transformed variate.

The SPI can produce not only monitoring information of index values but also the information of probability, percent of average, and precipitation deficit during a drought. Positive SPI values indicate greater than median precipitation, while negative values indicate less than median precipitation. The magnitude of departure from zero represents the probability of an occurrence so that decisions can be made based on this SPI. The precipitation used in the SPI can be used to calculate the precipitation deficit for the current period and to calculate the current percent of average precipitation for the time period under study (McKee et al., 1993; Hayes et al., 2000).

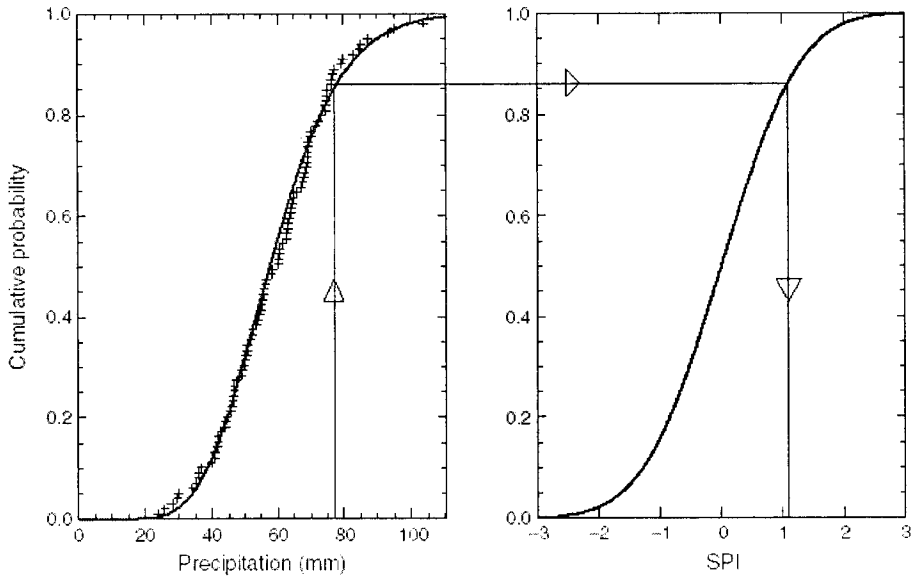

Figure 3.2. Schematic diagram of an equiprobability transformation from a fitted gamma distribution to the standard normal distribution (from Lloyd-Hughes and Saunder, 2002).

The SPI can be calculated for a variety of time scales and for different water variables such as soil moisture, ground water, snow-pack, reservoir, and streamflow. This feature allows the SPI to monitor both short-term and longer-term water resources. Since the precipitation data are transformed to a normal distribution, the SPI allows for comparison between different locations. Guttman (1998) compared the historical time series of the Palmer Drought Index with the time series of the corresponding SPI through spectral analysis and found that the SPI was spatially consistent (invariant) and easily interpreted.

Although the SPI has the strengths mentioned above, it also has some limitations. Hayes et al. (2000) stated that the SPI is only as good as the data used in

calculations. Before the SPI is applied to a specific region, knowledge of the climatology for that region is necessary. For short time scales, the SPI is similar to the percent of normal representation of precipitation, which can be misleading in regions with low seasonal precipitation totals. Guttman (1999) pointed out that at least 50 years of data are needed for drought periods of 1 year or less and that SPIs with time scales longer than 24 months may be unreliable.

The SPI is now used by the Colorado Climate Center, the Western Regional Climate Center, and the National Drought Mitigation Center of the United States to monitor drought conditions.

(2) Rainfall Anomaly Index (RAI)

The RAI was developed by van Rooy (1965). Although it is simple in terms of calculation, Oladipo (1985) concluded that RAI performed relatively equally in detecting meteorological drought periods by comparing to the more complicated Palmer drought index and Bhalme and Mooley drought index.

The positive and negative RAI indices are computed by using the mean of ten extremes. Let $\overline{M}$ be the mean of the ten highest precipitation records for the period under study, $\overline{P}$ the mean precipitation of all the records for the period, and P the precipitation for the specific year. Then the positive RAI (for positive anomalies) for that year is

$$RAI = 3\frac{P-\overline{P}}{\overline{M}-\overline{P}}.$$

Let $\overline{m}$ be the mean of the ten lowest precipitation records for the period under study. Then the negative RAI (for negative anomalies) for that year is

$$RAI = -3\frac{P - \overline{P}}{\overline{m} - \overline{P}}.$$

The classification of the index used by van Rooy (1965) is as follows.

RAI	Class description
≥ 3.00	Extremely wet
2.00 to 2.99	Very wet
1.00 to 1.99	Moderately wet
0.50 to 0.99	Slightly wet
0.49 to –0.49	Near normal
-0.50 to –0.99	Slightly dry
-1.00 to –1.99	Moderately dry
-2.00 to –2.99	Very dry
≤ -3.00	Extremely dry

(3) Rainfall Decile Index (RDI)

The RDI is defined by dividing the distribution of occurrences over a long-term precipitation record into sections for each ten percent of the distribution. Each of these categories is called a "decile." The first decile is the rainfall amount not exceeded by the lowest 10% of the precipitation occurrences. The second decile is the precipitation amount not exceeded by the lowest 20% of occurrences. The fifth decile is considered the median and is the precipitation amount not exceeded by 50% of the occurrences over the period of record (Hayes, 2000). The deciles are grouped into five classifications according to a decile's departure from the normal condition (Gibbs and Maher, 1967).

Deciles 1-2	lowest 20%	much below normal
Deciles 3-4	next lowest 20%	below normal
Deciles 5-6	middle 20%	near normal
Deciles 7-8	next highest 20%	above normal
Deciles 9-10	highest 20%	much above normal

A region is considered to be "drought affected" if the total precipitation of the preceding three months falls within the lowest decile of the historical distribution (Kinninmonth et al., 2000). The conditions end when either of the following happens:

1) The precipitation of the past month places the following three-month total in or above the fourth decile.

2) The total precipitation for the past three months is in or above the eighth decile.

The advantages of the RDI are that (1) it is simple to compute, and (2) it requires less data and fewer assumptions than the Palmer Drought Severity Index. Unlike the SPI, the RDI computation makes no assumption about the precipitation distribution. As Hayes (2000) and Keyantash and Dracup (2002) stated, however, the RDI has some limitations. It requires a long climatological record to calculate the deciles accurately. The two criteria to indicate the end of the "drought-affected" condition can lead to conceptual difficulties when the region under study has highly seasonal precipitation.

The RDI is used in the Australian Drought Watch System and appears to be very effective.

(4) Standardized Anomaly Index (SAI)

SAI is an index that was commonly used to monitor precipitation in drought-prone regions such as the West African Sahel and the Brazilian Northeast (Kraus, 1977; Katz and Glantz, 1986). In our research, the SAI is defined by

$$SAI(t) = \frac{1}{N}\sum_{i=1}^{N}\frac{R_i(t)-\mu_i}{\sigma_i},$$

where $R_i(t)$ denotes the precipitation for the i th EDP and t th year, μ_i is the long-term mean (i.e., the climatology) of $R_i(t)$, σ_i is the standard deviation of $R_i(t)$, and N denotes the total number of EDP polygons inside an ecoregion.

For the monthly time scale, a specific month has to be identified. The index is computed for this month, say, June. The $R_i(t)$ is the June total precipitation for the i th EDP from $t = 1901$ to $t = 2002$. The mean μ_i and standard deviation σ_i are the values specified for the June data. The June SAI has 102 values, one for each year from 1901 to 2002. An index curve can be drawn accordingly.

Katz and Glantz (1986) stated that the SAI is conceptually the conversion of the observed rainfall at a station into units, the number of standard deviations from the long-term station mean. In order to make comparisons of index values meaningful, it is desirable to have a fixed expected value and variance for an index. The SAI meets the first goal of possessing an expected value (i.e., zero) that is invariant under any changes in the locations on which the index is based, but it does not achieve the unit variance.

The SAI can be re-expressed as

$$SAI(t) = c + \frac{1}{N}\sum_{i=1}^{N} w_i R_i(t),$$

where $w_i = 1/\sigma$ and c is a constant given by

$$c = -\frac{1}{N}\sum_{i=1}^{N} \frac{\mu_i}{\sigma}.$$

Thus, the SAI can be viewed as a weighted average or linear combination of the rainfall for the N polygons, with the weights being inversely proportional to the station's standard deviations. Because sites with higher mean rainfall tend to also have higher standard deviations, the SAI results in weighting the drier sites more than the wetter ones (Katz and Glantz, 1986).

3.4 Wheat drought in Canada's Palliser Triangle

The Palliser Triangle is part of the Northern Great Plains and covers southern Alberta, southern Saskatchewan and northern Montana. Because of the barrier provided by the Rockies, the moisture flow from the Pacific Ocean is lifted and cooled, resulting in the dry air mass in southern Alberta (PFRA, 1998). This semi-arid prairie region was called the northern extension of the notorious "Great American Desert" by Captain John Palliser, a British explorer after whom the "Palliser Triangle" was named. In drought years, wheat yields are very sensitive to low antecedent moisture reserves, below average rainfall in the crop-growing season, summer heat waves, and hot dry winds. Using a water-budget approach to estimate the wheat yield, Williams (PFRA, 1998) mapped the areal extent of 26 annual wheat droughts occurring from 1929 to 1980 in Canada. Six of these drought areas, plus those of 1984 and 1985, are outlined in Fig. 3.3. These years can be used to validate whether the

indices mentioned in the previous section can be applied in the Palliser Triangle region. Thus, the four indices (SPI, RAI, SAI, RDI) are calculated by using the May to August precipitation for the Mixed Grassland ecoregion in the southwest corner of Alberta.

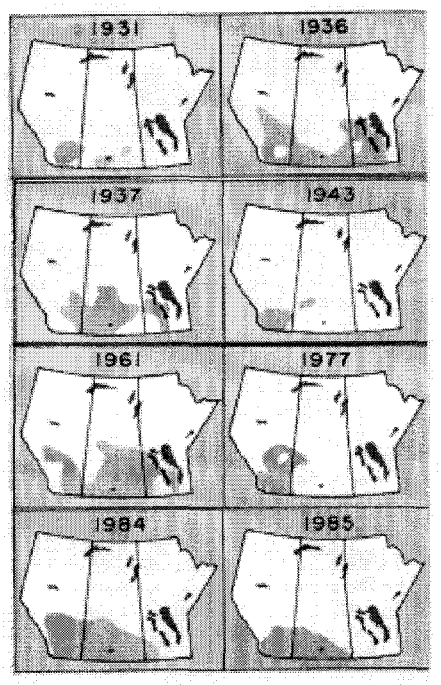

Figure 3.3. Historic Prairie wheat drought areas (from PFRA, 1998).

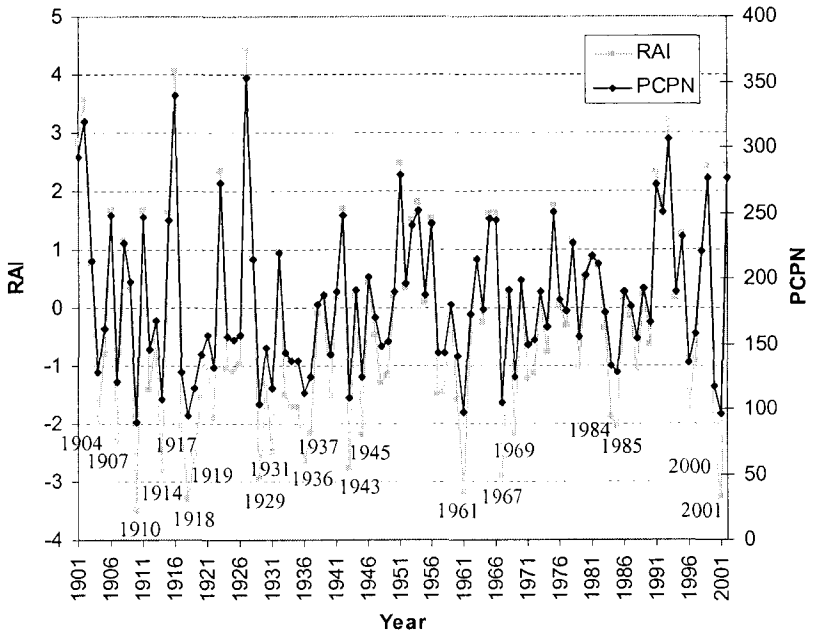

Figure 3.4. May to August precipitation from 1901 to 2002 and corresponding RAI over the Mixed Grassland region.

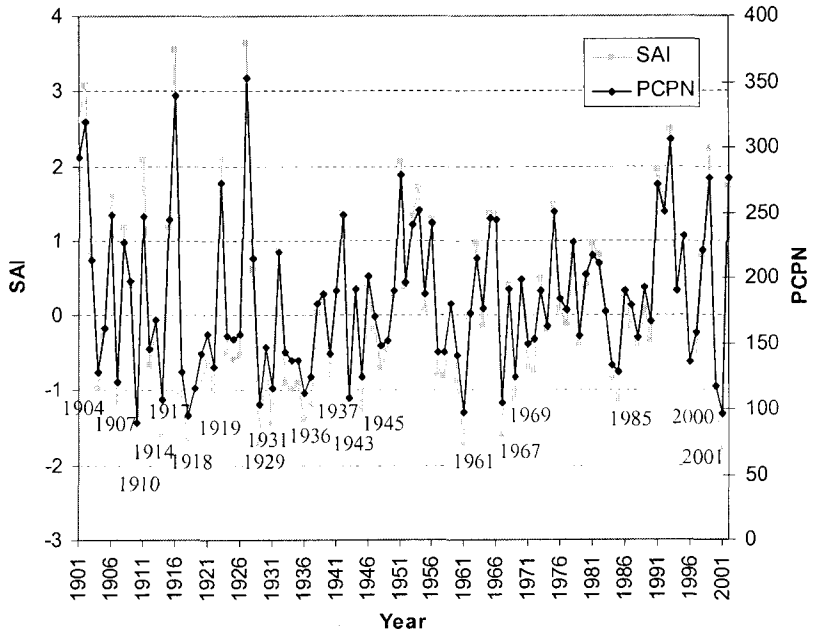

Figure 3.5. May to August precipitation from 1901 to 2002 and corresponding SAI over the Mixed Grassland region.

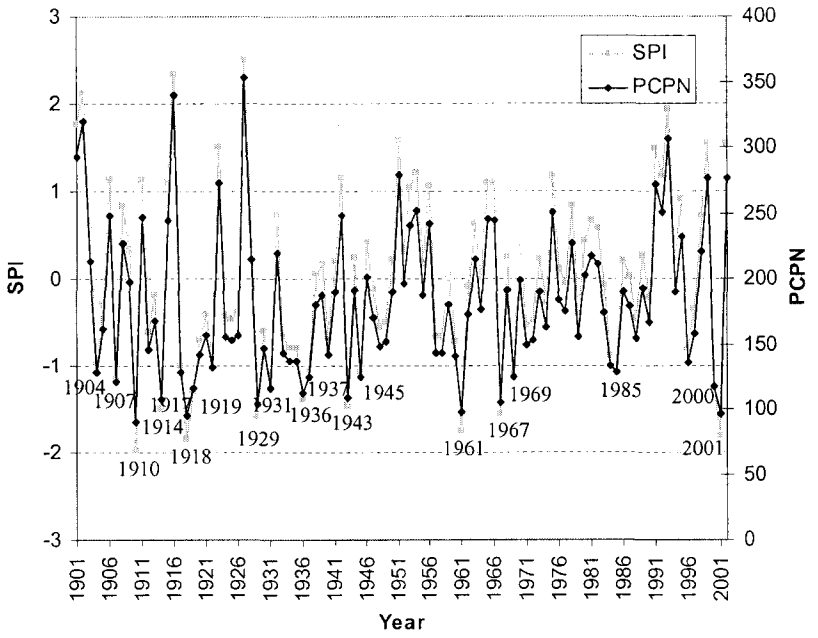

Figure 3.6. May to August precipitation from 1901 to 2002 and corresponding SPI over the Mixed Grassland region.

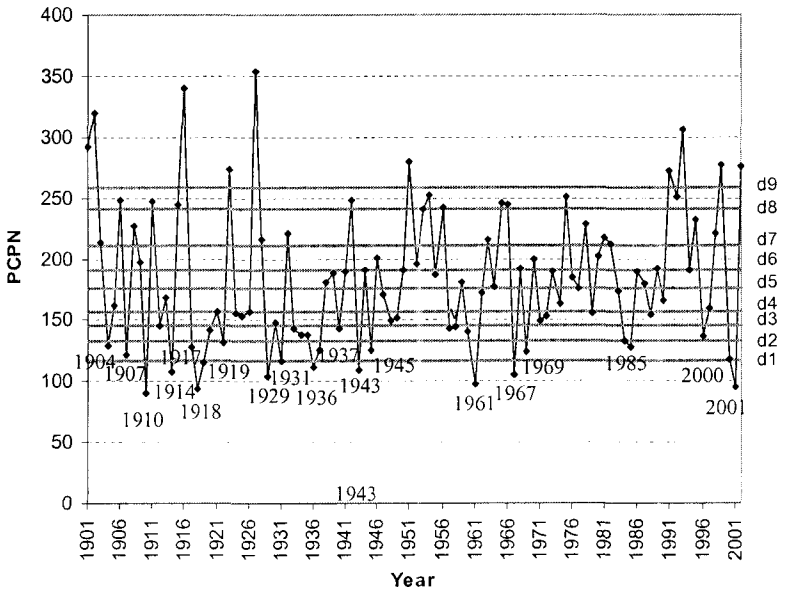

Figure 3.7. Rainfall Decile Index and precipitation (the black curve represents precipitation, and the gray straight lines represent deciles).

Figures 3.4-3.6 demonstrate the comparison of the RAI, SAI and SPI indices in terms of the precipitation over the Mixed Grassland ecoregion. The figures show that the indices captured the drought events of 1931, 1936, 1937, 1943, 1961, 1985, 2000 and 2001. The Rainfall Decile Index (Fig. 3.7) also captured those drought events. The years with precipitations below the d2 line are the years with "much below normal" precipitation.

3.5 Interpreting drought by probability of occurrence

Although the indices in Section 3.4 showed a similar ability to indicate the drought events, their drought classifications are different in scale, and their relevance to drought impacts are not clear and, thus, not comparable. In this study, a common drought category is used for all the indices to describe the drought condition of an area for a particular year. The drought classification adopted is the Drought Severity Classification, currently in use by the US Drought Monitor, administered by the NOAA National Climatic Data Center (Svoboda et al., 2000). The drought classification consists of numerical ratings of 0 to 4. The wet conditions are also classified with three classifications, which have opposite signs of the drought indices. The drought classification is made according to three factors: the extent of crop/pasture loss, current fire risk, and the water supply in the area.

Exceptional Drought, denoted by D4, is characterized by exceptional and widespread crop/pasture losses, exceptional fire risk, and shortages of water in reservoirs, streams, and wells creating water emergencies. Extreme Drought, denoted

by D3, is classified by major crop/pasture losses, extreme fire danger, and widespread water shortages or restrictions. Severe Drought, denoted by D2, occurs when crop/pasture losses are likely, the fire risk is high, water shortages are common, and water restrictions are imposed. Moderate Drought, denoted by D1, is characterized by some damage to crops and pastures, a high fire risk, with streams, reservoirs, and wells low or some water shortages developing or imminent, and voluntary water use restrictions requested. Abnormally dry, denoted by D0, is the condition in a period for a region either going into drought or coming out of drought. Going into drought is characterized by short-term dryness, slowing planting and growth of crops or pastures, and above average fire risk; coming out of drought is characterized by lingering water deficits and pastures/crops not fully recovered.

The additions to this classifications system are -D1 to -D3, where -D1 denotes a normal precipitation condition, where there is enough moisture and sunlight for crops, little fire risk, and reservoirs and wells have adequate supplies. -D2 represents an abnormal amount of precipitation for the period, more than enough for crops, a low-to-none fire risk, and full reservoirs and wells. -D3 indicates a severe amount of precipitation, such as floods, or torrential downpours, possibly too much for crops, no fire risk, and possible overflowing of reservoirs.

Once the conceptual drought classification is defined, another important topic to address is the threshold for drought categories, i.e., the drought triggers. Our principal basis for the drought threshold is the probability of occurrence. The exceptional drought D4 is defined as an event once in 50 years; extreme drought D3 once in 20 years; severe drought D2 once in 10 years; moderate drought D1 once in 5

years; and abnormally dry D0 once in 3 years. Because of this basis, the probability-based drought indices are easy to use for drought interpretation. Of the four indices introduced in Section 3.4, only the SPI and RDI take into account the probability of occurrence. The classification of the other indices, RAI and SAI, are either arbitrary or not clear at all. This section will analyze all the drought indices in the probability sense and develop methods for calculating the threshold values when an index is not probability-based.

The percentile-based indices, such as indices using the percent of normal precipitation, are explicit probability-based indices and do not need further clarification. However, the probability-based SPI still needs a drought classification. SPI is calculated from fitting a probability distribution model and being compared for the equivalent probability with a standard normal distribution. The fitting part is often problematic and the major source of error. Our probability interpretation of the SPI trigger is displayed in Table 3.1. The threshold values in the table correspond to the z values of a normal distribution. For example, for a percentile trigger 10%, the z value found from the normal distribution (mean zero and standard deviation one) gives –1.28. The threshold value for D3 is then –1.3 (rounded to the one decimal place), and the probability of occurrence is the probability of z smaller than or equal to –1.3, which is 9.7%.

When McKee et al. originally developed the SPI in 1993, they classified the drought intensity differently (Table 3.2.)

Table 3.1. SPI probability for drought interpretation

Category	Threshold Values	Probability of Occurrence	Event Frequency	Percentile Trigger
D0	-0.5 to –0.7	30.9%	Once in 3 years	21-30%
D1	-0.8 to –1.2	21.2%	Once in 5 years	11-20%
D2	-1.3 to –1.5	9.7%	Once in 10 years	6-10%
D3	-1.6 to –1.9	5.5%	Once in 20 years	3-5%
D4	-2.0 to - ∞	2.3%	Once in 50 years	0-2%

Table 3.2. Original SPI classification used by McKee

SPI Value	Probability of Occurrence	Drought Category
0 to –0.99	50.0%	mild drought
-1.00 to –1.49	15.9%	moderate drought
-1.50 to –1.99	6.7%	severe drought
≤ -2.00	2.3%	extreme drought

Table 3.3. The threshold values of drought classification for the growing season in the entire Alberta agricultural region

Category	Threshold Values		
	RAI	SAI	PCPN (mm)
D0	-0.9 to -1.5	-0.5 to -0.7	217.3 to 199.0
D1	-1.6 to -2.1	-0.8 to -1.0	198.9 to 184.9
D2	-2.2 to -2.7	-1.1 to -1.2	184.8 to 170.9
D3	-2.8 to -3.6	-1.3 to -1.5	170.8 to 149.4
D4	-3.7 to -∞	-1.6 to -∞	149.3 to 0

Table 3.4. The threshold values of drought classification for the growing season in the Mixed Grassland region

Category	Threshold Values		
	RAI	SAI	PCPN (mm)
D0	-1.4 to -1.8	-0.7 to -0.9	145.9 to 133.1
D1	-1.9 to -2.4	-1.0 to -1.2	133.0 to 116.2
D2	-2.5 to -2.8	-1.3 to -1.5	116.1 to 104.8
D3	-2.9 to -3.2	-1.6 to -1.7	104.7 to 95.4
D4	-3.3 to -∞	-1.8 to -∞	95.3 to 0

To make all the indices comparable, the threshold values for RAI and SAI are calculated according to the percentile trigger of SPI. That is, the second, fifth, tenth, twentieth, and thirtieth percentiles are used as the threshold values. Tables 3.3 and 3.4 give the threshold values of each of the indices for the Mixed Grassland region and the entire Alberta agricultural region (including the Peace Lowland, Boreal Transition, Moist Mixed Grassland, Aspen Parkland, Fescue Grassland and Mixed Grassland) for the growing season (i.e., from May to August.)

The results show differences in the threshold values for different regions, especially the SAI. This difference indicates the regional variance of the indices, so that a category suitable for one region may not work well for another.

The range of RAI values is

$$(-3\frac{P_m - \overline{P}}{\overline{m} - \overline{P}}, 3\frac{P_M - \overline{P}}{\overline{M} - \overline{P}}),$$

where P_M and P_m are the maximum and minimum precipitations. However, calculating $\overline{M}$ from the ten largest precipitation values and $\overline{m}$ from the ten smallest precipitation values appears arbitrary. Van Rooy (1965) chose 10 because he thought the average of 10 extremes could represent the mean conditions of an extremely dry year or an extremely wet year. In our study, we consider an event once in 50 years as an exceptional drought (D4) and an event once in 20 years as an extreme drought (D3). Therefore, we suggest that $\overline{M}$ be the mean of the top 5% precipitation records and $\overline{m}$ be the mean of the bottom 5% precipitation records. When P reaches $\overline{m}$, the index will reach –3.0. If 102 years of data are used, then $\overline{M}$ is the mean of the largest 5 values. Similarly, $\overline{m}$ is the mean of the smallest 5 values. Tables 3.5 and 3.6 give

the comparison of the threshold values for the two different RAIs. RAI_{10} uses the average of the 10 maximum or minimum records as the mean extrema, and RAI_5 uses the 5 maximum or minimum records.

Table 3.5. The threshold values of different RAIs for the growing season in the entire Alberta agricultural region

Category	Threshold Values	
	RAI_{10}	RAI_5
D0	-0.9 to -1.5	-0.8 to -1.3
D1	-1.6 to -2.1	-1.4 to -1.9
D2	-2.2 to -2.7	-2.0 to -2.4
D3	-2.8 to -3.6	-2.5 to -3.2
D4	-3.7 to -∞	-3.3 to -∞

Table 3.6. The threshold values of different RAIs for the growing season in the Mixed Grassland region

Category	Threshold Values	
	RAI_{10}	RAI_5
D0	-1.4 to -1.8	-1.3 to -1.6
D1	-1.9 to -2.4	-1.7 to -2.2
D2	-2.5 to -2.8	-2.3 to -2.6
D3	-2.9 to -3.2	-2.7 to -2.9
D4	-3.3 to -∞	-3.0 to -∞

3.6 Probability transition of drought conditions

Drought preparedness is an integral part of an effective drought-monitoring system. The knowledge of the probabilities of the transition of one drought condition to another will provide practical information for the drought-monitoring system and drought risk management to ensure that effective actions can be taken before a drought crisis, farmers will be more prepared and less vulnerable to drought, drought impacts can be reduced through planning and preparedness.

The drought-wet condition of the weekly precipitation for an EDP is divided into 5 categories according to percentiles of precipitation: extremely dry (0-20 percentile), dry (21-40 percentile), normal (41-60 percentile), wet (61-80 percentile), and extremely wet (81-100 percentile). The probability of the transition from one drought category this week to another in the next week is illustrated in Fig. 3.8.

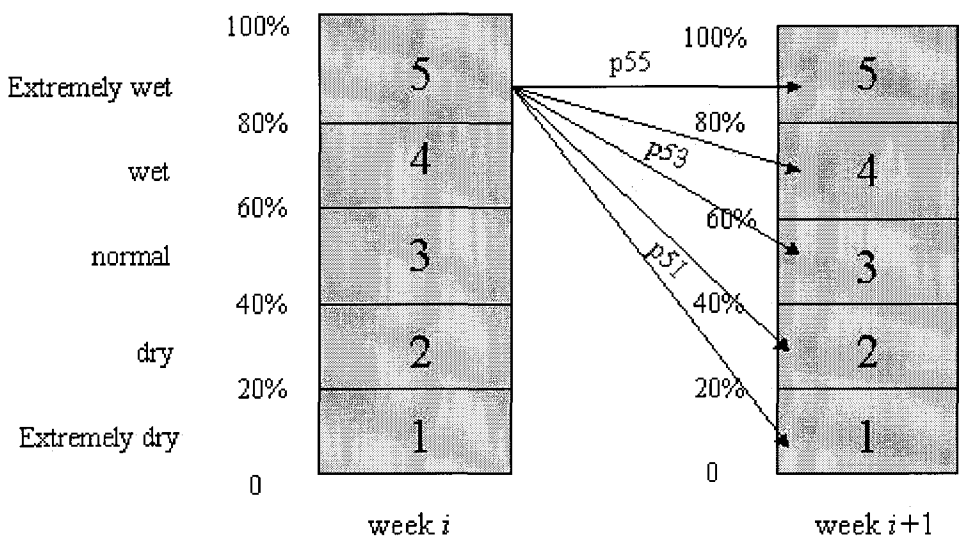

Figure 3.8. The illustration of the probability of the transition of weekly precipitation.

For week i, the 1901 to 2000 weekly total precipitations are classified into the five categories. Each category will have twenty years of precipitation. The twenty years in one category, say 5, of week i will fall into one of the categories in week $i+1$. The probabilities of the transition from category 5 in week i to the category 1~5 in week $i+1$ are denoted by $P_{51}, P_{52}, \cdots, P_{55}$. If the number of years transited from category 5 to category 1 is three, then $P_{51} = 3/20$. Since the sample size is small if only 20 years are used to calculate the probability transition, the probabilities are calculated for ecoregions instead of single EDPs. For an ecoregion, the number of years transited from one category to another is the sum of the corresponding number for each EDP in the ecoregion and the probability is then the ratio of the total number of years transited to the total number of years in the category (the multiplication of 20 and the number of EDPs).

Figures 3.8-3.9 give the probability transition of the wet-to-dry condition and dry to wet condition for the Mixed Grassland ecoregion. The chance of transition from normal to extremely dry is the highest in May. The chance of transition from normal to dry is the highest in the beginning of January, end of April, and middle of June. The transition of dry to extremely dry will most probably occur in January, April, the end of August, and the beginning of September. The transition of the extremely wet to the normal condition will most probably occur in the beginning and end of September. The middle of June and the middle of August are the periods when the recovery from the extremely dry to the normal condition will most probably occur. The alleviation from the extremely dry to the dry condition will most probably occur in the middle of February and late July. The chance of transition from dry to normal

is highest in the middle of February, the middle of May, and the middle of August. Apparently, the transitions from-dry-to-wet and from-wet-to-dry are asymmetric.

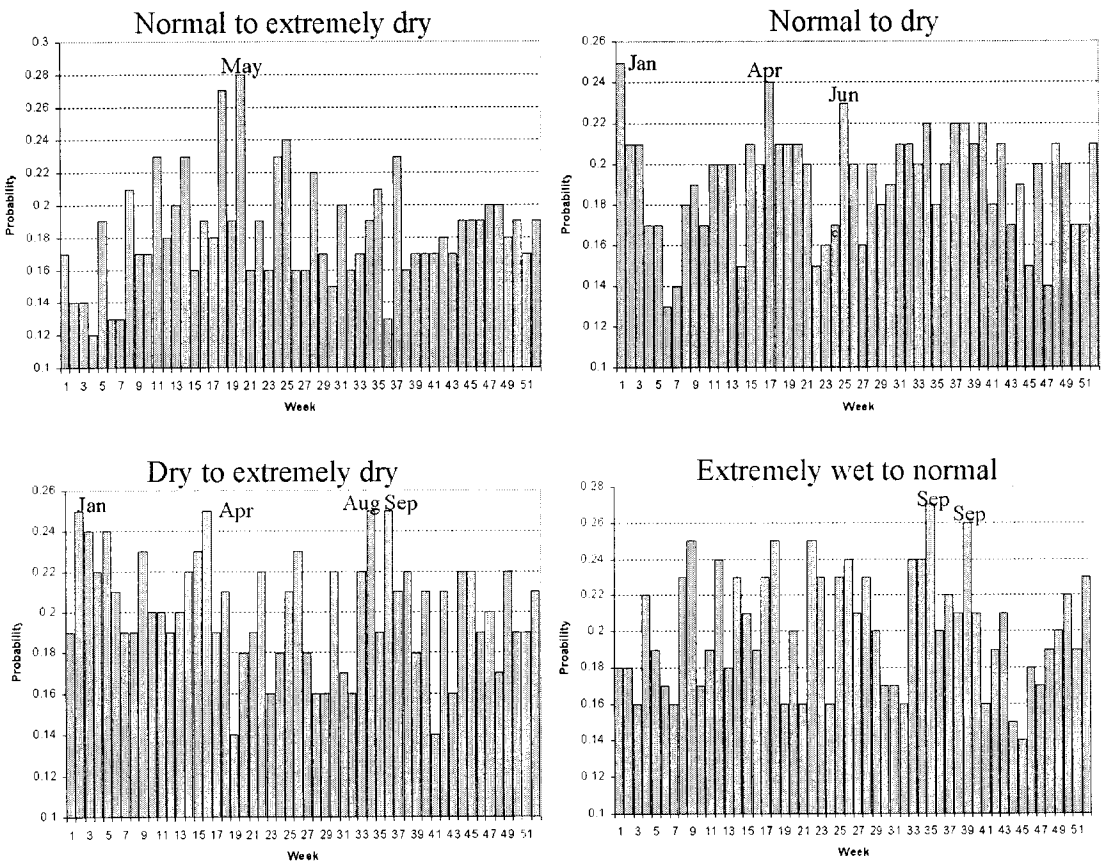

Figure 3.9. The wet-to-dry probability transition for Mixed Grassland.

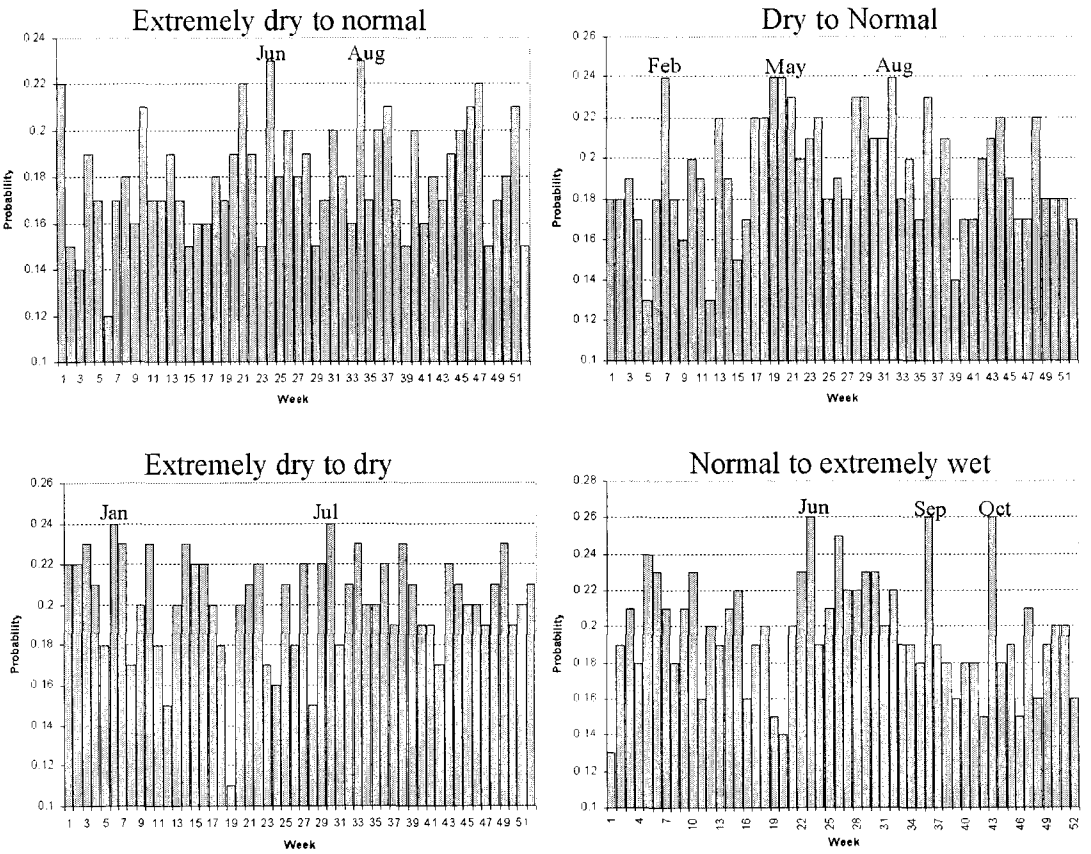

Figure 3.10. The dry-to-wet probability transition for the Mixed Grassland region.

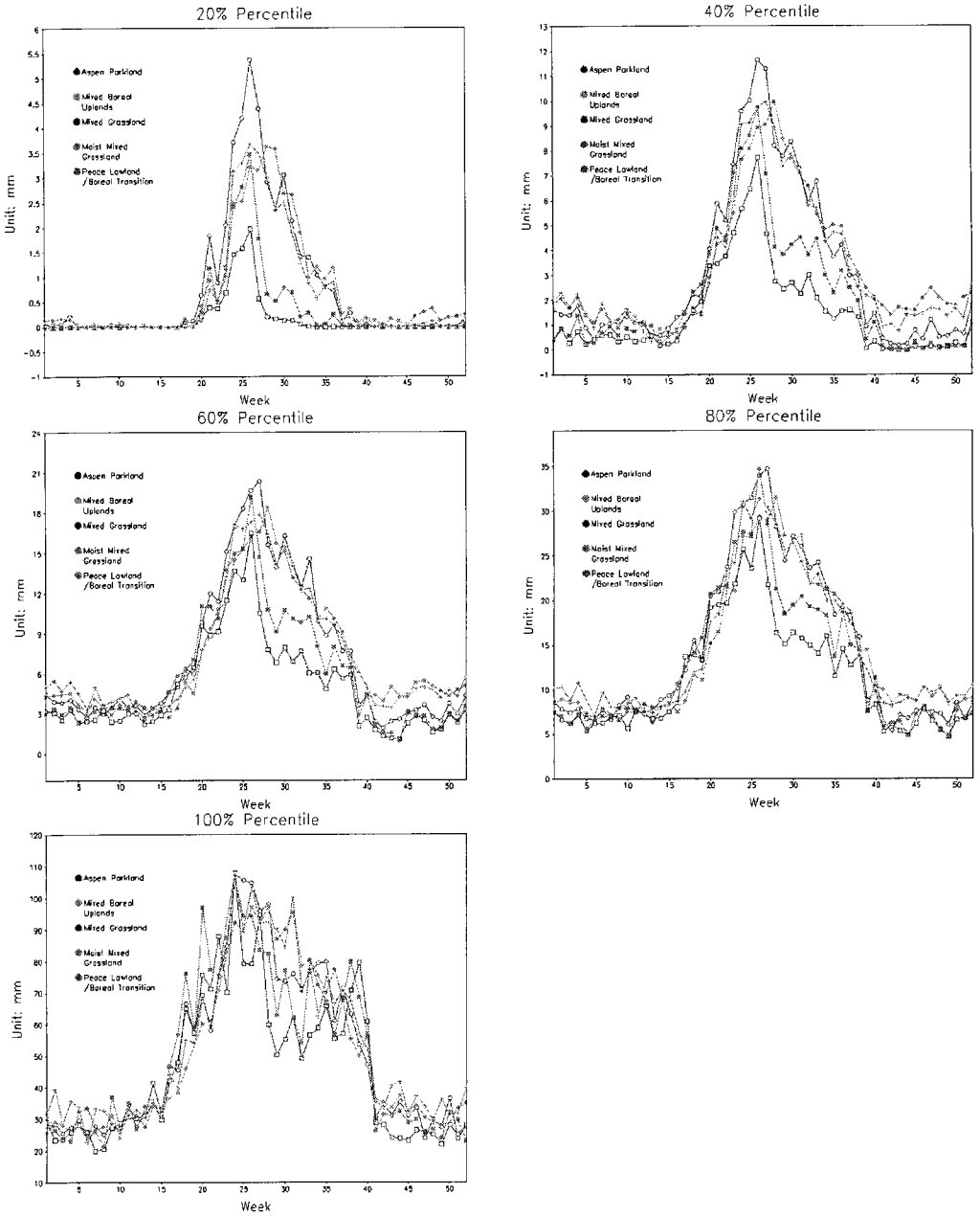

Figure 3.11. The 20% to 100% percentiles for five of the ecoregions.

Figure 3.11 demonstrates the averaged 20, 40, 60, 80, and 100 percentiles for five ecoregions: Aspen Parkland, Mixed Boreal Uplands, Mixed Grassland, Moist Mixed Grassland and Peace lowland/Boreal transition. The much lower 20 percentile in the Mixed Grassland ecoregion indicates that the region has the lowest precipitation among the five ecoregions and thus is the driest region in Alberta. However, the intensities of the heavy precipitation events (100 percentiles) for those regions are similar.

3.7 Summary and discussion

Four meteorological drought indices have been investigated in this chapter. The numerical results over the Mixed Grassland ecoregion show that these four indices can capture most of the drought events of Alberta in the 102-year (1901-2002) period. In the future, further studies are needed to compare the performance of the drought indices for various time scales, for instance, 1 week, 2 weeks, or 1 month.

Although the above drought indices behave similarly in detecting drought events, their drought classifications are different in scale. To solve this problem, we adopted a common drought category for all the indices to describe the drought condition of an area for a particular year. In addition, the thresholds for each drought category were derived by using the concept of probability of occurrence. This approach uses percentiles as drought triggers and allows the different indices' classification of the drought events to be compared with each other. By using this approach, the threshold values for the SPI, RAI and SAI are derived for the Mixed Grassland region and the Alberta agricultural region as a whole. The results indicate

the regional variance of the thresholds. Therefore, one should be cautious when applying a drought category to different regions since a category suitable for one region may not work well for another.

In order to provide practical information for the drought-monitoring system and drought risk management, the probability transition of the weekly precipitation was calculated. It was found that for the Mixed Grassland region, the chance of transition from normal to extremely dry is the highest in the middle of May. The chance of transition from normal to dry is the highest in early January, late April, and the middle of June. The transition from dry to extremely dry most probably occurs in January, April, late August and early September. The transition from an extremely dry condition to normal most probably occurs in the middle of June and the middle of August. Nevertheless, the robustness of the probability transition needs further investigation.

As mentioned before, snowmelt is an important source of water in Alberta. Snowmelt is related to the temperature, which should also be considered when analyzing precipitation deficit. However, determining if the water supply due to snowmelt is from the current year or from the year before is difficult, so how to relate the temperature to the snowmelt still needs investigation. This statement leads to a question: why use meteorological drought indices? Although drought indices in the Palmer class contain various types of information including precipitation, stream flow, and soil wetness, the complicated parameter estimation in the index calculation often makes the index insensitive to the drought conditions. On the other hand, the meteorological indices are appropriate for reflecting the balance of the water content

of the agricultural soil when the meteorological data are sufficiently accurate. Our study takes advantage of the long-term meteorological dataset that was obtained from optimal interpolation (Shen et al., 2001). However, the accuracy of the dataset for the mountainous regions is still questionable and needs further investigation.

Chapter 4

PPCI as a Drought Indicator

4.1 Introduction

This chapter introduces a new drought-monitoring index — the probabilistic principal component index (PPCI). Various kinds of indices are available for monitoring droughts around the world. Depending on the climatic, agricultural, and ecological properties of a region, one or more indices are chosen to be its drought indicators. The most commonly used drought indices are the Standardized Precipitation Index (SPI, Mckee et al., 1993, 1995) and the Palmer Drought Severity Index (PDSI, Palmer, 1965). The SPI is a probabilistic index and is hence applicable to any region. However, the SPI does not contain the rich physical content that the PDSI does. Neither does the SPI reflect the space-time structure of the precipitation field. The PDSI takes into account the rainfall, potential evapotranspiration, antecedent soil moisture, and runoff. But despite its rich meteorological and hydrological contents, the PDSI can be difficult to use because of its empirical method for calculating the weighting factor and the need to adjust the regional correction factor. Furthermore, the threshold values for the drought categories D0-D4 can vary from one region to the other, and determining the range of the PDSI values is

very difficult. Thus, the physically sound index, the PDSI, cannot be easily used to infer a drought category.

In order to provide a drought indicator that is both physical and probabilistic, this chapter proposes a new index, which can reflect the space-time structure of the precipitation field as well as the probability of the drought occurrence. This new index is essentially a conversion of the so-called principal component index (PCI) into the probabilistic PCI, referred to as the PPCI. The PCI is the precipitation field's first principal component obtained through principal component analysis, or empirical orthogonal function (EOF) analysis. Since the PCI is highly correlated to the spatial average of the precipitation (as is proven in Section 4.3), and provides more physical content than the simple spatial average, the PCI may be used as a new, or perhaps very reliable, drought indicator over a region. Another advantage of using the PCI to indicate drought occurrence is that the EOFs can reflect the spatial patterns of the variability and thus can be used to quantitatively assess the drought risk over a region. To make this physically sound index probabilistic, an equi-probability transformation is conducted similar to the calculations performed with the SPI. The difference is that SPI needs to fit the precipitation to a gamma distribution and then calculate the cumulative probability, while our PPCI calculation method uses the empirical cumulative probability directly to find the corresponding Z value from the normal distribution. A smoothing spline approach is used to fit the cumulative probability into the PCI-PPCI transformation.

4.2 Principal component index (PCI)

The PCI is defined as the coefficient of the first empirical orthogonal function (EOF) when data are decomposed into a product of the spatial components (i.e., EOFs) and the temporal components (i.e., the principal components, or the PCs). The precipitation anomaly data are denoted by $a_i(t) = R_i(t) - \mu_i$, where μ_i is the climate normal for the location i, $a_i(t)$ denotes the precipitation anomaly for the location i at time t, and $i = 1,2,\cdots,N$ and $t = 1,2,\cdots,T$. The $N \times T$ data matrix A is

$$A = \begin{bmatrix} a_1(1) & a_1(2) & \cdots & a_1(T) \\ a_2(1) & \cdots & \cdots & a_2(T) \\ \cdots & \cdots & \cdots & \cdots \\ a_N(1) & \cdots & \cdots & a_N(T) \end{bmatrix}.$$

The matrix A can be decomposed into

$$A = EP, \tag{4.1}$$

where E is the $N \times N$ EOF matrix

$$E = \begin{bmatrix} e_1(1) & e_2(1) & \cdots & e_N(1) \\ e_1(2) & \cdots & \cdots & \cdots \\ \cdots & \cdots & \cdots & \cdots \\ e_1(N) & e_2(N) & \cdots & e_N(N) \end{bmatrix},$$

and P is the $N \times T$ PC matrix

$$P = \begin{bmatrix} p_1(1) & p_1(2) & \cdots & p_1(T) \\ p_2(1) & \cdots & \cdots & p_2(T) \\ \cdots & \cdots & \cdots & \cdots \\ p_N(1) & \cdots & \cdots & p_N(T) \end{bmatrix}.$$

The E and P have the following orthogonality properties,

$$E_k' E_l = \sum_{i=1}^{N} e_k(i) e_l(i) = \delta_{kl}, \tag{4.2}$$

$$P_k P_l' = \sum_{j=1}^{T} p_k(j) p_l(j) = \lambda_k \delta_{kl}, \tag{4.3}$$

where δ_{kl} is the Kroneker delta that is equal to *1* when $k=l$ and 0 otherwise, and λ_k is the eigenvalue, paired with the eigenvector, of the covariance matrix

$$C = AA'. \tag{4.4}$$

In the above, the prime indicates the transpose of a matrix. Therefore, the principal components can be expressed as

$$P = E'A. \tag{4.5}$$

The k th PC is

$$P_k(t) = \sum_{i=1}^{N} a_i(t) e_k(i). \tag{4.6}$$

The first principal component PCI1 (or P_1) is used as the drought index.

4.3 PCI and its correlation with the average precipitation

Since the first EOF mode can usually explain a large percentage of the variance of a stochastic field, it is expected that the first PC, which is defined as the PCI, will be highly correlated with the spatial average of the field. Let $\bar{A}$ denote the spatial average of the field and P_1 the first PC. Their correlation can be expressed by the following formula,

$$Corr(\bar{A}, P_1) = \frac{Cov(\bar{E}_{1\times N} P_{N\times T}, [P_1]_{T\times 1})}{\sqrt{\|\bar{A}\|^2}\sqrt{\|P_1\|^2}} = \frac{1}{\sqrt{1+\sum_{n=2}^{N}(\lambda_n/\lambda_1)(\bar{e}_n/\bar{e}_1)^2}}, \tag{4.7}$$

where $E_{N\times N}$ is the orthogonal EOF matrix, and $\bar{E}_{1\times N}$ is the spatial average of the EOF matrix. The derivation of Eq. (4.7) is as follows. Let

$$\bar{A}_{1\times T} = \left[\sum_{j=1}^{N} a(j,t)/N\right]_{1\times T}$$

be the spatial average of the anomaly field, and

$$P_1 = \left[P_1(t)\right]_{1\times T}$$

be the PCI. Their covariance is

$$Cov(\bar{A}, P_1) = Cov(\bar{E}_{1\times N}P_{N\times T}, [P_1]_{T\times 1}) = \bar{E}_{1\times N}P_{N\times T}[P_1]_{T\times 1} = \bar{e}_1\left\|P_1\right\|^2 = \bar{e}_1\lambda_1, \qquad (4.8)$$

where

$$\bar{e}_1 = \sum_{j=1}^{N} e_1(j)$$

is the spatial average of the first EOF, and $\bar{e}_n$ is, similarly, the spatial average of the nth EOF. The variance of the averaged data is

$$\left\|\bar{A}\right\|^2 = \bar{E}P(\bar{E}P)' = \bar{E}PP'\bar{E}' = \bar{E}\Lambda\bar{E}' = \sum_{n=1}^{N}\lambda_n\bar{e}_n^{\,2}. \qquad (4.9)$$

The variance of PC1 is λ_1. Thus, the correlation between the average precipitation and the first principal component is

$$Corr(\bar{A}, P_1) = \frac{Cov(\bar{E}_{1\times N}P_{N\times T}, [P_1]_{T\times 1})}{\sqrt{\left\|\bar{A}\right\|^2}\sqrt{\left\|P_1\right\|^2}} = \frac{\bar{e}_1\lambda_1}{\sqrt{\sum_{n=1}^{N}\lambda_n\bar{e}_n^{\,2}}\sqrt{\lambda_1}} = \frac{1}{\sqrt{1+\sum_{n=2}^{N}(\lambda_n/\lambda_1)(\bar{e}_n/\bar{e}_1)^2}}$$

.

Usually, this value is very close to one since $(\bar{e}_n/\bar{e}_1)^2$ is very small. The reason is as follows. Since the covariance matrix C is symmetric and positive definite, every

entry of the first EOF has the same sign, say, positive. The second EOF will have a zero-crossing, so that half of the entries will have opposite signs to the other half. Similarly, the *n*th EOF will have $n-1$ zero-crossings. The sum of the first EOF entries is positive, while the sum of the entries of an EOF of a higher order will have a small absolute value. Even in many cases, $\bar{e}_n$ is almost or exactly equal to zero when $n \geq 2$. Then the correlation is almost or strictly equal to one.

One can also derive a similar formula for a spatially continuous field $R(\vec{x},t)$. This field can be decomposed as an infinite sum of EOFs,

$$R(\vec{x},t) = \sum_{n=1}^{\infty} R_n(t)\psi_n(\vec{x}),$$

where $\psi_n(\vec{x})$ are the EOFs and $R_n(t)$ are the principal components. The spatial average of the *R* field is

$$\bar{R}(t) = \frac{1}{\|\Omega\|}\int_{\Omega} R(\vec{x},t)d\Omega = \sum_{n=1}^{\infty} R_n(t)\bar{\psi}_n, \tag{4.10}$$

where Ω is the domain of the field *R*, and $\|\Omega\|$ is the area of the domain, and $\bar{\psi}_n$ is the spatial average of the *n*th EOF defined as

$$\bar{\psi}_n = \frac{1}{\|\Omega\|}\int_{\Omega} \psi_n(\vec{x})d\Omega. \tag{4.11}$$

The covariance between $\bar{R}$ and R_1 is

$$Cov(\bar{R},R_1) = \sum_{n=1}^{\infty} Cov(R_n(t),R_1(t))\bar{\psi}_n = \|R_1\|^2 \bar{\psi}_1 = \lambda_1\bar{\psi}_1. \tag{4.12}$$

The variance of the *R* field's average is

$$Var(\bar{R}^2) = \sum_{m,n=1}^{\infty} R_m' R_n \bar{\psi}_m \bar{\psi}_n = \sum_{n=1}^{\infty} \lambda_n \bar{\psi}_n^{\,2}. \tag{4.13}$$

The variance of R_1 is λ_1. Thus, the correlation between $\bar{R}$ and R_1 is

$$Corr(\bar{R}, R_1) = \frac{Cov(\bar{R}, R_1)}{\sqrt{Var(\bar{R})}\sqrt{Var(R_1)}} = \frac{\lambda_1 \bar{\psi}_1}{\sqrt{\sum_{n=1}^{\infty} \lambda_n \bar{\psi}_n^{\,2}}\sqrt{\lambda_1}} = \frac{1}{\sqrt{1 + \sum_{n=2}^{\infty} (\lambda_n / \lambda_1)(\bar{\psi}_n / \bar{\psi}_1)^2}}. \tag{4.14}$$

Usually, $(\bar{\psi}_n / \bar{\psi}_1)^2$ is very small and sometimes equal to zero strictly when $n \geq 2$. Thus, the correlation is again close to or exactly equal to one.

Because of this high correlation and also because all entries of the first mode have the same sign, the first PC can be used as an index to monitor drought (Katz and Glantz, 1986).

The first PC often explains a bit more variance than the field's average because the first PC is the projection of the anomaly data onto the first eigenvector of the covariance, and this projection maximizes the variance of the first PC. Let $\vec{a}(t) = \begin{bmatrix} a_1 \\ \vdots \\ a_N \end{bmatrix}(t)$ be the anomaly data, where $a_i(t) = R_i(t) - \mu_i, i = 1, \ldots, N$, μ_i is the mean of the i^{th} point. Let $\vec{u} = \begin{bmatrix} u_1 \\ \vdots \\ u_N \end{bmatrix}$ be the unit directional vector for projection and $Q(t) = \vec{u}' \cdot \vec{a}(t)$ be the projection. If $\vec{u} = \vec{e}_1$, the first eigenvector of the covariance of $A = [\vec{a}(1) \quad \cdots \quad \vec{a}(t)]$, then $Q(t) = P_1(t)$, the first PC. If $\vec{u} = \frac{1}{\sqrt{N}} \begin{bmatrix} 1 \\ \vdots \\ 1 \end{bmatrix}$, then

$$Q(t) = L(t) = \frac{1}{\sqrt{N}} \sum_{i=1}^{N} a_i(t) = \frac{N}{\sqrt{N}} \cdot \frac{1}{N} \sum_{i=1}^{N} a_i(t) = \sqrt{N}\bar{a}(t). \tag{4.15}$$

Therefore,

$$\text{var}(L(t)) \le \text{var}(P_1(t)) \Rightarrow \text{var}(\sqrt{N}\bar{a}(t)) \le \text{var}(P_1(t)) \Rightarrow N \cdot \text{var}(\bar{a}(t)) \le \text{var}(P_1(t)) \Rightarrow$$

$$\text{var}(\bar{a}(t)) \le \frac{1}{N}\text{var}(P_1(t)) = \frac{\lambda_1}{N}. \tag{4.16}$$

Thus, the proportion of the variance explained by the first PC is greater than that explained by the field's average, and these proportions satisfy the following inequality,

$$\frac{\lambda_1}{\sum_{i=1}^{N}\lambda_i} \ge \frac{N \cdot \text{var}(\bar{a}(t))}{\sum_{i=1}^{N}\lambda_i}.$$

Our analysis of the data at four townships in Alberta (the townships near Beaverlodge, Vegreville, Lacombe, and Lethbridge) gives the following two percentages:

$\frac{\text{var}(\bar{a}(t))}{\sum_{i=1}^{N}\lambda_i}$ =10.2% for average and $\frac{\lambda_1}{\sum_{i=1}^{N}\lambda_i}$ = 41.3% for the PC1, and

$$41.3\% = \frac{\lambda_1}{\sum_{i=1}^{N}\lambda_i} \ge \frac{4 \cdot \text{var}(\bar{a}(t))}{\sum_{i=1}^{N}\lambda_i} = 40.8\%.$$

As Katz and Glantz (1986) pointed out, if the standardized precipitation instead of the anomaly is used, the variance of the average field equals

$$\frac{1+(N-1)\bar{\rho}}{N}, \tag{4.17}$$

where N is the total number of stations, and $\bar{\rho}$ is the average correlation between each pair of stations. If the correlations between the pairs of stations are equal, then

the proportion of the total variance explained by the first PC of the standardized precipitation equals Eq. (4.17). However, due to the strong inhomogeneity of a precipitation field, the first PC explains a greater fraction of the total variance than does the average. Therefore, the first PC will explain a larger fraction of the total variance than the average field no matter if the field is the anomaly or the standardized precipitation.

Since the EOF patterns reflect the fundamental dynamical behavior of the stochastic precipitation field, using the PCI to monitor the drought conditions can reflect more properties of climate dynamics than using the spatial average precipitation. The pattern of the first EOF has ups and lows in the working domain. Although this spatial variance is not very large, the pattern can reflect the likelihood of drought vulnerability for a given location in the domain under investigation. The location with a large value for the EOF1 is more vulnerable to climate change and hence is more likely to suffer from drought.

4.4 EOF patterns and the PCI of the Alberta agricultural region

The leading mode (EOF1) of the May-August precipitation of Alberta agricultural region shows a north-south pattern (Fig. 4.1a). The large EOF1 values are in the southern agricultural regions: the Aspen Parkland, Moist Mixed Grassland, and Mixed Grassland areas, while the northern Peace Lowland and part of the Boreal Transition areas have relatively small EOF1 values. The regions with large EOF1 values are very sensitive to the variations of the PC1 values. Thus, the EOF1 pattern reflects the drought characteristic of southern Alberta, especially the area within the

Palliser Triangle, showing the high risk of drought in the region. During the 1930s and 1980s, southern Alberta experienced both single-year and multi-year droughts. For the farmers in southern Alberta, drought is a normal, recurrent feature, and they have a long history of struggling with it. Although southern Alberta is the most drought-prone region, other areas of Alberta have experienced drought as well. The extreme droughts in the years 2000 and 2001 occurred across the entire province and had a severe effect on the agricultural industry.

The EOF2 of the May-August precipitation (Fig. 4.1b) reveals that besides being large in the southern areas, the absolute value of the EOF2 is also large in the Peace region, indicating a secondary vulnerable region for agriculture. Since the EOFs can quantitatively assess the drought vulnerability, the values of the leading EOFs in these regions may be used to predict the drought risk in a region. The EOF1 and EOF2 modes explained a total of 63% (41% for EOF1 and 22% for EOF2) of the variability of the precipitation field in the agricultural region.

Section 4.2 also indicates that the inner product of the data matrix and the PC will yield EOF patterns. This result leads to another way of presenting the spatial patterns, i.e., plotting the k^{th} homogeneous correlation map, which is the vector of the correlation values between the PC of the k^{th} mode and the precipitation values of the field at each location. The 1^{st} homogeneous map (Fig. 4.2a) of the Alberta agricultural region also presents a north-south pattern. The correlations are the highest in the center of the Mixed Grassland, the center of the Moist Mixed Grassland, and the northern half of the Fescue Grassland with a correlation value between 0.78 and 0.9. Since the square of the correlations represents the variance explained locally, this

mode accounts for 61%-81% of the variance in these regions. The fraction of the local variance explained decreases towards the north, with the variance explained locally

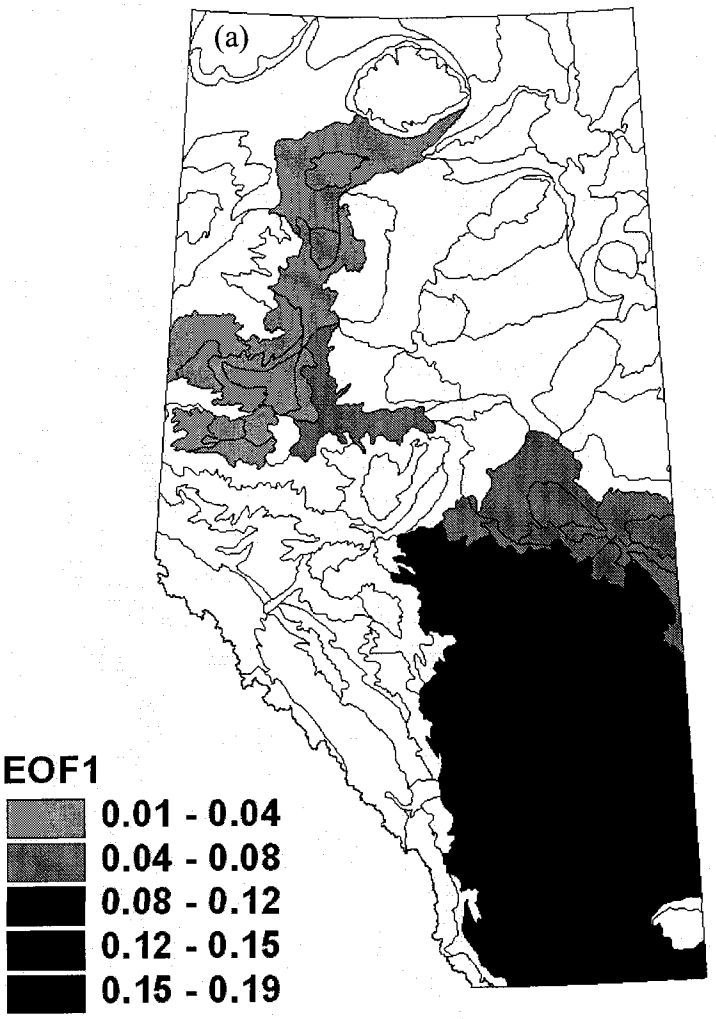

Figure 4.1. The (a) EOF1 and (b) EOF2 modes of the May-August precipitation for the Alberta agricultural region.

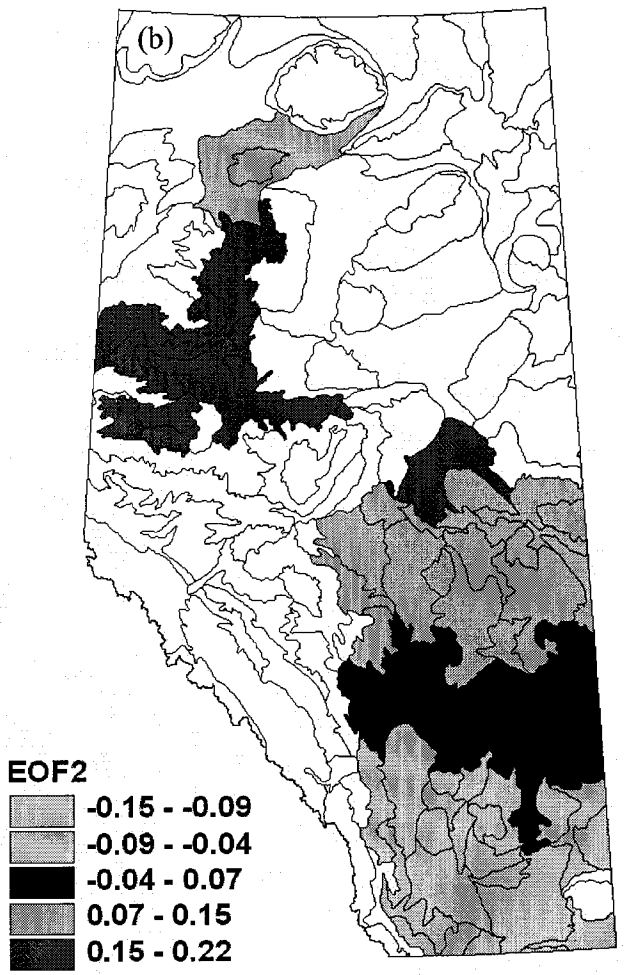

Figure 4.1.Continued.

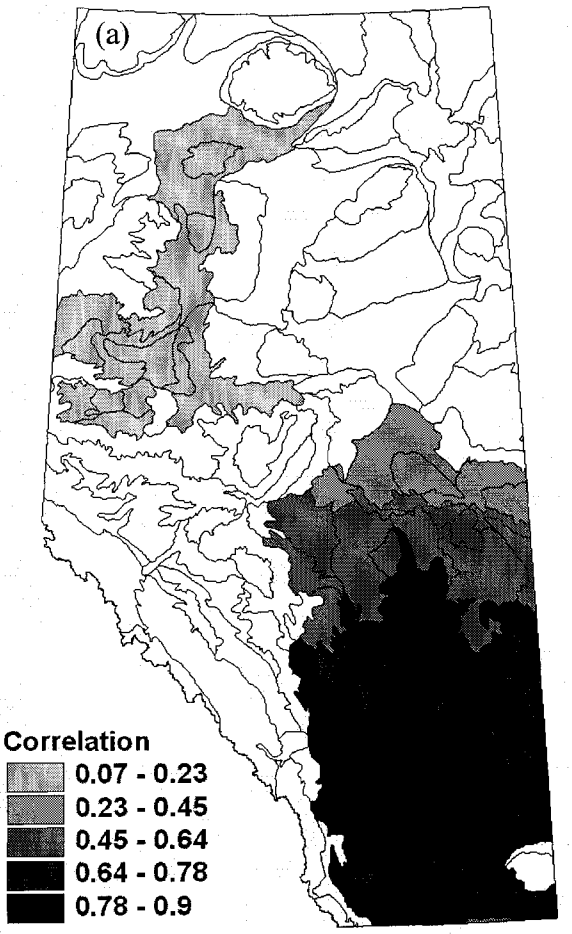

Figure 4.2. The (a) first and (b) second homogeneous correlation maps of the May-August precipitation for the Alberta agricultural region.

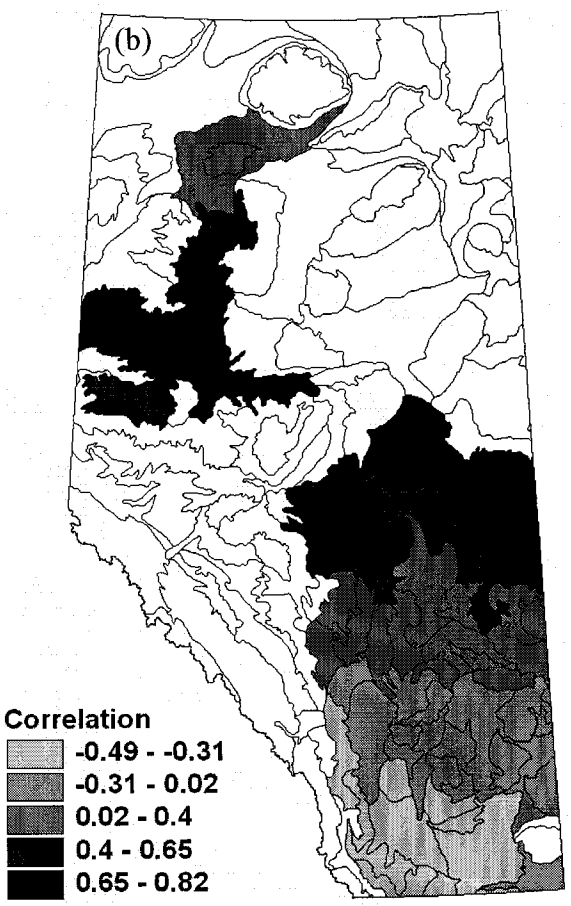

Figure 4.2. Continued.

being between 4.9% and 5.3%. The 2nd homogeneous map (Fig. 4.2b) displays a high correlation in the southern part of the Peace region and part of the Boreal Transition (0.65-0.82), and the variance explained in the regions is between 42% and 67%. The map also shows an out-of-phase relationship between the precipitation in the north and in the south.

The EOF1 and EOF2 patterns from the four townships are also plotted (Fig. 4.3) to compare these patterns with those derived from the whole agricultural region. The EOF1 pattern in Fig. 4.3a also shows an increase from the north to the south, but the increment is very small compared to the increment in Fig. 4.1a. The EOF2 (Fig. 4.3b) of the four townships displays a similar pattern to that of the agricultural regions (Fig. 4.1b). The large absolute value of EOF2 in the Peace region is also evident.

The PCs reflect the time variation of the spatial patterns. The first PC of the precipitation field in the agricultural region (Fig. 4.4a) shows mainly the interannual fluctuations. The PC1 captures the drought events of 1910, 1917, 1918, 1919, 1929, 1936, 1958, 1967 and 2001 (Wheaton, 2001). Only one of the eight wheat drought events reported by PFRA (1998) is captured by the agricultural regions' PC1 (year 1936) because these droughts occurred mainly in southern Alberta. Since the PC1's variation is similar to that of the average precipitation of the field (Figs. 4.4 and 4.5), the PC1 calculated only from the southern regions is expected to show more evidence of these drought events. Fig. 4.4b presents the PC1 calculated for the Mixed Grassland region. Seven out of eight of the wheat drought events reported by PFRA (1998) are captured (1931, 1936, 1937, 1943, 1961, 1984, and 1985). Other drought events reported by Wheaton (2001) are also captured (1910, 1914, 1917, 1918, 1919,

1929, 1945, 1967, 1969, 2000, and 2001). Since the PCs calculated are not dimensionless, the values vary when the amplitude of the average precipitation changes. Thus, comparing the PC values computed from different climatologic regions in this way is difficult. A commonly used way to compute the dimensionless PC (normalized PC) is to divide the PC by its standard deviation. Fig. 4.5 shows the normalized PC1 of the agricultural region and the Mixed Grassland region. The normalized PC1s are more comparable.

As stated previously, the correlation of the PC1 with the averaged precipitation is close to one. To demonstrate this result, Table 4.1 lists the correlations of the precipitation to the corresponding four drought indices. All four indices have a high correlation with the precipitation field, and the correlation is the highest for the PCI.

Table 4.1. The correlations of the May-August precipitation with SPI, RAI, SAI and PCI in the Mixed Grassland region.

	May-August				
	PCPN	SPI	RAI	SAI	PCI
May-August PCPN	1				
SPI	0.992740952	1			
RAI	0.994790765	0.999227	1		
SAI	0.994829299	0.987234	0.989557	1	
PCI	0.997422608	0.989194	0.991658	0.997666	1

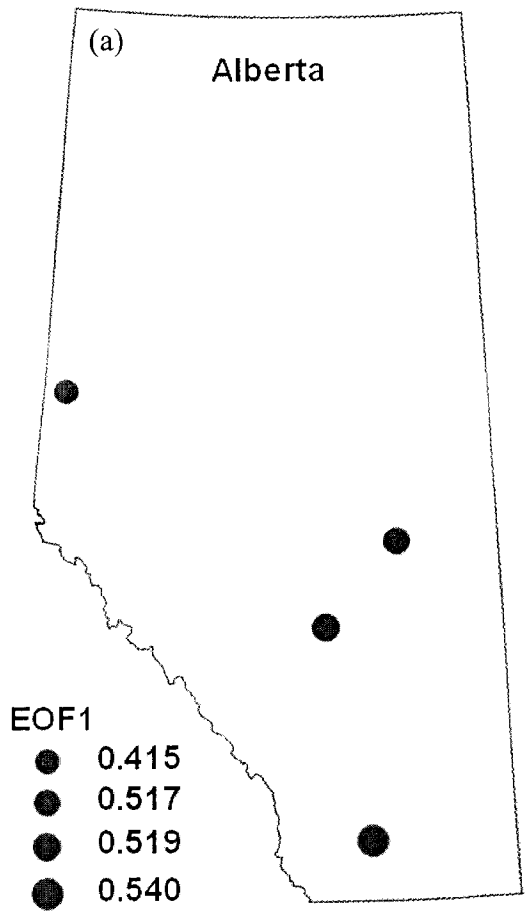

Figure 4.3. The (a) EOF1 and (b) EOF2 modes of the May-August precipitation for four townships.

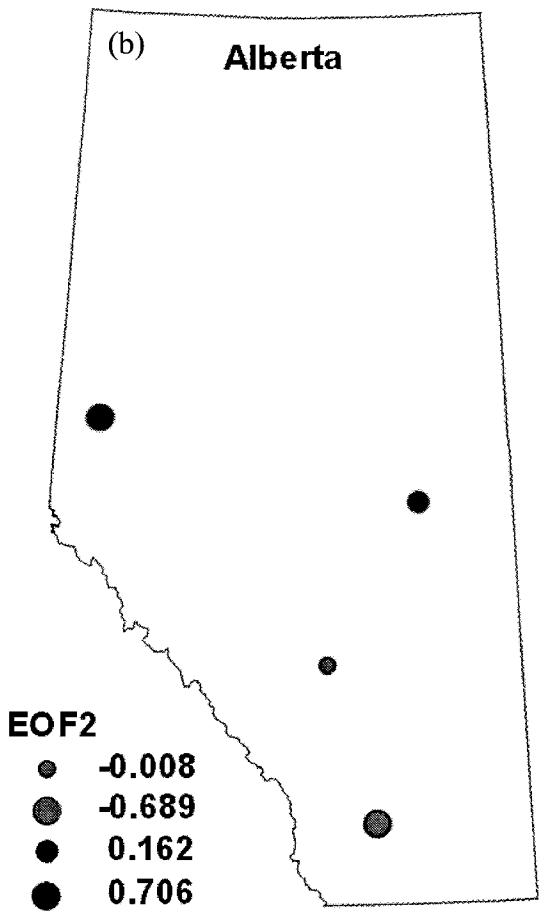

Figure 4.3. Continued.

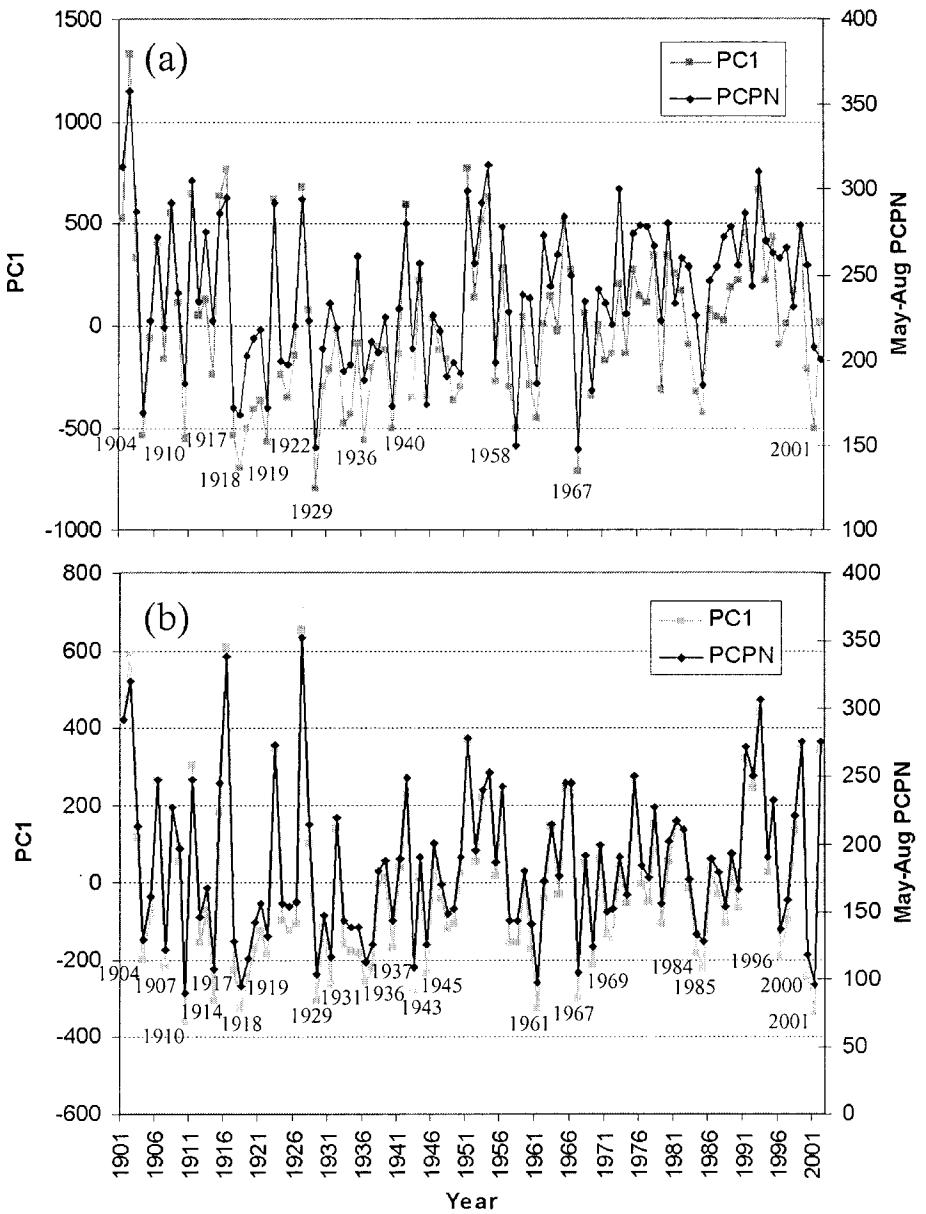

Figure 4.4. The PC1 and the May-August precipitation in (a) the agricultural region and (b) the Mixed Grassland region.

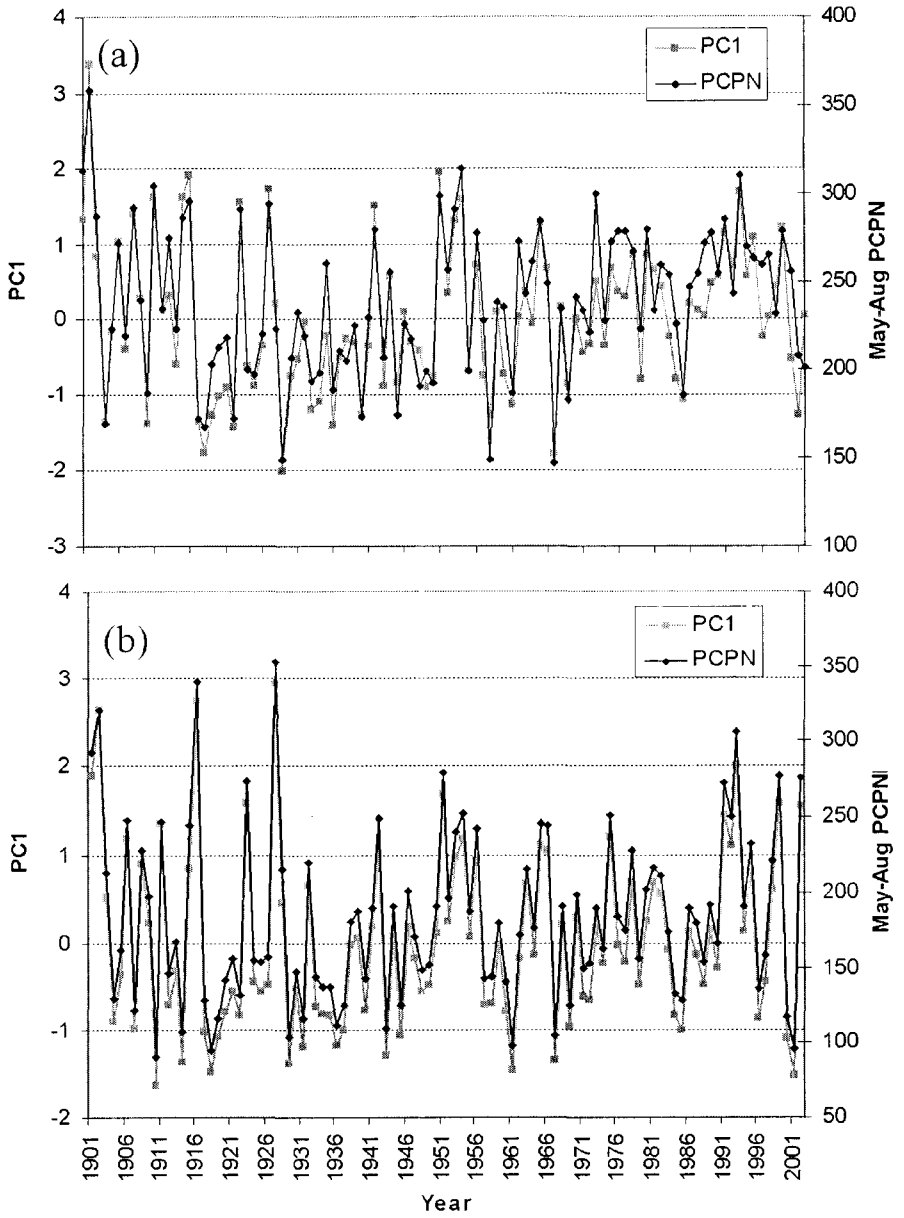

Figure 4.5. The dimensionless PC1 and the May-August precipitation in (a) the agricultural region and (b) the Mixed Grassland region.

4.5 Probabilistic principal component index

The advantage of using the PCI instead of the average precipitation as a drought index is that when the SPI-type of probabilistic approach is combined with the PCI, the transformed probabilistic PCI (i.e., the PPCI) can reflect both the dynamic and probabilistic properties of the drought conditions over a large area.

The transformation of the PCI into the PPCI is based on the idea of SPI calculation. It follows two steps. First, the empirical cumulative probability of the PCI is calculated by using the method of Panofsky and Brier (1958). The PCI time series is sorted in increasing order, and the empirical cumulative probability (ECP) is defined as

$$ECP = \frac{k}{n+1},$$

where k denotes the k^{th} PCI of the sorted data series, and n is the sample size. Therefore, each PCI value has its corresponding cumulative probability. Then the inverse of the normal cumulative distribution function with mean $\mu = 0$ and variance $\sigma = 1$ at the corresponding probability can be calculated for each PCI. The resulting values are our PPCI. The PCI values can take either positive or negative or zero. They cannot be used for the gamma fitting since it requires data to be non-negative. Thus, the smoothing spline is used to find the corresponding probability of a given PCI value.

Figure 4.6 gives the schematic diagram of the transformation of the PCI into the PPCI for the Mixed Grassland region. In the left panel, the "plus" sign denotes the ECP of each of the 102 PCI values from 1901 to 2002; the smooth curve is the fitted

cumulative probability. The smoothing spline fitting here is achieved by using the Matlab curve-fitting tool. The smoothing spline f is constructed by using piecewise polynomial to minimize

$$p\sum_i w_i(y_i - f(x_i))^2 + (1-p)\int\left(\frac{d^2 f}{dx^2}\right)^2 dx,$$

where the (x_i, y_i) is the data point, p and w_i are the smoothing parameter and the weights, respectively. The p and w_i are chosen to be 0.0001 and 1.0 in this fitting. The coefficient of determination, R^2, equals 0.9995 and the SSE equals 0.004036. The 1901-2002 PPCI for the agricultural region and the Mixed Grassland region are given in Fig. 4.7.

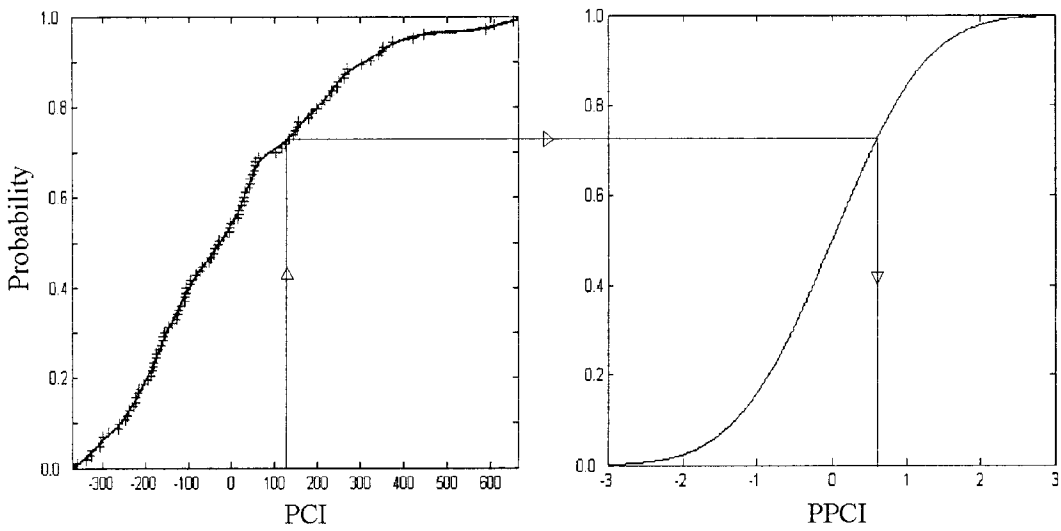

Figure 4.6. The transformation of the PCI to PPCI for the Mixed Grassland region.

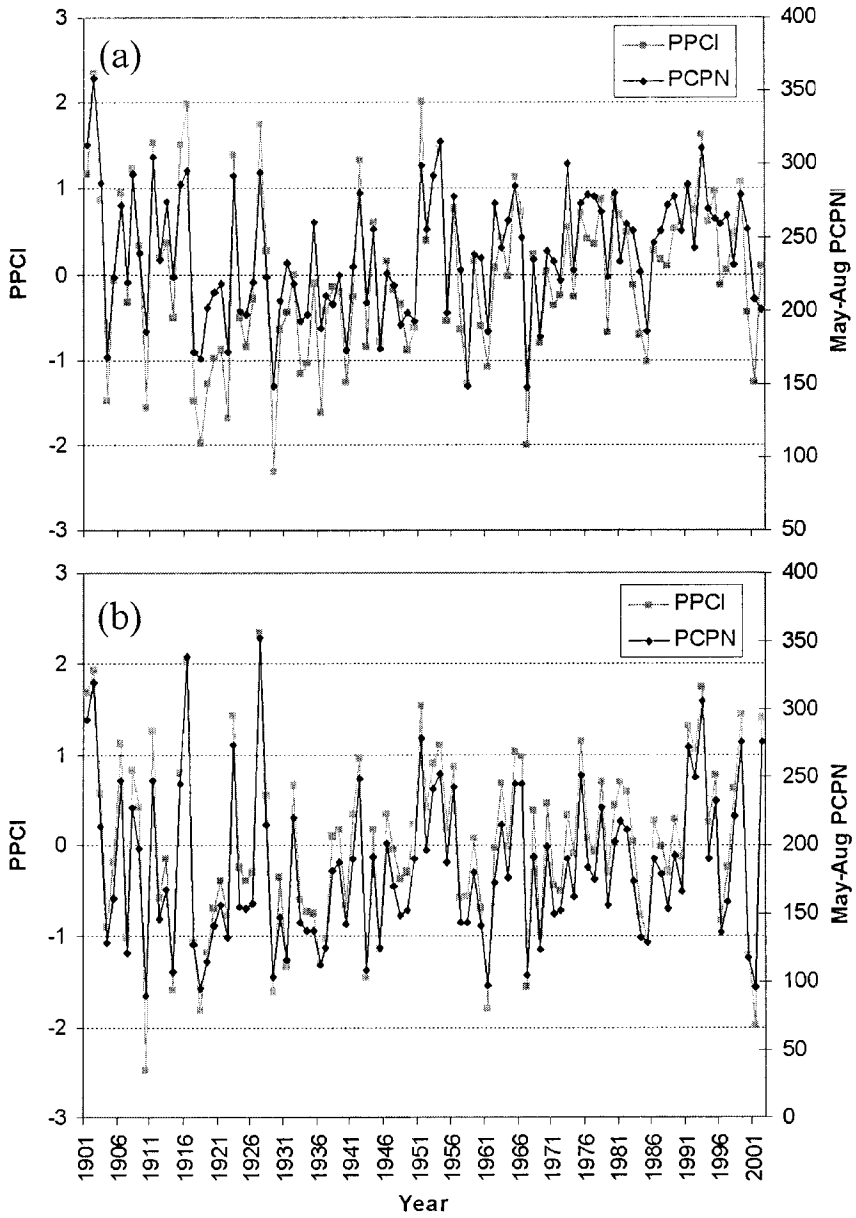

Figure 4.7. The PPCI and the May-August precipitation in (a) the agricultural region and (b) the Mixed Grassland region.

The above analysis provides the procedure for the PPCI calculation. However, to understand the drought triggers, i.e., the threshold values of drought severity, one has to define a standard by using the probabilistic approach. Normally, drought severity is classified according to chance of recurrence, say, once in 10 years. To make the study self-contained, the probability for drought interpretation according to a normal distribution is listed in Table 4.2. Droughts are classified into the 5 categories described in the last chapter. The exceptional drought D4 occurs once in 50 years; extreme drought D3 once in 20 years; severe drought D2 once in 10 years; moderate drought D1 once in 5 years; and abnormally dry D0 once in 3 years. The impacts of the droughts in the different categories can be found in Section 3.5 or the US National Drought Mitigation Center's website http://drought.unl.edu/dm/monitor.html. In terms of the exact probability of occurrence based on the PPCI threshold values, the droughts are classified according to Table 4.2.

Table 4.2. PPCI probability for drought interpretation

Category	Threshold Values	Probability of Occurrence	Event Frequency	Percentile Trigger
D0	-0.5 to –0.7	30.8%	Once in 3 years	21-30%
D1	-0.8 to –1.2	21.2%	Once in 5 years	11-20%
D2	-1.3 to –1.5	10.7%	Once in 10 years	6-10%
D3	-1.6 to –1.9	5.5%	Once in 20 years	3-5%
D4	-2.0 to - ∞	2.3%	Once in 50 years	0-2%

4.6 Summary and discussion

This chapter proposed a new drought index, the PPCI, which can not only reflect the probabilistic property of the drought event occurrence but also can show the dynamic behavior of the average field through the dominant spatial patterns. An advantage of using PPCI as a drought indicator is that the drought vulnerability of a region can be quantitatively evaluated by the leading EOF mode, which provides a possible means to predict drought risks. Furthermore, because the PPCI is derived by an equi-probability transformation, the drought categories can be classified into D0 to D4 according to the chance of occurrence based on the normal distribution.

In deriving the PPCI, a probabilistic approach is used similar to the derivation of SPI. But instead of using a gamma fitting, we used the empirical cumulative probability and smoothing spline to fit the curve. Since the smoothing parameter in the fitting process can be adjusted subjectively to reach the level of smoothing, the result is not unique. Other fitting tools such as polynomial, cubic spline, and shape-preserving interpolation could also be tested.

Chapter 5

An Estimate of the Error Variance of the GHCN Monthly Surface Air Temperature Data

5.1 Introduction

The purpose of this study is to estimate the sampling error of the $5^{o} \times 5^{o}$ gridded data in the Global Historical Climatology Network (GHCN) developed by the United States' National Climatic Data Center (NCDC). In calculating the optimal global or regional average of seasonal or annual mean temperatures, accurate estimate of errors is an important issue that has attracted much attention. The "error" is known to the general public as "uncertainties" in estimating global warming. Folland et al. (2001) made the first attempt to quantify the major sources of uncertainties. These uncertainties result from several error sources including the sampling error and random data error. In addition, systematic data biases can also cause uncertainties.

Reducing the uncertainties by optimal averaging and interpolation is a recognized, worthwhile effort for increasing our understanding of the climate change throughout history. Folland et al. (2001) calculated the global average temperature anomaly following the theory of spectral optimal averaging (SOA) (or called "reduced space optimal averaging") developed by Shen et al. (1998) and minimized the explicitly defined mean square error (MSE):

$$\varepsilon^2 = \sum_{n=1}^{M} \lambda_n \left[\overline{\psi_n} - \sum_{i \in N} w_i \psi_n(i) \right]^2 + \sum_{i \in N} w_i^2 \left\langle E_i^2 \right\rangle, \tag{5.1}$$

where the MSE is between the true spatial average and the estimated average, λ_n is the eigenvalue of the EOF (empirical orthogonal functions) mode n, $\psi_n(i)$ is the value of the EOF mode n at box i, $\overline{\psi_n}$ is the "true" spatial average of the EOF mode n, M is the number of EOFs used, $\left\langle E_i^2 \right\rangle$ is the data error variance for box i, and $\langle \cdot \rangle$ stands for the ensemble average, and w_i is the optimal weight for box i. This theory has assumed stationarity (i.e. the mean, variance, higher statistical moments, and autocorrelation structure do not change over time) and ergodicity (i.e. ensemble average is equal to the long-time temporal average). Folland et al. (2001) improved it and attempted to take non-stationarity into account by using a moving time window (MTW), i.e., assuming only piecewise stationarity. They computed their eigenvalues and EOFs in a MTW and applied the results to calculate the optimal global average of the surface temperature anomalies from 1861 to 2000. The grid box data were the variance-adjusted version of the combined land and marine dataset of surface temperature anomalies (HadCRUTv) archived at the Climate Research Unit of the University of East Anglia, U.K. (Jones et al., 2001). The error variances $\left\langle E_i^2 \right\rangle$ required in the optimal averaging were estimated from the error variances for the decadal data (Jones et al., 1997, referred to as J97 hereafter). The optimal average and its error from Folland et al. (2001) are also included in the Intergovernmental Panel for Climate Change (IPCC) 2001 report.

J97 was the first publication on the systematic calculation of the error variance on gridded data in the decadal scale by estimating two parameters: the average variance (s_0^2) of all the stations in a grid box, and the average inter-correlation (r) of these stations based upon the output of GCMs (general circulation models). However, the error variances at the monthly scale and the error variances for the GHCN gridded monthly surface air temperature anomalies over the land have not been systematically estimated. Since optimal averages and interpolations based on the GHCN data require the error variances, the objective of this study is to estimate the required error variances of the monthly, gridded surface air temperature data of the GHCN. Thus, each GHCN gridded datum corresponds to an error variance. Both the GHCN gridded data and the corresponding error variances are archived at the United States' NCDC. The differences between the current dataset and the J97 dataset of error variances are listed below.

(i) Different datasets: Ours is for the GHCN gridded temperature data and J97's is for the HadCRUT data.

(ii) Different time scales: Ours is for the monthly data, and J97's is for decadal data.

(iii) Different methods: Ours is based on spatial variances and a regressional parameter, while J97's was based on the spatially averaged temporal variances and averaged inter-correlations.

(iv) Different results: Our error estimate attempts to take non-stationarity into account, and hence, a large spatial variance of a given month of a GHCN

grid box leads to a large error variance, while J97 does not have this feature.

5.2 Data

The GHCN is a comprehensive, global, and station-based climate dataset composed by NCDC scientists. This dataset includes temperature, precipitation, and pressure. The GHCN Version 1 was released in 1992 and Version 2 in 1997 (Peterson and Vose, 1997). The adjusted monthly-mean station temperature dataset from Version 2 is used in this research, and the data were downloaded from the NCDC GHCN website http://www.ncdc.noaa.gov/oa/pub/data/ghcn/v2/ghcnftp.html. The data site includes both the "Temperature Station Inventory File"(740KB) and "Adjusted Monthly Mean Temperature Data" (31MB). This version of GHCN records started from January 1702 and ended on February 2004. Before 1835, less than 10 stations existed over the entire globe during a given month. January of 1835 had 27 stations (all of them were in the United States and Europe), and the number of stations increased to 158 stations in January of 1851, to 446 stations in January of 1881, until the maximum of 4230 stations was reached in July of 1969, before the number of stations began to decrease. The number of stations dropped sharply during the period from 1990 to 1993, and then from 2003 to 2004. These two sharp decreases were due mainly to the time lag between the NCDC's data archiving and the station observations. The total number of stations contributing to the GHCN temperature data is around 6,000. Since few stations were in the GHCN system before January 1835

and after December 2003, this study considers the data between January 1835 and December 2003. The history of the number of stations from January 1835 to February 2004 is shown in Fig. 5.1. The spatial distributions of the stations of February 1853,

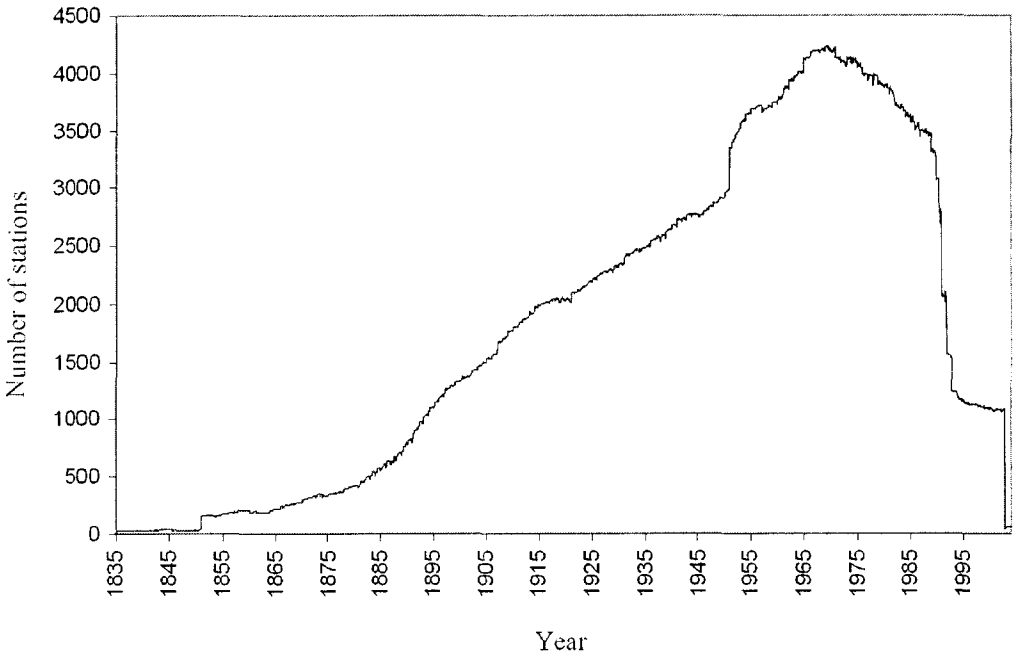

Figure 5.1. History of the number of stations in the GHCN network from January 1835 to February 2004.

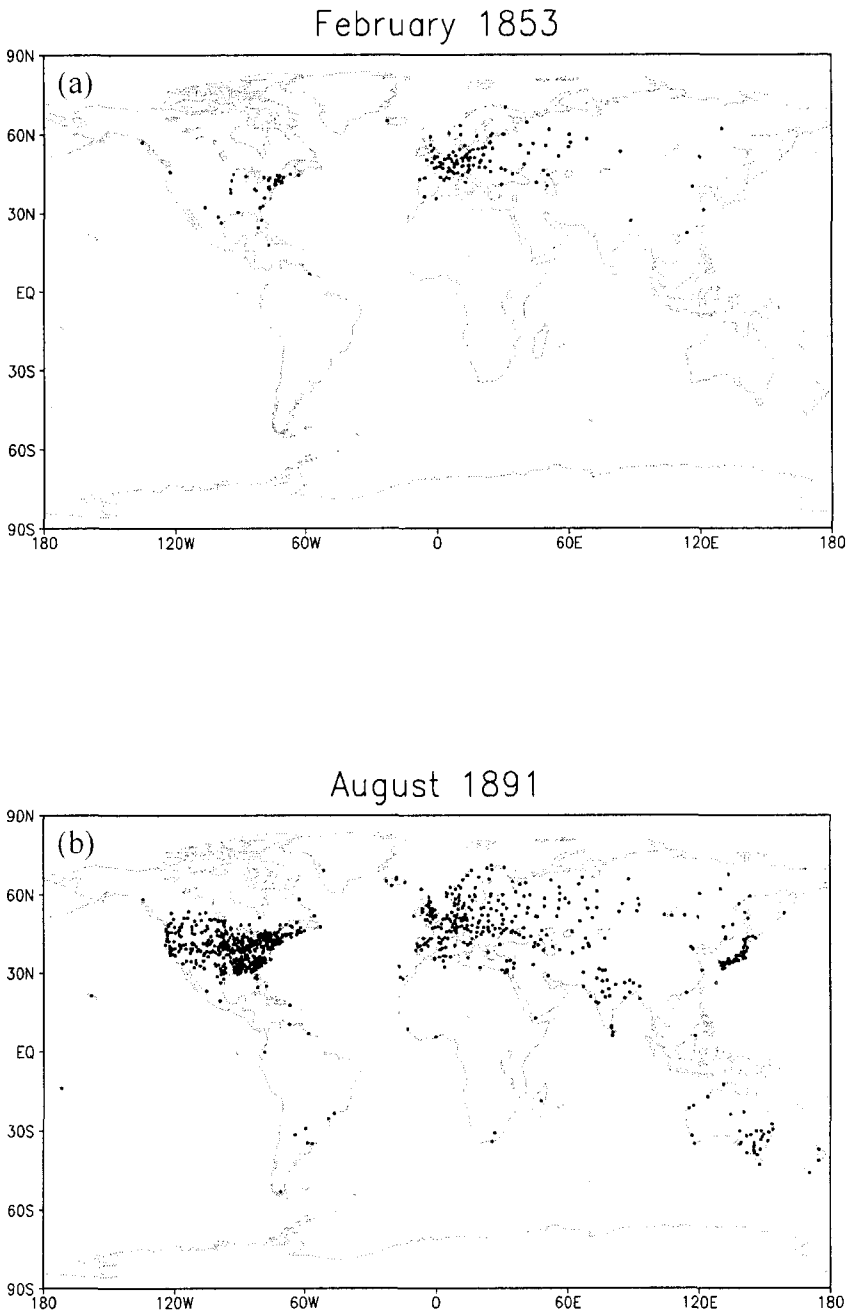

Figure 5.2. Spatial distribution of stations.

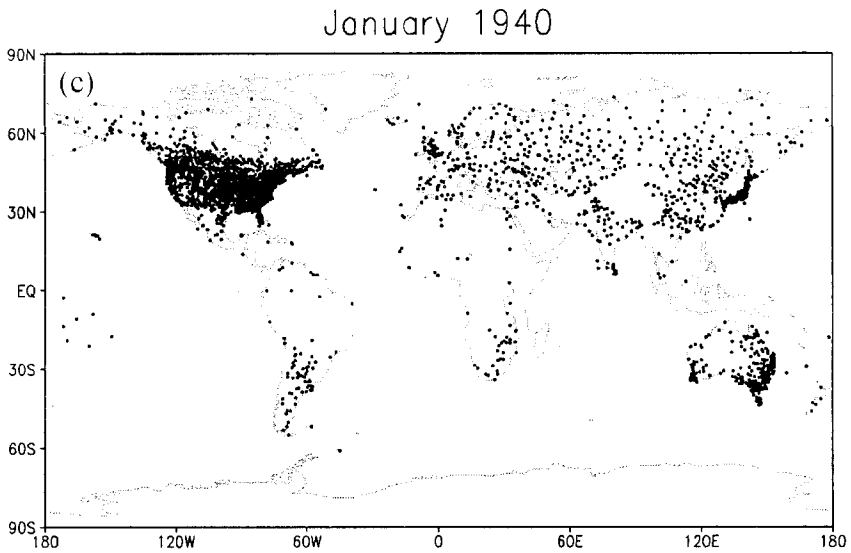

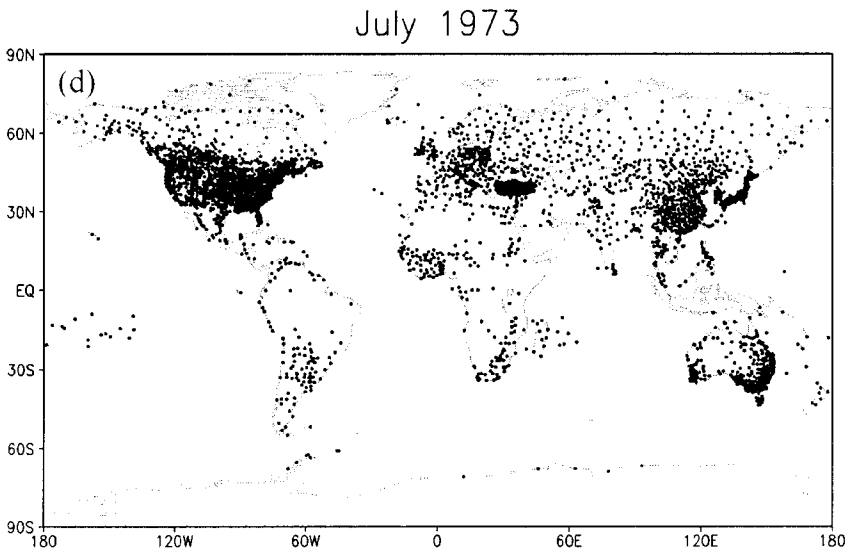

Figure 5.2. Continued.

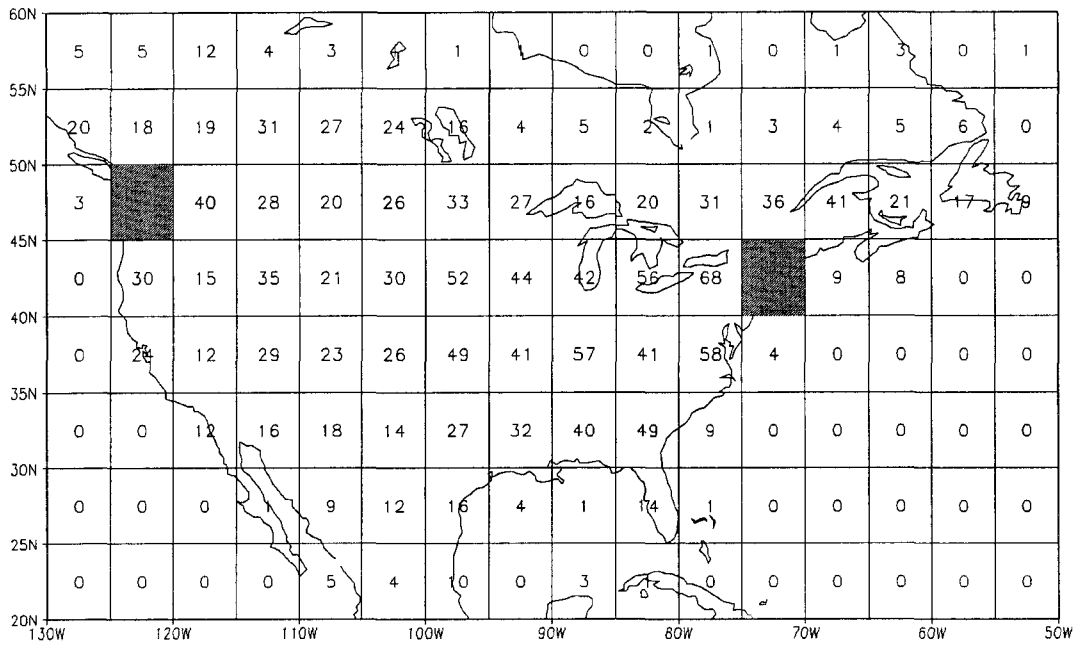

Figure 5.3. Grid boxes in the contiguous United States and southern Canada, total number of stations in a box in the GHCN history, and two error-validation boxes in the United States: (120°-125°W, 45°-50°N) with 55 stations and (70°-75°W, 40°-45°N) with 68 stations.

August 1891, January 1940, and July 1973, representing both station-sparse and station-dense months, are displayed in Fig. 5.2.

Two 5° ×5° station-dense boxes in the United States are selected to validate our error-estimation theory. They are (120°-125°W, 45°-50°N) in the western US and (70°-75°W, 40°-45°N) in the eastern US. The locations of the two boxes (highlighted) can be seen in Fig. 5.3. The number in each box in Fig. 5.3 is the total number of stations, each of which appeared once in the box, but might not have continued throughout the entire time period from 1835 to 2003. This number might not have been reached at any month of the GHCN's history. For a given month, the number of stations with data was usually less than this number, since most stations had incomplete records from 1835 to the present. Our two validation boxes had a total of 55 stations in (120°-125°W, 45°-50°N). The maximal number of stations appearing in a single month was 52, which was reached in only 42 months including January 1970. A total of 74 stations were in the box (70°-75°W, 40°-45°N) and the maximal number of stations appearing in a single month was 68, which was reached in only 78 months including March 1947.

5.3 Method

5.3.1 Basic formulas

It is well known that the formula of the standard error for the spatial average

$$E^2 = \left\langle \left(\overline{T} - \hat{\overline{T}} \right)^2 \right\rangle = \frac{\sigma^2}{N} \tag{5.2}$$

is applicable to a spatial white noise field $T(\vec{r})$. Here $\overline{T}$ is the true average of the white noise field over the spatial domain Ω whose area is $\|\Omega\|$:

$$\overline{T} = \frac{1}{\|\Omega\|} \int_{\Omega} T(\hat{\mathbf{x}})\, d\Omega . \tag{5.3}$$

Its estimator is

$$\hat{\overline{T}} = \frac{1}{N} \sum_{i=1}^{N} T_i . \tag{5.4}$$

In the above, $T_i = T(\vec{r}_i)$ is a sampling datum, N is the number of samples, and $\sigma^2 = \langle T^2(\vec{r}) \rangle$ is the uniform variance of the white noise field. When the monthly surface air temperature anomaly of a grid box is computed from the simple average of the anomaly data of the stations within the box, intuition implies a smaller standard error than that estimated by formula (5.2) due to the correlation among the temperature anomaly time series measured at different stations. The question is how to quantify the reduction from the error determined by formula (5.2) due to the correlation. The temperature field, even within a $5^{\circ} \times 5^{\circ}$ box, may be inhomogeneous, and hence has non-uniform variances at different station locations within the box. This inhomogeneity feature is distinct for a grid box in a mountainous or coastal region. Thus, the constant, ensemble variance σ^2 in formula (5.2) is usually not true.

Normally, in statistical climatology, ergodicity is automatically assumed, and hence, the ensemble variance is computed by temporal variance. If the constant

temporal variance is invalid, the alternative variance quantities of a grid box need to be considered. The possible alternative variances include (i) the spatial average of the point, temporal variances, (ii) the temporal mean of spatial variances, and (iii) the relevant covariances. J97 used (i) and (iii), and we choose to use (ii) and (iii) in the current study. J97 employed the concepts of spatially averaged correlation ($\bar{r}$) and the average of the point variance (s_0^2), and derived the error estimate formula

$$SE^2 = \frac{s_0^2(1-\bar{r})}{N}, \tag{5.5}$$

where

$$\bar{r} = \frac{2}{N(N-1)} \sum_{i>j=1}^{N} r_{ij} \tag{5.6}$$

is the spatially averaged correlation, r_{ij} is the correlation between station i and station j, and

$$s_0^2 = \frac{1}{N} \sum_{i=1}^{N} s_i^2 \tag{5.7}$$

is the spatially averaged point variance since s_i^2 is the temperature's temporal variance of station i. J97 used the GCM model's outputs to estimate $\bar{r}$ and s_0^2, which are assumed to be temporally invariant. Thus, for a given season in a decade and a given grid box, J97's standard error varies only according to the mean number of stations in the grid box. Calculations of $\bar{r}$ and s_0^2 require the temperature anomaly data to be complete in a specified time period. J97 developed an *ad hoc* method of using gridded data and GCM data to estimate these two parameters.

Intuitively, the sampling error is obviously large for a month when the temperature has a large spatial variance and serious spatial inhomogeneity. Thus, we choose to take the spatial variance into account when estimating the sampling errors. A regressional approach is used to assess the inter-correlation among the stations in the same grid box. The sampling errors are finally estimated by using the spatial variance, the correlation factor, and the number of stations in a grid box. The underlying assumption of the error estimate is that the ratio of the sampling-error-variance (ε^2) to the spatial variance of the temperature field (σ_s^2) is inversely proportional to the number of stations in the grid box (N):

$$\frac{\varepsilon^2}{\sigma_s^2} = \frac{\alpha_s}{N} + \varepsilon_E, \tag{5.8}$$

where α_s is the regressional coefficient, σ_s^2 is the spatial variance of the temperature field defined by

$$\sigma_s^2 = \left\langle \frac{1}{N} \sum_{j=1}^{N} \left(T_j(t) - \bar{T}(t) \right)^2 \right\rangle, \tag{5.9}$$

and ε_E is the Gaussian random error of the regression model (5.8). Formula (5.8) is mathematically similar to formula (5.5), but provides a different algorithm of calculation because the temporal variance (s_0^2) in (5.5) is replaced by the spatial variance (σ_s^2) in (5.8).

The meaning of the regression coefficient α_s can be interpreted as follows. The sampling error variance for a grid box is defined as the ensemble mean of the

square difference between the true spatial average and the estimated spatial average and can be written in the following form:

$$E^2 = \left\langle \varepsilon^2 \right\rangle = \left\langle \left(\hat{\bar{T}} - \bar{T} \right)^2 \right\rangle = \alpha_s \times \frac{\sigma_s^2}{N} \quad , \tag{5.10}$$

where the regression coefficient α_s, i.e., the correlation factor, is equal to

$$\alpha_s = 1 + \frac{1}{N} \sum_{\substack{i,j=1 \\ i \neq j}}^{N} \left\langle \frac{(T_i - \bar{T})}{\sigma_s} \frac{(T_j - \bar{T})}{\sigma_s} \right\rangle \quad . \tag{5.11}$$

The derivation of this formula is as following. The mean square error is

$$\begin{aligned}
E^2 &= \left\langle \left(\bar{T} - \hat{\bar{T}} \right)^2 \right\rangle \\
&= \left\langle \left[\frac{1}{N} \sum_{i=1}^{N} \left(\bar{T} - T_i \right) \right]^2 \right\rangle \\
&= \frac{1}{N} \left[\left\langle \frac{1}{N} \sum_{i=1}^{N} \left(\bar{T} - T_i \right)^2 \right\rangle + \left\langle \frac{1}{N} \sum_{\substack{i \neq j \\ i,j=1}}^{N} \left(\bar{T} - T_i \right) \left(\bar{T} - T_j \right) \right\rangle \right] \\
&= \frac{1}{N} \left[\sigma_s^2 + \left\langle \frac{1}{N} \sum_{\substack{i \neq j \\ i,j=1}}^{N} \left(\bar{T} - T_i \right) \left(\bar{T} - T_j \right) \right\rangle \right] \\
&= \frac{\sigma_s^2}{N} \left[1 + \frac{1}{N} \sum_{\substack{i \neq j \\ i,j=1}}^{N} \left\langle \frac{\left(\bar{T} - T_i \right)}{\sigma_s} \frac{\left(\bar{T} - T_j \right)}{\sigma_s} \right\rangle \right].
\end{aligned}$$

If the temperature field is homogeneous in a grid box, i.e., the point variance is same everywhere and the inter-station correlation depends only on the distance between two stations, then formula (5.10) degenerates into formula (5.5) and is in agreement with the interpretation of J97's formula. The advantage of error model

(5.10) is its tolerance of the inhomogeneity of the temperature field in a grid box, and the spatial inhomogeneity is mainly taken account by the spatial variance σ_s^2.

5.3.2 Computation of anomalies and estimation of σ_s^2

The first step of computation is to calculate anomalies from the real readings of the temperature gauges. Not all the stations have data for each month from January of 1835 to December of 2003. As a matter of fact, not even a single station has complete data. This problem complicates the computing algorithm for anomalies. Because one of the main purposes of the error calculation is to quantify the uncertainties in global warming via climate anomalies, the first step is to select the stations whose anomalies can be computed. Our anomaly calculation method is the same as that of J97. For a given month from January to December, if a station has 21 or more years of data (i.e., 21 or more data entries) from 1961 to 1990, the station is then retained. The climatology is then computed as the mean of the at-least 21 data in the 30-year period. The at-least 21 anomalies for a station are the departures from the climatology. The format of the anomaly data is presented in Table 5.1.

This way of calculating anomalies inevitably results in the inability to compute the anomalies for a station for a specified month of a year even though it has data. The station that had data but had no anomalies is denoted by –8888, while the station that had no data is denoted by –9999 in Table 5.1. A station without anomalies is not used in the optimal average of global surface air temperature anomalies. Using a reference station, the first difference method, another way to calculate the anomalies, enables one to compute anomalies of more stations (Peterson et al., 1998).

Table 5.1. A sample data set of climate anomalies for the Little Falls Mill ST station (ID 4257448004) of the United States. Unites is [°C], –9999 stands for missing data, and –8888 indicates the existence of station data whose anomaly cannot be calculated

Year	J	F	M	A	M	J	J	A	S	O	N	D
1961	-2.44	0.36	-0.82	-1.52	-8888	-0.51	-0.23	0.31	-8888	-8888	-0.56	-8888
1962	0.36	-1.34	-0.12	0.08	-8888	1.09	-1.13	-0.19	-8888	-8888	-2.46	-8888
1963	-0.94	-2.84	-0.32	-0.52	-8888	0.49	0.87	-1.39	-8888	-8888	3.04	-8888
1964	-9999	-9999	-9999	-9999	-8888	-9999	-9999	-9999	-8888	-8888	-9999	-8888
1965	-9999	-9999	-9999	-9999	-8888	-0.71	-1.43	0.61	-8888	-8888	-0.76	-8888
1966	0.16	0.86	0.98	-1.32	-8888	0.59	0.97	0.61	-8888	-8888	2.04	-8888
						.....						
1987	-0.14	-2.54	1.78	1.98	-8888	0.19	0.17	-1.69	-8888	-8888	-0.96	-8888
1988	-9999	-9999	-9999	-9999	-8888	-1.71	1.17	0.41	-8888	-8888	-9999	-8888
1989	-9999	0.16	-9999	-2.42	-8888	-9999	-0.83	-0.79	-8888	-8888	-0.86	-8888
1990	5.26	2.26	0.18	-9999	-8888	-9999	-9999	-1.49	-8888	-8888	-9999	-8888

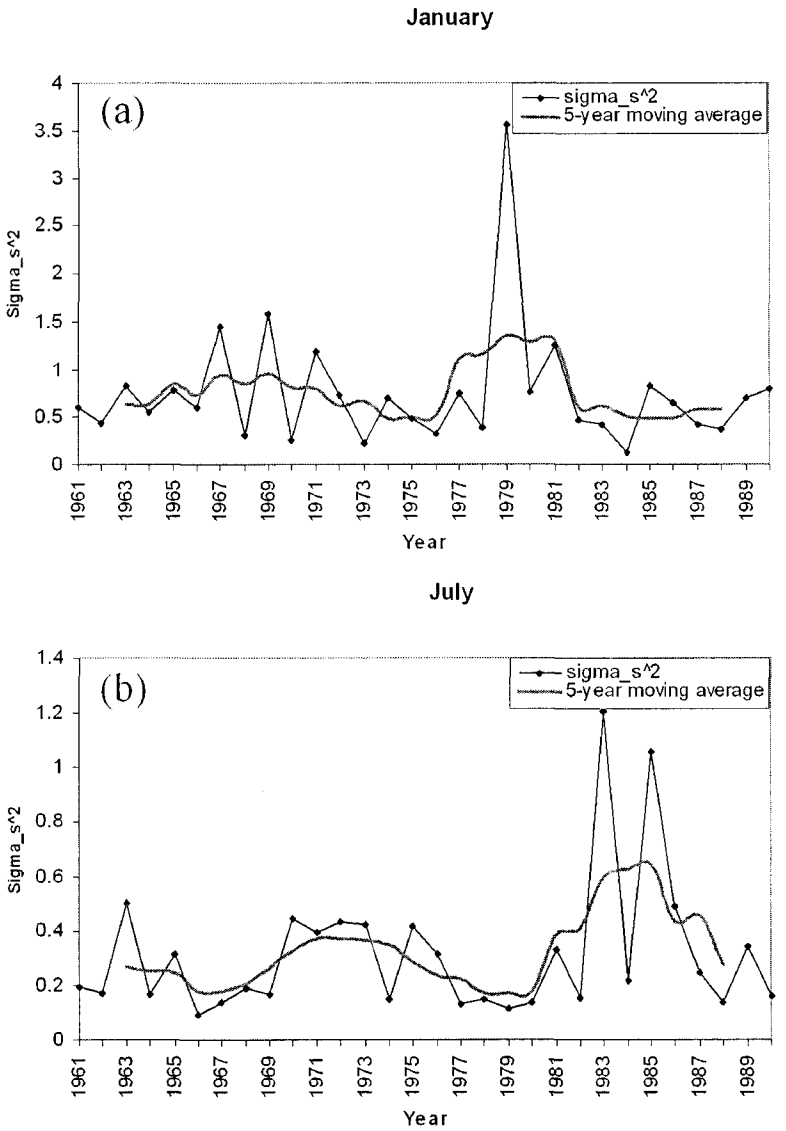

Figure 5.4. Time series and their 5-year MTW smoothed series of the spatial variances over a validation box (120°-125°W, 45°-50°N). The January results are computed from 41 stations with complete records and the July results from 35 stations with complete records. Units: $[°C]^2$.

The error variance is intended to be calculated for the anomalies data. For a given month in the GHCN history from January of 1835 to December of 2003, a grid box has K stations, of which N stations have anomalies, where $N \le K$ and, K is zero for the data-void grid boxes.

The spatial variance σ_s^2 needs an approximation since $\bar{T}$ is unknown. In this study, σ_s^2 is estimated by

$$\hat{\sigma}_s^2 = \left\langle \frac{1}{N} \sum_{j=1}^{N} \left(T_j(t) - \hat{\bar{T}}(t) \right)^2 \right\rangle. \tag{5.12}$$

Then two questions remain: what time window should be used for the temporal mean that replaces the ensemble average? How large should the N be when the spatial variance is computed? Following the idea of piecewise stationarity and the MTW of Folland et al. (2001), a 5-year MTW is chosen for the temporal mean. After some numerical tests of regression, $N=4$ is chosen as the minimum number of stations of a box on which the spatial variance is estimated. The estimation procedure is given below.

The spatial variance for the tth year, for a given month, is computed by

$$\sigma_{s,t}^2 = \frac{1}{N} \sum_{j=1}^{N} \left(T_j(t) - \bar{T}_N(t) \right)^2 . \tag{5.13}$$

This variance $\sigma_{s,t}^2$ varies from year to year. A 5-year MTW is chosen to smooth the year-to-year fluctuation

$$\hat{\sigma}_s^2(t) = \frac{1}{\|MTW(t)\|} \sum_{\tau \in MTW(t)} \sigma_{s,\tau}^2 . \tag{5.14}$$

Here, the 5-year *MTW(t)* is centered around year *t*, and $\|MTW(t)\|$ denotes the number of years of the *MTW(t)* with data. If $\|MTW(t)\| \geq 3$, the above calculation for $\hat{\sigma}_s^2(t)$ is implemented. Otherwise, $\hat{\sigma}_s^2(t)$ is not computed. For the validation grid box (120°-125°W, 45°-50°N), the $\hat{\sigma}_s^2(t)$ variations and their moving averages in a 5-year MTW from 1961 to 1990 for January and July are shown in Fig. 5.4. This figure used 41 stations for January and 35 stations for July in the grid box with 30 years of complete data.

5.3.3 Validation of the regression error model

The following will validate the regression error model (5.10). The validation is made for the year 1975 over the two station-dense validation grid boxes in the United States: (70°-75 °W, 40 °-45 °N) and (120°-125°W, 45°-50°N). Since each box contained over 30 stations in the MTW centered around 1975, the simple average of all the stations is considered the "true" average, i.e., the "true" grid box value. The square differences of the "true" average and the average of the sub-samples enables the computation of "true" mean square error. The computing scheme may be described as follows. Suppose that a box has *N* station anomalies and *N* is reasonably large, then the "true" average temperature anomaly of the box is

$$\hat{\bar{T}}_N(t) = \frac{1}{N}\sum_{i=1}^{N} T_i(t)\,. \tag{5.15}$$

Sub-samples of the N stations are taken. The average of the sub-sampled temperatures with *n* stations is

$$\hat{\bar{T}}_n(t) = \frac{1}{n}\sum_{i=1}^{n} T_{n,i}(t), \tag{5.16}$$

where $T_{n,i}$ is the ith station's anomaly temperature in the sub-sample network of size n.

Sub-samples of size n are taken from the N stations, where $1 \le n \le N \ge 4$. The total number of sampling ways is equal to $C_N^n = \frac{N!}{(N-n)!n!}$. This number can be very large when both N is large and $n = N/2$ or $(N+1)/2$. For example, if N=20 and n=10, the total number of sub-samples is 184,756. A long computing time is required to exhaust the sub-samples. Further, the GHCN network has over 30 grid boxes with more than 25 stations, and hence, the exhaustive sub-sampling is computationally unrealistic. Fortunately, it is unnecessary in climate physics to exhaust all the combinations since (i) some samples have all the stations in a small sub-region of the grid box, and this situation is undesirable, and (ii) some samples result from the replacement of only one station nearby, and hence, these samples are highly correlated. Thus, it is decided that only 1000 random sub-samples are used in the calculation.

If the average of the N-station sample is regarded as the "truth", we estimate the mean square error (MSE) between the "truth" and n-station sub-sample. The MSE is

$$E_n^2 = \frac{1}{1000}\sum_{n \in S_{1000}} \left(\hat{\bar{T}}_N - \hat{\bar{T}}_n\right)^2, \tag{5.17}$$

where S_{1000} stands for the set of 1000 random sub-samples. The MSE for the exhaustive samplings is calculated according to the formula

$$E_n^2 = \frac{1}{C_N^n} \sum_{n \in S_{Ex}} \left(\hat{\bar{T}}_N - \hat{\bar{T}}_n \right)^2 , \tag{5.18}$$

where S_{Ex} stands for the set of exhaustive sub-samples.

To examine the difference between the 1000 random n-station samplings without replacement and the exhaustive samplings, a comparison is made for the results from both samplings. Figure 5.5 shows the comparison for the case of *N=27* stations for the grid box (120°-125°W, 40°-45°N) in January 1961. The error results from the 1000 random samplings and those from the exhaustive samplings are almost the same. In January 1961, the grid box had 50 stations. We choose not to use all the 50 stations since the number of exhaustive samples is $C_{50}^{25} = 126{,}410{,}606{,}437{,}752$. This number is too large to be handled by our computers. A smaller number 27 is thus chosen. Even with 27 stations, when the sub-sample size is 13, the number of exhaustive samples is as large as 280,816,200. Figure 5.5 implies that 1,000 random sub-samples are appropriate to assess the "true" MSE E_n^2.

Since the purpose of our model validation is to verify whether E_n^2 is inversely proportional to n, applying the 5-year MTW to E_n^2, the estimated $\hat{E}_n^2 = \frac{1}{\|MTW(t)\|} \sum_{\tau \in MTW(t)} E_n^2(\tau) \approx \langle E_n^2 \rangle$ MSE values are regressed against $1/n$. For each month and each grid box of N station anomalies, the *N-1* data pairs

$$\left(\frac{\hat{E}_n^2}{\hat{\sigma}_s^2}, \frac{1}{n} \right) \quad (n = 1, 2, 3, \ldots, N-1) \tag{5.19}$$

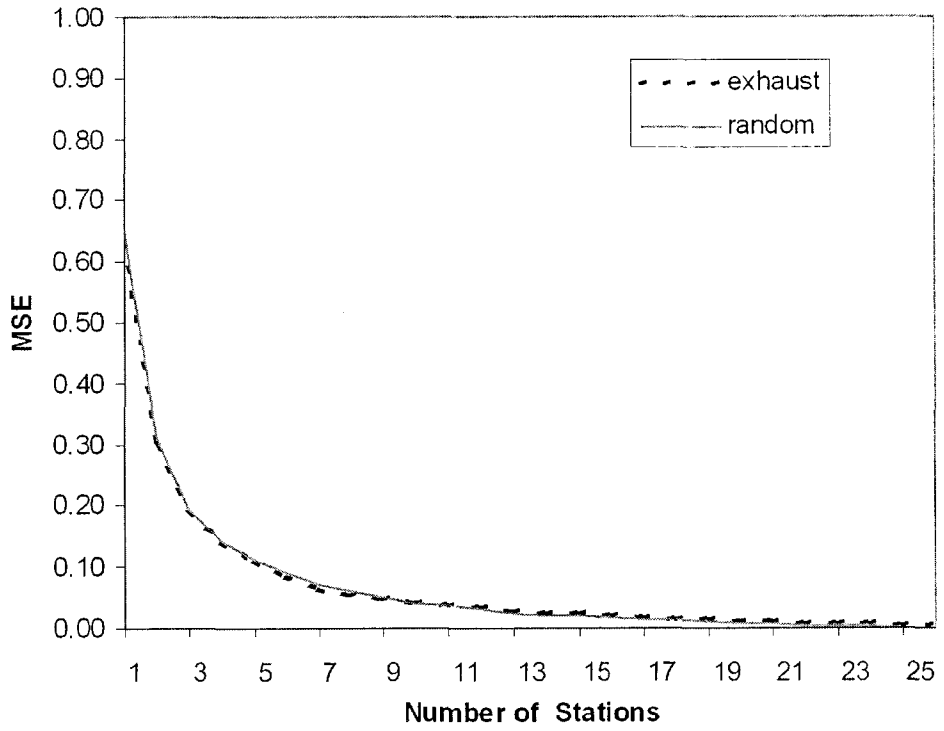

Figure 5.5. The "true" MSE of January 1961 computed from the 1,000 random samplings and the exhaustive samplings, respectively, for the grid box (120°-125°W, 45°-50°N). Twenty seven stations in the grid box are used.

are used in the regression

$$\frac{\hat{E}_n^2}{\hat{\sigma}_s^2} = \alpha_s \times \frac{1}{n} \tag{5.20}$$

to find the correlation factor α_s. Again, since the correlation factor α_s is expected to be a physical property of the temperature anomalies over a grid box, we wish to demonstrate that the α_s value is insensitive to the size of full samples. Table 5.2 shows the results of α_s values for the sizes of the full samples *N=30, 20, 10, 9, 8, 7, 6, 5*, and *4* stations for the two validation grid boxes (70°-75°W, 40°- 45°N) and (120°-125°W, 45°-50°N) for January and July of 1975. Of course, the largest full sample gives the best approximation to the "true" α_s value for the grid box at a given month. The samples of 20, 10, ..., 4 are sub-sets of the 30-station sample and are picked visually to maintain an even spatial distribution. The α_s value differences among the nine samples are less than 20%. Considering the observational uncertainties of the monthly temperature, this difference may be attributed to the random errors.

The robustness of the α_s value is further demonstrated by the regression curves shown in Fig. 5.6. The regression curves indicate that the 1/n decay of the error variance is an appropriate formulation to measure the error variance. This figure provides evidence to support both J97's and our own error formulations. The α_s values in Table 5.2 are derived from these regression curves.

The same test is used to demonstrate that the spatial variance σ_s^2 is a physical property of a grid box. The results in Table 5.2 indicate that σ_s^2 fluctuations

according to the sample size may be attributed to random errors. Thus, this table supports that σ_s^2 is insensitive to the number of stations when the number is sufficiently large.

It is well known that both the temporal and spatial variances of the surface air temperature have clear seasonality over the validation grid boxes. However, the correlation factor varies little throughout the seasons. Figures 5.7(a) and (b) show that the seasonal variation is less than 5% for 1973 and less than 15% for 1891. The 1891 results might be due to sparse sampling, and hence, much of the variation may be attributed to random errors.

Figures 5.7 (c) and (d) show the seasonality of the sampling error variance. Since the correlation factor does not vary much with season, the error variance's seasonal variation is driven by the seasonality of the spatial variance and the variations of the number of stations in the grid box. As one may expect, the error is larger in winter than in summer, particularly when the sample size is not very large.

The last validation step of the regressional error model is to check the goodness of the fit by considering the "true" MSE $\hat{E}_n^2$ and the estimated MSE $E^2 = \alpha_s \hat{\sigma}_s^2 / n$ over the two validation grid boxes. Only the stations with complete records from 1959 to 1992 are used in this step. The grid box (120°-125°W, 45°-50°N) had 33 stations in January and 28 stations in July. The grid box (70°-75°W, 40°-45°N) had 41 stations in January and 40 stations in July. The "true" MSE $\hat{E}_n^2$ is computed for

Table 5.2. Sensitivity test for the values of spatial variance $\hat{\sigma}_s^2$ and the correlation factor α_s over the grid boxes (70°-75°W, 40°- 45°N) and (120°-125°W, 45°-50°N) when the sub-sample size n= 30, 20, 10, 9, 8, 7, 6, 5, and 4. The results are for the year 1975

	Box (70-75W, 40-45N)				Box (120-125W, 45-50N)			
	January		July		January		July	
Number of stations	σ_s^2	α_s	σ_s^2	α_s	σ_s^2	α_s	σ_s^2	α_s
30	0.39	0.95	0.30	0.97	0.50	0.98	0.28	0.99
20	0.35	0.92	0.34	0.93	0.47	0.99	0.27	0.97
10	0.40	0.86	0.36	0.93	0.54	1.01	0.32	0.92
9	0.27	0.82	0.26	0.89	0.57	0.96	0.31	1.01
8	0.30	0.83	0.26	0.89	0.55	0.97	0.34	0.87
7	0.34	0.84	0.19	0.84	0.54	0.96	0.20	0.80
6	0.30	0.96	0.22	0.85	0.58	0.97	0.22	0.80
5	0.31	0.99	0.25	0.90	0.64	1.00	0.22	0.82
4	0.34	0.93	0.28	0.95	0.70	1.02	0.23	0.88

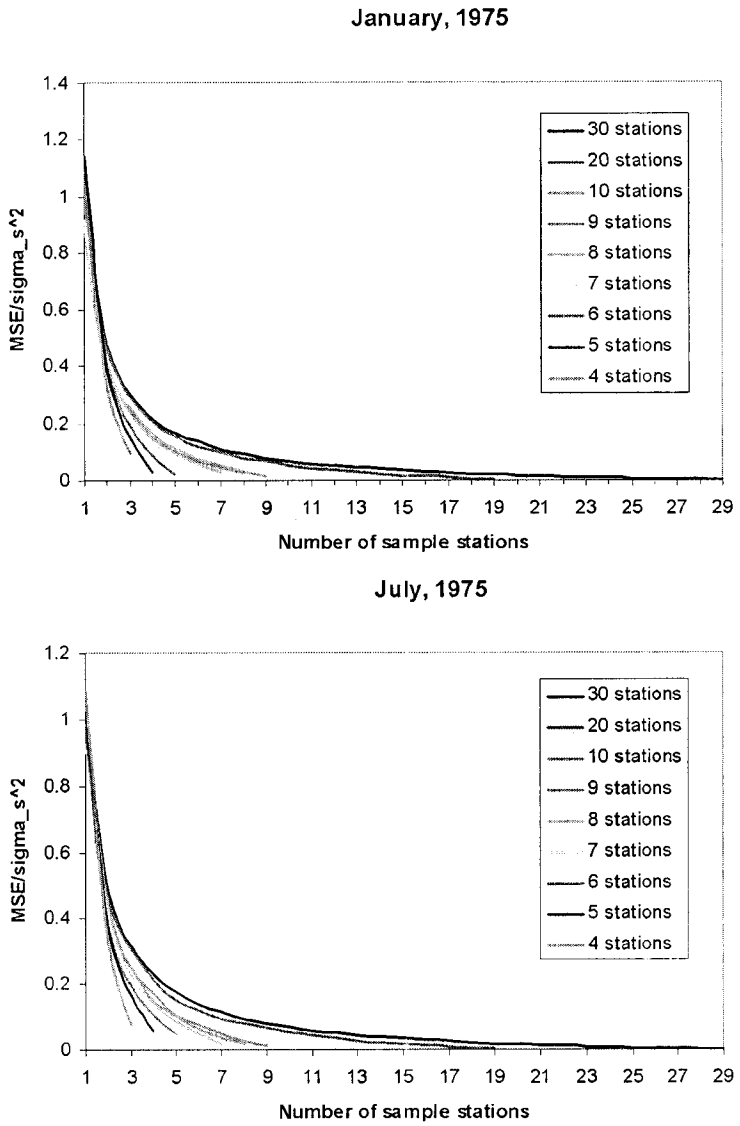

Figure 5.6. The ratio of the 5-year MTW smoothed "true" MSE $\hat{E}_n^2$ to the 5-year MTW smoothed spatial variance $\hat{\sigma}_s^2$ as a function of the number of sample stations for the grid box (70°-75°W, 40°- 45°N) in the eastern United States when the total number of stations is N= 30, 20, 10, 9, 8, 7, 6, 5, and 4 stations: (a) January 1975, and (b) July 1975.

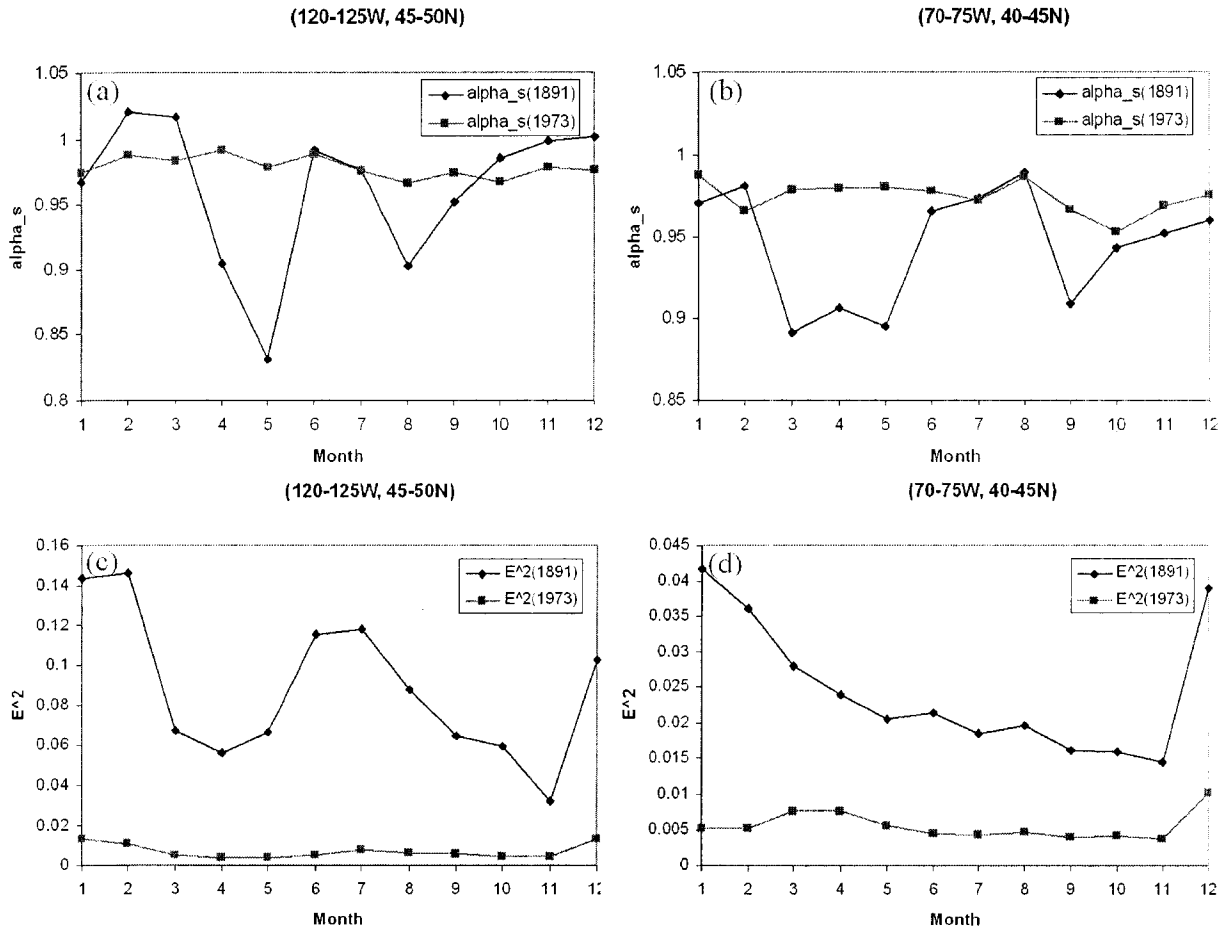

Figure 5.7. The regression parameter α_s, and error variance E^2 as a function of the month for the two grid boxes in the US. The units for the error variance is [°C]^2.

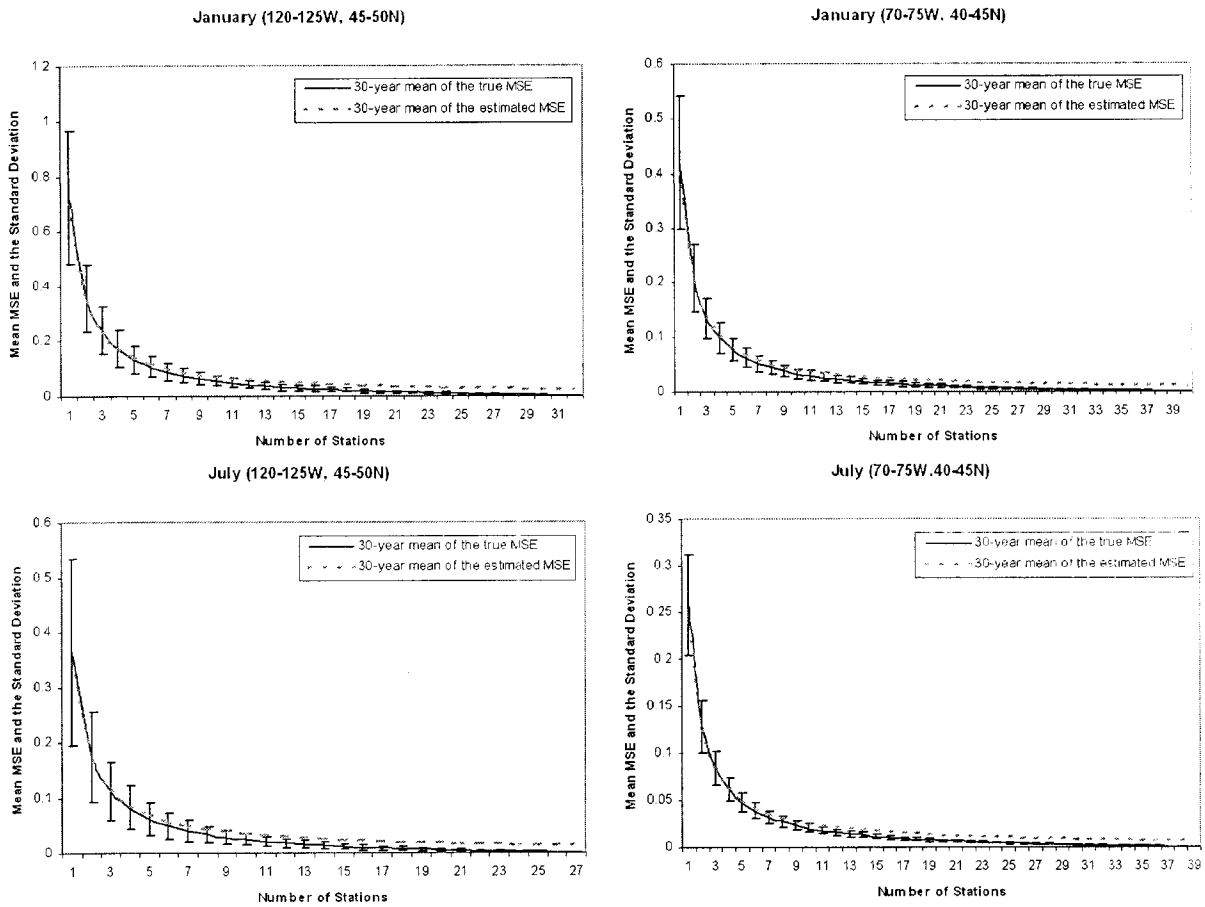

Figure 5.8. The 1961-1990 30-year mean of the "true" MSE (solid line) and the 1961-1990 30-year mean of the estimated MSE (dashed line) for the grid boxes (120°-125°W, 45°-50°N) and (70°-75°W, 40°-45°N). The bars on each side of the mean are the one-standard deviations of the 30 "true" MSE values. Units: $[°C]^2$.

January and July for every year from 1961 to 1990. The solid curve of Fig. 5.8(a) shows the mean of the 30 values of $\hat{E}_n^2$, and the bars indicate one-standard deviation on each side. The same mean is computed for the estimated MSE $E^2 = \alpha_s \hat{\sigma}_s^2 / n$ and is depicted by the dashed line in Fig. 5.8(a). The closeness of the solid and dashed line and the reasonable range of one-standard deviation imply the good fit of MSE to $\alpha_s \hat{\sigma}_s^2 / n$.

Figures 5.8(b), (c), and (d) are obtained in a similar way. Again, these results all support the $\alpha_s \hat{\sigma}_s^2 / n$ error variance model.

5.3.4 Interpolation of α_S and σ_S^2

The values of the regression coefficient α_s are obtained for the grid box at the month of at least four stations with temperature anomaly data. These values are interpolated onto other grid boxes so that every grid box has an α_s value. The interpolation method is a kind of nearest-neighbor-assignment method on a sphere and has two steps. First, the values of α_s are interpolated among the boxes of the same latitude. For a given grid box without an α_s value, one searches to the west and to the east and assigns the value from the nearest box to it. If two boxes with data are found to be the same distance from the box, then the average of the two values is assigned to the box. This step fills up all the boxes on the 5-degree latitude band as long as this band contains at least one grid box that has four or more stations with anomaly data. Second, for the 5-degree latitude band that does not contains any grid box with four or more stations, the α_s values for the grid boxes of this band have to be interpolated

from the north and south boxes. Since most of the blank bands that include land areas are in the north in both hemispheres, the southern grid boxes with the α_s values are given priority. Thus, for a grid box that has not acquired values from step 1, one searches to the south first and assigns the α_s value from the nearest grid box to it. If no value is found from the southern boxes, one searches to the north and assigns the value from the nearest grid box to it.

The $\hat{\sigma}_s^2$ values are interpolated to the globe in the same way as the α_s values. Thus for each month from January 1837 to December 2001, each grid box over the globe has α_s, $\hat{\sigma}_s^2$ and N values, where N is the actual number of stations in the grid box and is not the number of stations with anomaly data since they may be computed in different ways that may enable different grid boxes to be used to compute the anomaly data. Of course, when N=0, the error is not needed. Eventually, the error variance of the GHCN grid box data for a given box and a given month is computed by

$$E^2 = \frac{\alpha_s}{N}\hat{\sigma}_s^2 . \tag{5.21}$$

5.4 Results

5.4.1 Global results of the error variance on each grid box

According to the procedures described in the above section, the error variance can be calculated according to formula (5.21) for each grid box that had stations from

January 1837 to December 2001. Each month from January 1837 to December 2001 has an error map showing the error variance on each grid box with station data. Four error maps of selected months (February 1853, August 1891, January 1940, and July 1973) from data-sparse to data-dense cases are shown in Fig. 5.9. It is obvious that the fewer the number of stations, the larger the error variances. For the northern hemisphere, the errors are usually large in the north where the numbers of stations are few and spatial variances are large. Some costal grid boxes have large error variances, which are attributed mainly to strong temperature inhomogeneity, and hence, large spatial temperature variances. The large errors of the northern and coastal grid boxes for the northern hemisphere imply that smaller weights should be assigned to these grid boxes when their data are used to calculate the global or regional average or interpolation. Optimal averaging and interpolation methods should automatically take these weights into account.

The maximal error variance in a grid box from January 1837 to December 2001 was 9.506$[°C]^2$ in January 1935 in some grid boxes in the latitude band 60-75N where the grid box has only one station and a large spatial variance. The minimal error variance was 0.001$[°C]^2$ and occurred in October 1993 due to large number of stations in this grid box.

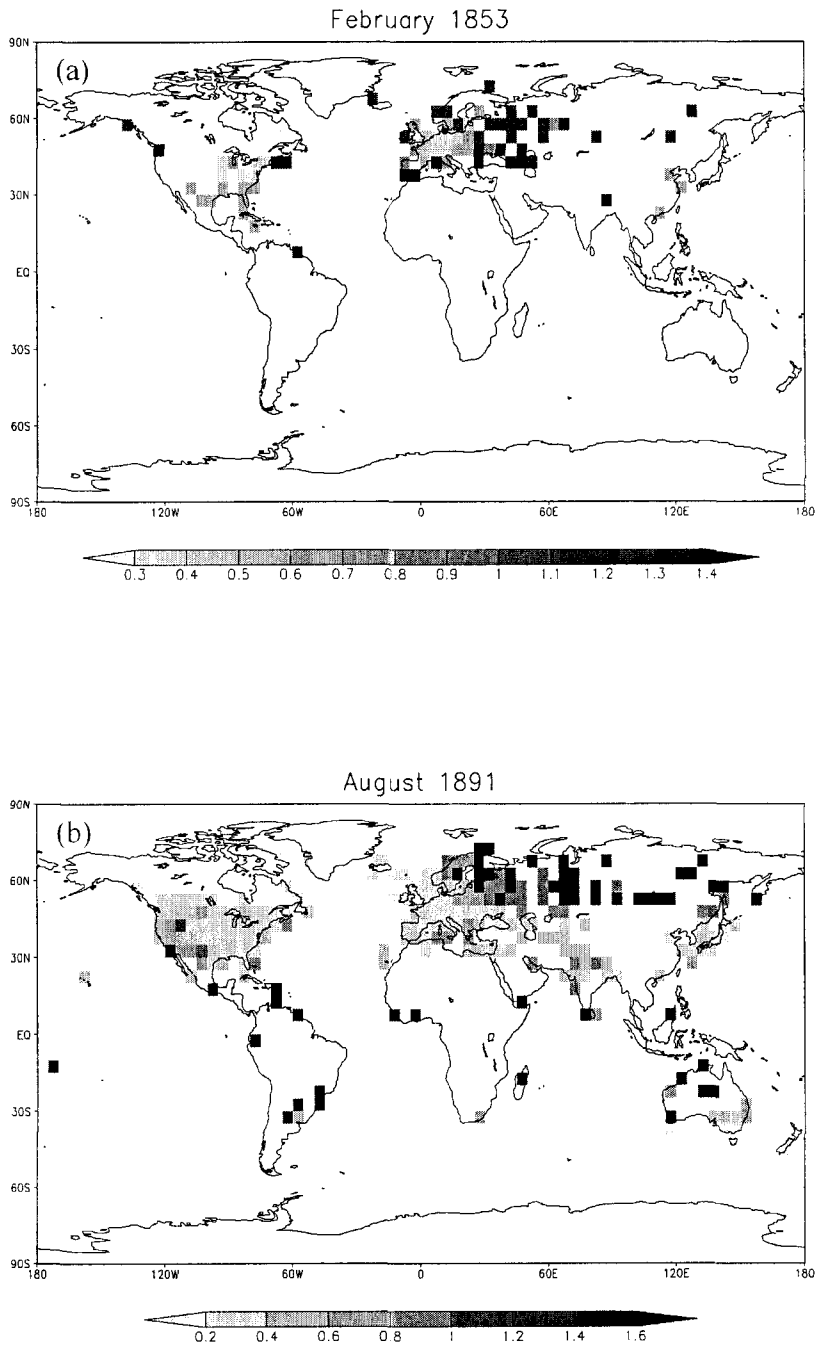

Figure 5.9. Maps of the estimated error variances of the grid boxes with data for four selected months. Units: $[°C]^2$.

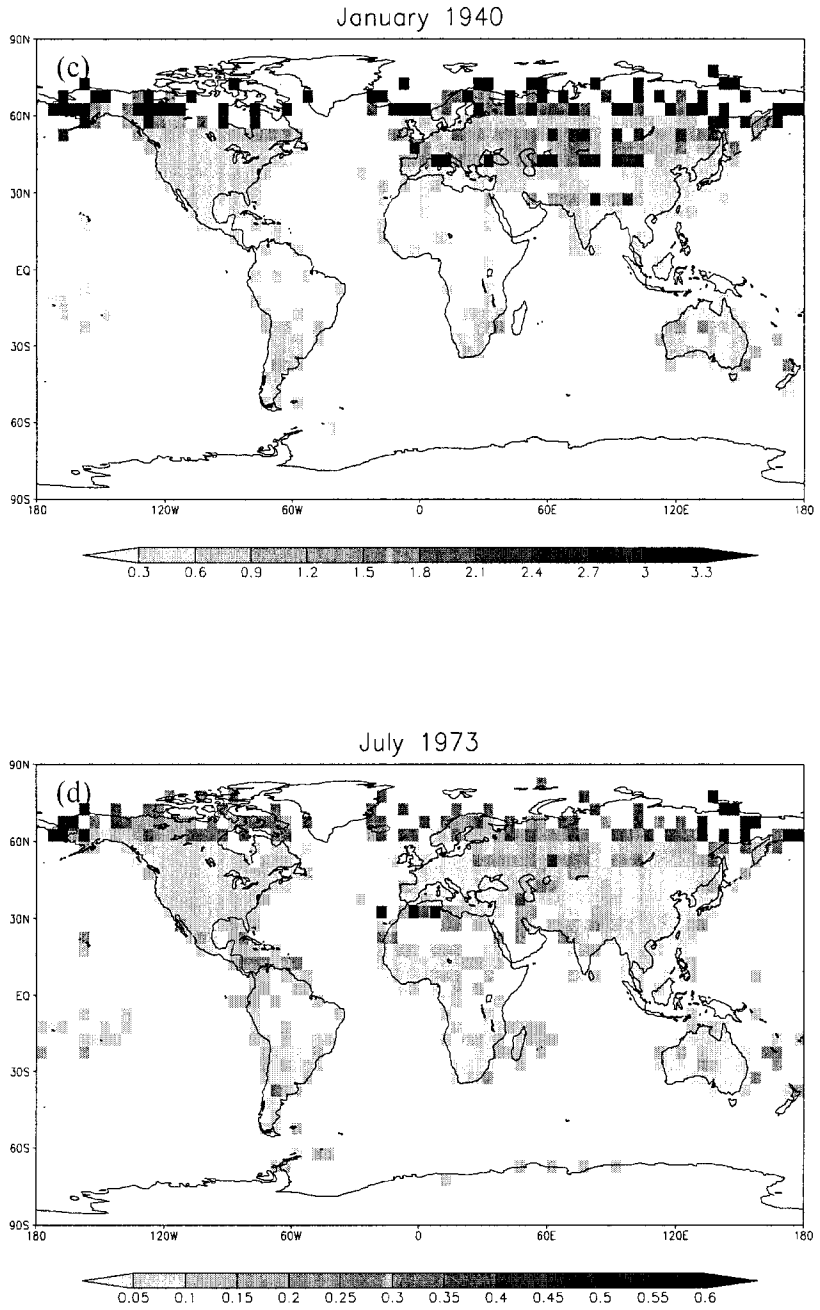

Figure 5.9. Continued.

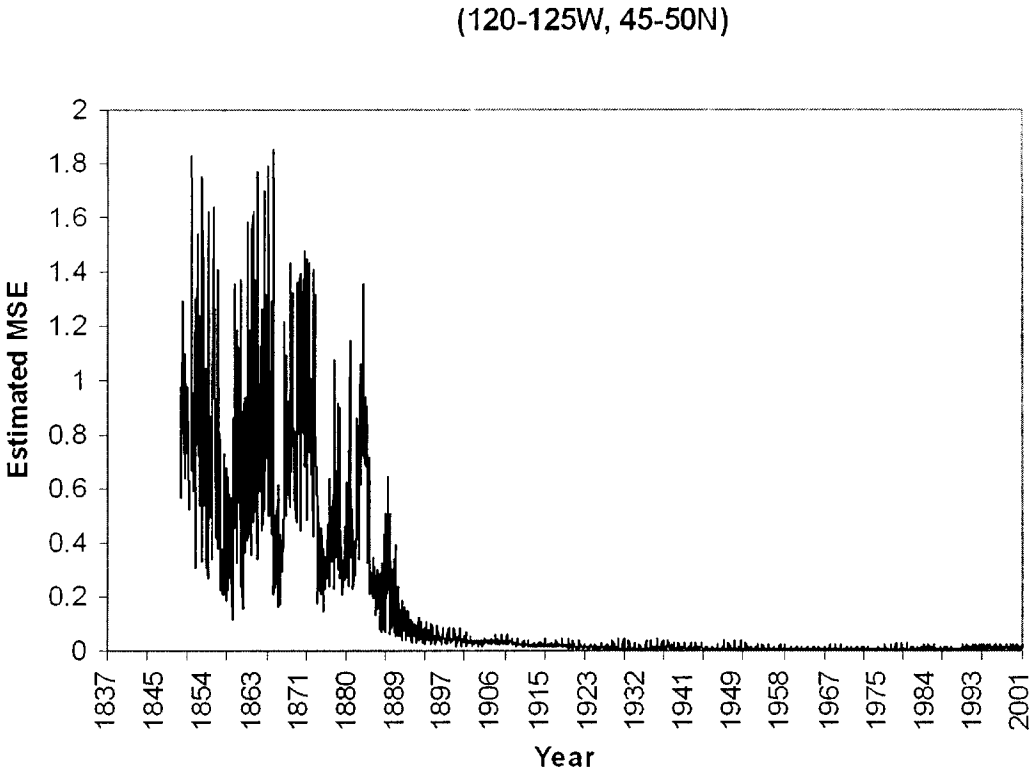

Figure 5.10. Monthly time series of the estimated MSE for the grid box (120°-125°W, 45°-50°N) from December 1849 to December 2001. Units: $[°C]^2$.

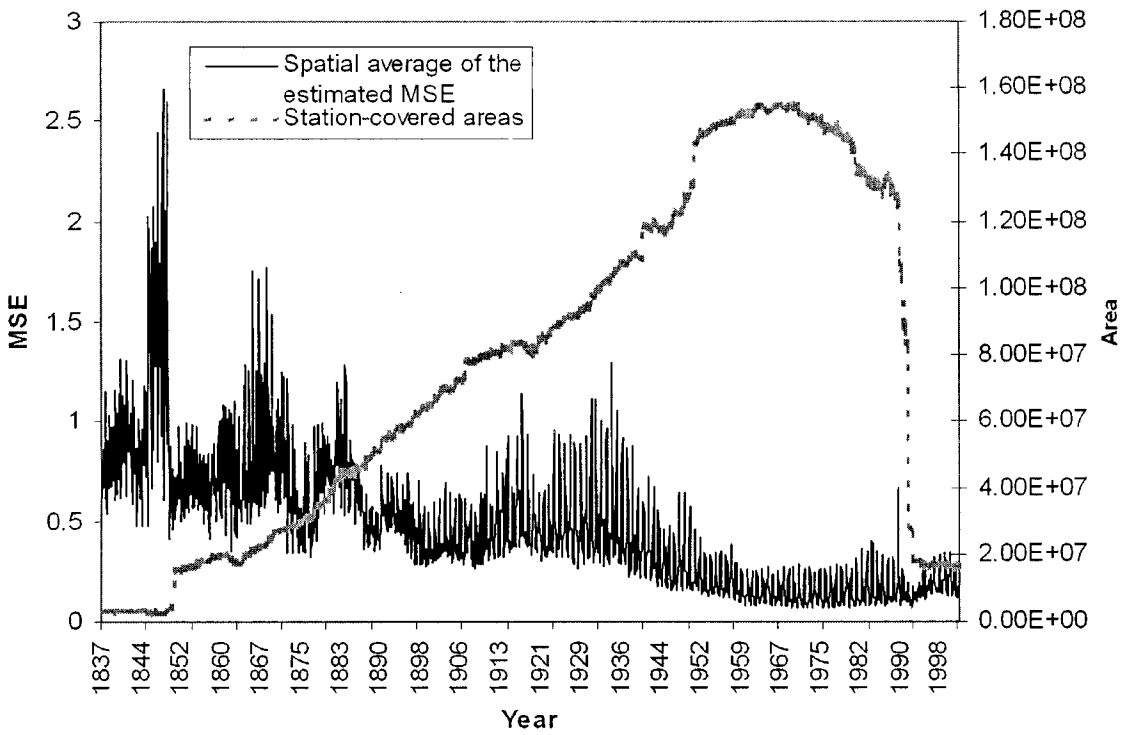

Figure 5.11. Time series of the spatial average of the estimated MSE (solid line, units: $[°C]^2$) and the time series of the station-covered areas (dashed line, units: $[km]^2$) from January 1837 to December 2001.

To examine the temporal variations of the error variance of a grid box in detail, the validation grid box (120°-125°W, 45°-50°N) is used and the estimated error variance is still computed according to formula (5.21). The time series of the error variance for this grid box started from December 1849 and ended at December 2001 (Fig. 5.10). This time series demonstrates two properties of the error: seasonality and station density. The error is larger in the winter months than in the summer months due to the larger spatial variances of the winter temperature. This seasonality is also demonstrated in Figs. 5.7(c) and (d). Fig. 5.4 shows that the spatial variance of the winter temperature for this validation box is about 2-3 times larger than that of summer. After 1890, the station density of this validation box became large, and the seasonal fluctuation of the error variance was effectively suppressed and small.

Another interesting property of the error variance is the change of its average value in the global scale. The global spatial average (i.e., area-weighted average) of the error variance values is calculated and displayed in Fig. 5.11. The station-covered areas are also displayed in the figure. The clear seasonality of the globally averaged error variance is attributed mainly to the northern hemisphere data since they were numerous. The figure shows the clear increase of the station-covered areas from 1837 to the early 1980s. The station density did not increase uniformly, and hence, the average error variance did not decrease sharply during this period. Also, although there is a drop of the station-covered areas since 1990s, the average error variance did not jump up. Note that the spatially averaged MSE shown in Fig. 5.11 is the average of error variances of all the data boxes. Although the coverage of the station observations sharply decreased (due to the NCDC's data gathering time-lag of about

10 years), sixty percent of these boxes had at least four stations (Fig. 5.12), thus the error variances of these boxes with data are small. Consequently, the average of these boxes' error variances is small. However, many boxes were data void during this period.

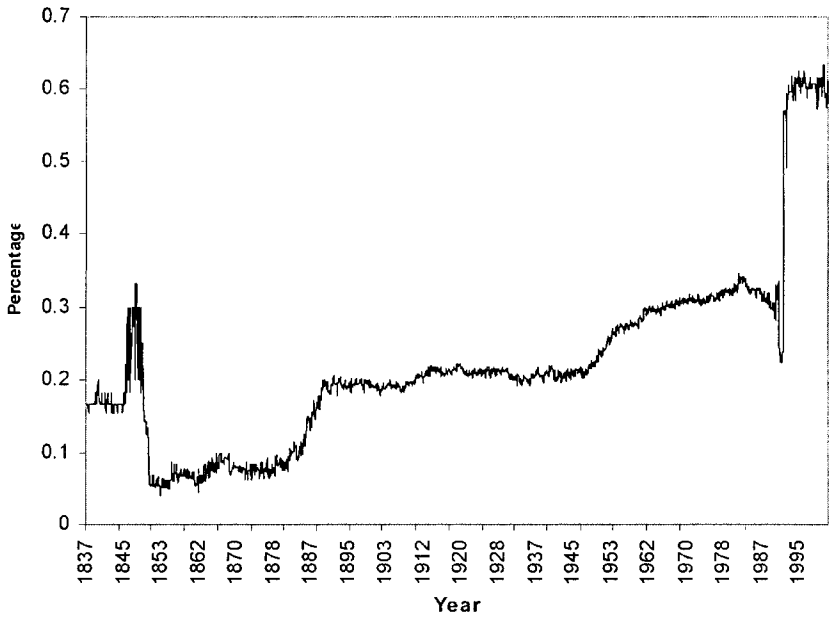

Figure 5.12. The ratio of the number of boxes with at least four stations to the number of boxes with data.

5.4.2 Comparison with J97's data

The output of J97's error estimates were in seasons defined by each consecutive three months starting from DJF in every decade from 1851 for two time scales: interannual and interdecadal. The error variances were calculated for every $5^{\circ} \times 5^{\circ}$ grid box. For the grid box without observational data, error variance was also computed, where it was slightly smaller than the spatially averaged temporal variance.

The output of our error values for the monthly $5^{\circ} \times 5^{\circ}$ data also begins January 1851, when the GHCN network had 158 stations. For each month from January 1851 to December 2001, if a grid box had observed data, this box datum is assigned an error variance. The grid box without observations in a certain month has no error variance values and is assigned –999.000.

Due to different time scales and different output, it is not fair to compare directly the values of the error variances of J97 and ours from grid to grid and from month to month. A method of fair comparison is that the parameters of the errors formulas of J97 and ours are re-calculated under the same time scale and the same number of sampling stations. From J97's error formula (5.5) and our error formula (5.10), the comparison can thus be made by comparing the values of the following two quantities $s_0^2(1-\bar{r})$ and $\alpha_s \hat{\sigma}_s^2$, which are the error variance of a box with one single sample station. Again the station-dense grid boxes (120°-125°W, 45°-50°N) and (70°-75° W, 40° -45° N) are used for the comparison since they allow one to estimate the "true" error variances and, hence, to compare J97's and our own error results with

the "true" errors. The year 1975, which is in the middle of climatology period 1961-1990, is chosen for the comparison.

Since the interdecadal and interannual means were used in J97, two MTWs of different window lengths are considered here: one of 5 years and another of 29 years. The 29-year MTW covers almost the entire climatology period of 1961-1990. The results computed from the 29-year MTW are included in the round brackets (Table 5.3). The last column contains the values of the "true" error variance.

Table 5.3 implies the following. (i) Our errors and those of J97 are in the same order, but ours are consistently larger in both the 5-year and 29-year MTWs. The differences are large and in the range of 30-100% in the 5-year MTW, and they become very small (less than 10%) in the 29-year MTW. (ii) In most cases, our error variances are closer to the "true" error variances than those of J97 (this difference is due mainly to our regressional method of error estimate since our errors are the fitting results with the "true" errors when more than four stations are in a grid box). And (iii) the parameter estimates are smoother for the 29-year MTW than for the 5-year MTW, but the realistic error variances of the GHCN grid box temperature anomaly data should take the less smooth results because of the anomalies' spatial variations. Thus, the final product of our error variances for the GHCN data is calculated by using the 5-year MTW.

Table 5.3. Comparison between the results from the formula (5.10) and J97's formula. The comparison is done for the year 1975. The 29-year MTW results are in round brackets, and the other results are from the 5-year MTW. The MSE(1) is the "true" MSE computed from the mean of the 1000 random 1-station samplings

	Box (120-125W, 45-50N)						
	s_0^2	r	$s_0^2(1-r)$	α_s	σ_s^2	$\alpha_s\sigma_s^2$	MSE(1)
January	1.27(4.18)	0.73(0.86)	0.34(0.58)	0.98(0.97)	0.50(0.75)	0.48(0.73)	0.50
February	1.94(2.70)	0.83(0.84)	0.34(0.45)	0.98(0.97)	0.49(0.52)	0.48(0.50)	0.51
March	0.70(1.53)	0.83(0.86)	0.12(0.22)	0.98(0.97)	0.24(0.23)	0.23(0.22)	0.24
April	1.33(1.38)	0.90(0.87)	0.13(0.18)	0.97(0.97)	0.22(0.19)	0.22(0.19)	0.21
May	0.81(0.98)	0.89(0.80)	0.09(0.19)	0.97(0.97)	0.20(0.20)	0.19(0.20)	0.20
June	0.92(1.54)	0.87(0.81)	0.12(0.29)	0.98(0.97)	0.30(0.31)	0.29(0.31)	0.31
July	0.60(0.99)	0.71(0.68)	0.18(0.32)	0.98(0.97)	0.29(0.32)	0.28(0.31)	0.29
August	2.12(1.54)	0.91(0.82)	0.20(0.28)	0.98(0.97)	0.30(0.31)	0.29(0.30)	0.30
September	1.18(1.75)	0.84(0.85)	0.19(0.27)	0.97(0.97)	0.29(0.31)	0.28(0.30)	0.31
October	0.28(1.15)	0.40(0.79)	0.17(0.24)	0.97(0.97)	0.22(0.26)	0.21(0.25)	0.22
November	1.31(2.69)	0.89(0.90)	0.14(0.26)	0.97(0.97)	0.26(0.31)	0.26(0.30)	0.28
December	0.56(3.35)	0.47(0.86)	0.30(0.48)	0.96(0.97)	0.48(0.61)	0.46(0.59)	0.47

Table 5.3. Continued.

	Box (70-75W, 40-45N)						
January	8.05(5.61)	0.96(0.93)	0.30(0.39)	0.97(0.97)	0.43(0.42)	0.42(0.40)	0.44
February	2.29(4.91)	0.89(0.93)	0.25(0.36)	0.95(0.96)	0.35(0.44)	0.34(0.42)	0.36
March	3.54(2.74)	0.95(0.89)	0.19(0.30)	0.97(0.96)	0.44(0.35)	0.43(0.34)	0.45
April	2.66(2.07)	0.94(0.84)	0.16(0.33)	0.97(0.96)	0.34(0.37)	0.33(0.35)	0.36
May	2.70(2.11)	0.89(0.83)	0.30(0.37)	0.96(0.95)	0.44(0.38)	0.42(0.36)	0.43
June	1.27(1.04)	0.85(0.74)	0.19(0.27)	0.97(0.95)	0.30(0.27)	0.30(0.26)	0.31
July	0.71(0.79)	0.74(0.67)	0.19(0.26)	0.96(0.97)	0.29(0.26)	0.28(0.25)	0.29
August	0.85(1.17)	0.80(0.80)	0.17(0.23)	0.98(0.97)	0.31(0.25)	0.30(0.24)	0.30
September	0.48(1.65)	0.62(0.84)	0.18(0.27)	0.96(0.96)	0.28(0.28)	0.27(0.27)	0.26
October	2.56(2.36)	0.92(0.90)	0.20(0.24)	0.97(0.97)	0.33(0.26)	0.32(0.25)	0.32
November	3.17(2.25)	0.95(0.89)	0.15(0.25)	0.96(0.97)	0.26(0.26)	0.25(0.25)	0.26
December	4.53(5.83)	0.94(0.92)	0.29(0.46)	0.96(0.97)	0.48(0.54)	0.46(0.52)	0.48

For the interannual seasonal data, the maximal standard error (i.e., the square root of the error variance) of J97 is 4.184 °C in DJF for the grid box (50-55E, 80-85N) and the periods of 1851-1920 and 1961-1994, and the minimal standard error is 0.007 °C in JJA for the grid box (75°-80°W, 25°-30°N) and the period of 1991-1994. For the interdecadal data, the maximal standard error of J97 is 3.267 °C in DJF for the grid box (10°-15°E, 75°-80°N) for the decades of 1851-1920, while the minimal error is 0.002 °C in several grid boxes and decades. Our maximal standard error is smaller than J97's even in the interannual scale, and our minimal standard error is larger than that of J97's interdecadal results but smaller than its interannual results.

An obvious and important application of the error variances is the assessment of the uncertainties of the global average temperature. The methods of J97 and ours are different in this respect. The formulas (11) and (12) of J97 are based on the theory

of white spatial noise under the condition of effective degrees of freedom, while our formula (1) of this chapter is based on the explicit MSE estimation with spatial correlation and tele-connection taken into account by EOFs. Thus, we require only the error variances on the grid box with observations, while J97 required the values of error variances on all the grid boxes.

5.5 Summary and discussion

The error variances of the GHCN $5^{o} \times 5^{o}$ gridded data have been estimated using a regression approach. The calculation method is mathematically supported. The underlying assumption of the method is that the correlation coefficient is a physical parameter and is insensitive to the number of stations when the number is sufficiently large. Our method differs from that of J97. Our results are in the same order as those of J97, but our error variance values are consistently larger.

The errors for most grid boxes are from the extrapolation or interpolation of the two parameters: the spatial variance and the correlation factor. Fig. 5.13 shows the history of the number of grid boxes with the two parameters being computed and the total number of grid boxes with at least one station. The latter was usually more than three times of the former. Therefore, a question arises: is the interpolation of the two parameters valid? The answer to this question might need high-resolution GCM simulation results and the use of the spectral method for MSE over each grid box (Shen et al., 1998). Namely, the MSE expression by EOFs and their corresponding eigenvalues that were designed for global and regional optimal averages can be

applied to the spatial average over a grid box. The simulation data from atmospheric GCMs with high resolution are needed to prepare the EOFs and eigenvalues.

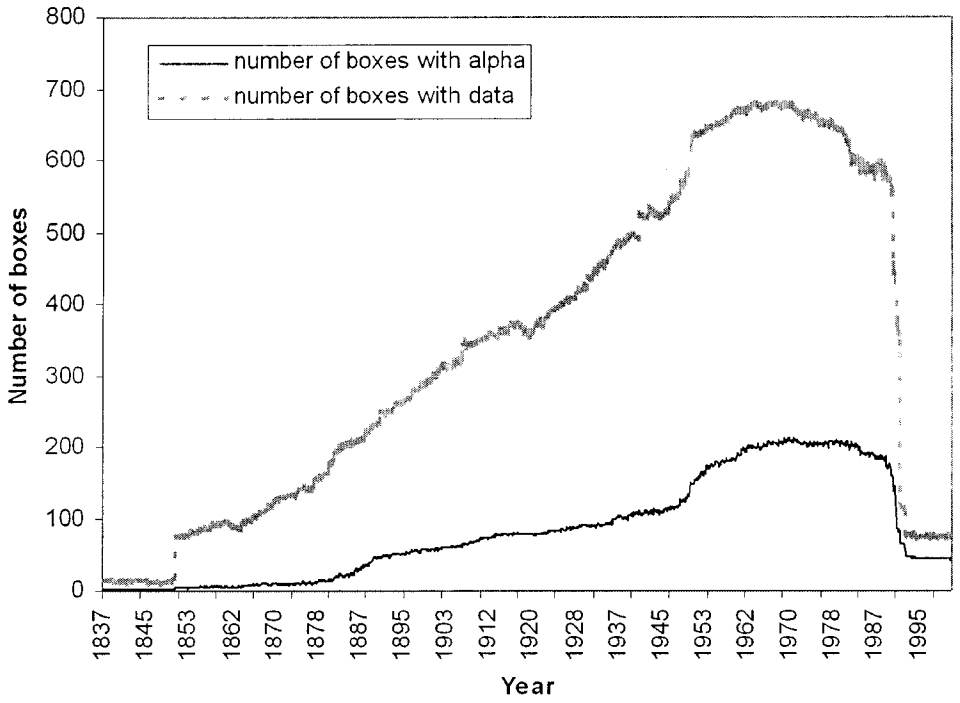

Figure 5.13. History of the number of grid boxes with the calculated values of spatial variance and correlation factor (solid line) and the total number of grid boxes with at least one station (dashed line).

These error variances can be used for various applications of optimal estimations, such as optimal averaging for the assessment of global or regional warming (Smith et al., 1994, Shen et al., 1998, and Folland et al., 2001). The applications of the estimated error variance product are not limited to optimal spatial averaging, it can be used for optimal spatial interpolation and any other optimal estimates based on minimizing the MSE between the true parameter and the estimated parameter as well. For example, Shen et al. (2004) derived a MSE formula for optimal interpolation, which also needs the error variances of the data.

Chapter 6

Summary and Discussion

Three topics related to climate change have been addressed in this thesis: agroclimatic change, error variance estimation of the climate dataset, and drought monitoring. Specifically, for the first topic, we analyze the agroclimatic changes of Alberta during the period of 1901-2002; for the second topic, a new method is developed to estimate the error variances of the $5^{\circ} \times 5^{\circ}$ Global Historical Climatological Network (GHCN) monthly surface air temperature data; for the third topic, we analyze the applicability of various drought indices in detecting droughts in Alberta. Their drought classification is also studied and a new drought index, PPCI, is proposed. In this chapter, we will summarize some of the main results.

Chapter 2 analyzes the long-term (1901-2002) temporal trends in the agroclimate of Alberta and explores the spatial variations of the agroclimatic resources and the potential crop-growing area in Alberta. Nine agroclimatic parameters are investigated: May-August precipitation, start of growing season, end of growing season, length of growing season, date of last spring frost, date of first fall frost, length of frost-free period, growing degree days, and corn heat units. The results support the following conclusions: (1) The Alberta PCPN has increased 14% from 1901 to 2002 and the increment is the largest in the north and the northwest of Alberta, then diminishes (or even becomes negative over two small areas) in central

and southern Alberta, and finally becomes large again in the southeast corner of the province. (2) No significant long-term trends are found for the SGS, EGS, and LGS. (3) An earlier LSF, a later FFF, and a longer FFP are obvious all over the province. (4) The area with sufficient CHU for corn production, calculated according to the 1973-2002 normal, has extended to the north by about 200-300 km compared to the 1913-1932 normal, and by about 50-100 km compared to the 1943-1972 normal; this expansion implies that potential exists to grow crops and raise livestock in more regions of Alberta than the past. One can conclude from the above results that the climate change since the last century has benefited agriculture in Alberta.

Of course, in order to understand the impact of the changing climate on Alberta agriculture, more quantitative studies are needed on parameters such as soil moisture and evapotranspiration that are closely related to plant growth. The interpolation method used to derive the long-term dataset did not consider the elevation effect, thus the values of mountain region are not as reliable as those in other regions. Improvement could be made if the topographic variation is implemented in the interpolation. In addition, only linear trend was analyzed in our current study. Other methods that detect trend in non-linear and non-stationary process would be explored in the future.

In Chapter 3 and 4, we have analyzed four kinds of existing meteorological drought indices and validated their applicability for drought assessment in Alberta. The indices include: the standardized precipitation index (SPI), the rainfall anomaly index (RAI), the standardized anomaly index (SAI) and the rainfall decile index (RDI). The numerical results over the Mixed Grassland ecoregion show that these

four indices can capture most of the drought events of Alberta during the 102-year (1901-2002) period. The correlation coefficients indicate high correlations between the indices and the precipitation. Using a percentile approach, we have classified the drought conditions of the four indices based on the probability of occurrence of the drought events. Furthermore, we have analyzed the 1901-2000 weekly precipitation and calculated the probabilities of the transition of the drought condition from one week to another for each ecoregion. In addition, we have proposed a new index, PPCI, which can reflect the spatial patterns of the variability through the EOFs and also can reflect the probability of occurrence of the drought events through an equi-probability transformation. An application of the PPCI to Alberta agricultural regions shows a potential of using this index to quantitatively evaluate the drought vulnerability of a region by the leading EOF mode and to predict the drought risk.

The drought study in this thesis is conducted only in meteorological perspective. In the future, more information such as temperature could be considered in the drought assessment. Also, reliable and detailed historical drought records are needed to validate the performance of the drought-monitoring model.

In Chapter 5, the error variances of the $5^{\circ} \times 5^{\circ}$ Global Historical Climatological Network (GHCN) monthly surface air temperature data are estimated from January 1851 to December 2001. For each grid box of the GHCN and for each month in the above time interval, an error variance is computed. The error variance is calculated by using the proposed formula $E^2 = \alpha_s \hat{\sigma}_s^2 / N$, where N is the total number of observations for the grid box in the given month; $\hat{\sigma}_s^2$ is the spatial variance

of the grid box's temperature anomaly; α_s is a correlation-factor determined by using a regression. The estimated error variance can be used in optimal spatial averaging, optimal spatial interpolation and any other optimal estimates that minimize the MSE between the true parameter and the estimated parameter. However, problem may exist in our interpolation of the two parameters to the grid boxes with less than four stations. Some of the boxes could have α_s and $\hat{\sigma}_s^2$ interpolated from far away. Further investigation is needed to solve this problem.

Bibliography

Akinremi, O. O. and S. M. McGinn, 1996: Evaluation of the Palmer drought index on the Canadian prairies. *J. Climate*, **9**, 897-905.

Akinremi, O. O., S. M. McGinn, and H. W. Cutforth, 1999: Precipitation trends on the Canadian Prairies, *J. Climate,* **12**, 2996–3003.

Akinremi, O. O., S. M. McGinn, and H. W. Cutforth, 2001: Seasonal and spatial patterns of rainfall trends on the Canadian prairies, *J. Climate,* **14**, 2177–2182.

Alberta Agriculture, Food and Rural Development, 2005. Agriculture Industry Facts. [on line at http://www1.agric.gov.ab.ca/$department/deptdocs.nsf/all/com7126?opendocument].

Alley, W. M., 1984: The Palmer drought severity index: limitations and assumptions. *J. Clim. Appl. Metero.,* **23**, 1100-1109.

Bazzaz, F. A and W. G. Sombroek, 1996: Global climatic change and agricultural production: An assessment of current knowledge and critical gaps. Global Climate Change and Agricultural Production, F. Bazzaz, Ed., England: John Wiley & Sons.

Bhalme, H. N., and D. A. Mooley, 1980: Large-scale drought/floods and monsoon circulation. *Mon. Wea. Rev.,* **108**, 1197-1211.

Bonsal, B. R. and R. G. Lawford, 1999: Teleconnections between EL Nino and La Nina events and summer extended dry spells on the Canadian prairies. *Int. J. Climatol.*, **19**, 1445-1458.

Bonsal, B. R., X. Zhang, and W. D. Hogg, 1999: Canadian Prairie growing season precipitation variability and associated atmospheric circulation. *Clim. Res.*, **11**, 191-208.

Bonsal, B. R., X. Zhang, L. A. Vincent, and W. D. Hogg, 2001: Characteristics of daily and extreme temperatures over Canada. *J. Climate*, **14**, 1959-1976.

Bootsma, A., 1994: Long-term (100 years) climate trends for agriculture at selected locations in Canada. *Climatic Change*, **26**, 65-88.

Bootsma, A., and D. M. Brown, 1995: *Risk Analysis of Crop Heat Units Available for Corn and Other Warm-Season Crops in Ontario*. Technical Bulletin 1995-1E. Center for Land and Biological Resources Research, Research Branch, Agriculture and Agri-Food Canada, 13 pp.

Bootsma, A., 1997: A review of Impacts of Climate Variability and Change on Agriculture in Atlantic Canada. in Shaw, R.W. (ed.), *1997 Climate Change and Climate Variability in Atlantic Canada*, Workshop Proceedings, 3–6 December 1996, Environment Canada. pp. 348.

Bootsma, A., S. Gameda, and D. W. McKenney, 2001: *Adaptation of agricultural production to climate change in Atlantic Canada*. Final Report for Climate Change Action Fund Project A214. Agriculture and Agri-Food Canada, 30 pp.

Byun, H.-R. and D. A. Wilhite, 1999: Objective quantification of drought severity and duration. *J. Climate*, **12**, 2747-2756.

Charney, J. G., 1975: Dynamics of deserts and drought in Sahel. *Q. J. R. Meteorol. Soc.*, **101**, 193-202.

Chetner, S., and the Agroclimatic Atlas Working Group, 2003: *Agroclimatic Atlas of Alberta, 1971-2000.* Alberta Agriculture, Food and Rural Development, Agdex 071-1. Edmonton, Alberta, 97 pp.

Cutforth, H. W., 2000: Climate change in the semiarid prairie of southwestern Saskatchewan: temperature, precipitation, wind, and incoming solar energy. *Can. J. Soil Sci.,* **80**, 375–385.

Cutforth, H., E. G. O'Brien, J. Tuchelt, and R. Rickwood, 2004: Long-term changes in the frost-free season on the Canadian prairies. *Can. J. Plant Sci.,* **84**, 1085-1091.

Daniel, W. W., 1990: *Applied Nonparametric Statistics, 2nd Ed.*. PWS-Kent Publishing Co., 635 pp.

Dzikowski, P., and R. Heywood, 1989: *Agroclimatic Atlas of Alberta.* Alberta Agriculture, Food and Rural Development, Agdex 071-1, Edmonton, Alberta, 31 pp.

Environment Canada. 1995. The state of Canada's climate: monitoring variability and change. State of the Environment Report: SOE Report No. 95–1. Environment Canada, Downsview, ON. 52 pp.

Environment Canada, 1997. The Canada Country Study (CCS): Climate impacts and adaptation, National Summary for Policy Makers. Environment Canada Inquiry Centre, 351 St. Joseph Boulevard, Gatineau, Quebec, K1A 0H3.

Folland, C. K. , N. A. Rayner, S. J. Brown, T. M. Smith, S. S. P. Shen, D. E. Parker, I. Macadam, P. D. Jones, R. N. Jones, N. Nicholls, and D. M. H. Sexton, 2001:

Global temperature change and its uncertainties since 1861. *Geophys. Res. Lett.*, **28**, 2621-2624.

Gan, T. Y., 1995: Trends in air temperature and precipitation for Canada and North-eastern USA. *Int. J. Climato.*, **15**, 1115-1134.

Gan, T. Y., 2000: Reducing vulnerability of water resources of Canadian prairies to potential droughts and possible climatic warming. *Water Reso. Manag.*, **14**, 111-135.

Giannini, A., R. Saravanan, and P. Chang, 2003: Oceanic forcing of Sahel rainfall on interannual to interdecadal time scales. *Science*, **302**, 1027-1030.

Gibbs, W. J. and J. V. Maher, 1967: Rainfall deciles as drought indicators. Australian Bureau of Meteorology, Bull. 48, 37 pp.

Griffith, D. P., 2002. Processing of Daily Agroclimatic Data. M.Sc. Thesis, University of Alberta, Edmonton, Canada, 104 pp.

Gullet, D. W., and W. R. Skinner, 1992: *The State of Canada's Climate: Temperature Change in Canada 1895-1991.* Environment Canada, SOE Report No. 92-2, 36 pp.

Guttman, N. B., 1991: A sensitivity analysis of the Palmer hydrologic drought index. *Water Res. Bull.*, **27**, 797-807.

Guttman, N. B., 1998: Comparing the Palmer drought index and the standardized precipitation index. *J. Am. Water Resour. Assoc.*, **34**, 113-121.

Guttman, N. B., 1999: Accepting the Standardized Precipitation Index: a calculation algorithm. *J. Am. Water Resour. Assoc.*, **35**, 311-322.

Hall, C. L., M. Akbar, and A. Howard, 2003: A history of agricultural drought in Alberta. *Alberta Agriculture, Food and Rural Development.*

Hayes, M. , 2000: Drought indices. [online at http://www.drought.unl.edu/whatis/indices.htm].

Hayes, M., M. Svoboda and D. A. Wilhite, 2000: Monitoring drought using the standardized precipitation index. Drought: A Global Assessment, D. A. Wilhite, Ed., Routledge, 168-180.

Hegerl, G. C., P. D. Jones, and T. P. Barnett, 2001: Effect of observational sampling error on the detection of anthropogenic climate change. *J. Climate*, **14**, 198-207.

Heim, R. R. Jr., 2002: A review of twentieth century drought indices used in the United States. *Bull. Amer. Meteor. Soc.*, **83**, 1149-1165.

Herrington, R., R. Johnson, and F. Hunter, 1997: Responding to global climate change in the Canadian prairies. In: Canada Country Study: Climate impacts and adaptation. Vol. 3. Environment Canada. Ottawa, ON.

Hoerling, M. and A. Kumar, 2003: The perfect ocean for drought. *Science*, **299**, 691-694.

IPCC, 2001: Climate Change 2001, The Scientific Basis. Cambridge University Press, Cambridge, United Kingdom, 881pp.

Jones, P. D., T. J. Osborn, and K. R. Briffa, 1997: Estimating sampling errors in large-scale temperature averages. *J. Climate*, **10**, 2548-2568.

Jones, P. D., Osborn, T. J., Briffa, K. R., Folland, C. K., Horton, E. B., Alexander, L. V., Parker, D. E. and Rayner, N. A., 2001, Adjusting for

sampling density in grid box land and ocean surface temperature time series. *J.Geophys. Res.* **106**, 3371-3380.

Karl, T. R., R. W. Knight, and J. R. Christy, 1994: Global and hemispheric temperature trends: uncertainties related to inadequate spatial sampling. *J. Climate*, **7**, 1144-1163.

Karl, T. R., N. Nicholls, and J. Gregory, 1997: The coming climate. *Scientific American*, **276**, 79–83.

Karl, T. R., and R. W. Knight, 1998: Secular trends of precipitation amount, frequency, and intensity in the USA. *Bull. Am. Met. Soc.*, **79**, 231-241.

Katz, R. W. and M. H. Glantz, 1986: Anatomy of a rainfall index. *Mon. Wea. Rev.*, **114**, 764-771.

Keyantash, J. and J. A. Dracup, 2002: The quantification of drought: An evaluation of drought indices. *Bull. Amer. Meteor. Soc.*, **83**, 1167-1180.

Kinninmonth, W. R., M. E. Voice, G. S. Beard, G. C. de Hoedt, and C. E. Mullen, 2000: Australian climate services for drought management. Drought: A Global Assessment, D. A. Wilhite, Ed., Routledge, 210-222.

Kraus, E. B., 1977: Subtropical droughts and cross-equatorial energy transports. *Mon. Wea. Rev.*, **105**,1009-1018.

Kunkel, K., 2003: North America trends in extreme precipitation. *Natural Hazards*, **29**, 291-305.

Lau, K. M., S. S. P. Shen, K.-M. Kim, H. Wang: A multi-model study of the 20th century simulations of Sahel drought from the 1970s to 1990s. Manuscript.

Lloyd-Hughes, B. and M. A. Saunder, 2002: A drought climatology for Europe. *Int. J. Climatol.*, **22**, 1571–1592.

Madden, R. A., D. J. Shea, G. W. Branstator, J. J. Tribbia, and R. Weber, 1993: The effects of imperfect spatial and temporal sampling on estimates of the global mean temperature: Experiments with model data. *J. Climate*, **6**, 1057-1666.

McGinn, S. M., A. Shepherd and O. O. Akinremi, 2001: Assessment of climate change and impacts on soil moisture and drought on the prairies. Final report for the climate change action fund (CCAF) science, impacts and adaptation. Agriculture and Agri-Food Canada.

Mckee, T. B., N. J. Doesken and J. Kleist, 1993: The relationship of drought frequency and duration to time scales. Eighth conference on applied climatology, Anaheim, CA, American Meteorological Society.

Mckee, T. B., N. J. Doesken and J. Kleist, 1995: Drought monitoring with multiple time scales. Proceedings of the ninth conference on applied climatology, Boston, MA, American Meteorological Society.

McKenney, D. W., M. F. Hutchinson, J. L. Kesteven, and L. A. Venier, 2001: Canada's plant hardiness zones revisited using modern climate interpolation techniques, *Can. J. Plant Sci.*, **81**, 129-143.

Meyer, S. J., K. G. Hubbard, and D. A. Wilhite,1993: A crop-specific drought index for corn: I. Model development and validation. *Agron. J.*, **86**,388-395.

Meyer, S. J. and K. G. Hubbard, 1995: Extending the crop-specific drought index to soybean. Ninth conf. on Applied Climatology, Dallas, TX, Amer. Meteor. Soc. 25-259.

Motha, R. P and W. Baier, 2005: Impacts of present and future climate change and climate variability on agriculture in the temperate regions: North America. *Climatic Change*, **70**, 137-164.

North, G. R., J. B. Valdes, E. Ha, and S. S. P. Shen, 1994: The ground-truth problem for satellite estimates of rain rate, *J. Atmos. Oceanic Tech.* **11**, 1035-1041.

Oladipo, E. O., 1985: A comparative performance analysis of three meteorological drought indices. *Int. J. Climato.*, **5**, 655-664.

Palmer, W. C., 1965: Meteorological drought. Weather Bureau, Research Paper No.45, U.S. Dept. of Commerce, Washington, DC, 58 pp.

Palmer, W. C., 1968: Keeping track of crop moisture conditions, nationwide: The new crop moisture index. *Weatherwise*, **21**, 156-161.

Parry, M., 1990. Climate Change and World Agriculture. London: Earthscan. 157pp.

Peterson, T. C., and R. S. Vose, 1997: An overview of the global historical climatology network temperature database. *Bull. Amer. Meteo. Soc.* **78**, 2837-2849.

Peterson, T. C., T. R. Karl, P. F. Jamason, R. Knight, and D. Easterling, 1998: First difference method: Maximizing station density for the calculation of long-term global temperature change. *J. Geophys. Res.* **103**, 25967-25974.

PFRA, 1998, Drought in the Palliser Triangle (A Provisional Primer). Agriculture and Agri-Food Canada.

Pollution Probe, 2004. Primer on climate change and human health. Online reports, http://www.pollutionprobe.org/Reports/climatechangeprimer.pdf

Quiring, S. M. and T. N. Paparkryiakou, 2003: An evaluation of agricultural drought indices for the Canadian prairies. *Agric. For. Meteorol.*, **118**, 49-62.

Rosenzweig, C. and D. Hillel, 1995: Potential impacts of climate change on agriculture and food supply. Consequences, vol. 1, No. 2. [on line at http://www.gcrio.org/CONSEQUENCES/index.htm]

Schubert, S. D., M. J. Suarez, P. J. Pegion, R. D. Koster, J. T. Bacmeister,2004: On the cause of the 1930s dust bowl. *Science*, **303**, 1855-1859.

Shabbaar, A. and W. Skinner, 2004: Summer drought patterns in Canada and relationship to global sea surface temperatures. *J. Climate*, **17**, 2866-2880.

Shafer, B. A. and L. E. Dezman, 1982: Development of a surface water supply index (SWSI) to assess the severity of drought conditions in snow pack runoff areas. Proc. Western Snow Conf., 164-175.

Shen, S. S. P., G. R. North, and K.-Y. Kim, 1994: Spectral approach to optimal estimation of the global average temperature. *J. Clim.* **7**, 1999-2007.

Shen, S. S. P., T. M. Smith, C. F. Ropelewski, and R. E. Livezey, 1998: An optimal regional averaging method with error estimates and a test using tropical Pacific SST Data, *J. Climate,* **11**, 2340-2350.

Shen, S. S. P., K. Cannon, and G. Li, 2000a: *Alberta 1961-1997 climate data on EDP and SLC polygons: Data derivatives and data formation for soil quality models*. Alberta Agriculture, Food and Rural Development, Edmonton, Alberta, Canada, 32 pp.

Shen, S. S. P., P. Dzikowski, and G. Li, 2000b: *Interpolation of 1961-1997 daily climate data onto Alberta polygons of ecodistrict and soil landscapes of*

Canada. Alberta Agriculture, Food and Rural Development, Edmonton, Alberta, Canada, 60 pp.

Shen, S. S. P., P. Dzikowski, G. Li and D. Griffith, 2001: Interpolation of 1961-1997 daily temperature and precipitation data onto Alberta polygons of ecodistrict and soil landscapes of canada. *J. Appl. Meteor.*, **40**, 66-81.

Shen, S. S. P., A. Howard, H. Yin, F. Khurshed, and M. Akbar, 2003: *Statistical Analysis of Drought Indices and Alberta Drought Monitoring*. Alberta Agriculture, Food and Rural Development, Edmonton, Alberta, Canada, 40 pp.

Shen, S. S. P., A. N. Basist, G. Li, C. Williams, and T. R. Karl, 2004: Prediction of sea surface temperature from the Global Historical Climatology Network data, *Environmetrics* **15**, 233-249.

Smith, T. M., R. W. Reynolds, and C. F. Ropelewski, 1994: Optimal averaging of seasonal sea surface temperatures and associated confidence interval (1860-1989). *J. Climate,* **7**, 949-964.

Svoboda, M., D. Lecomte, M. Hayes, R. Heim, K. Gleason, J. Angel, B. Rippey, R. Tinker, M Palecki, D. Stooksbury, D. Miskus, and S. Stephens, 2002: The drought monitor. *Bull. Amer. Meteor. Soc.*, **83**,1181-1190.

Taylor, C. M., E. F. Lambin, N. Stephenne, R. J. Harding, and R. L. H. Essery, 2002: The influence of land use change on climate in the Sahel. *J. Climate*, **15**, 3615-3629.

Van Rooy, M. P., 1965: A rainfall anomaly index independent of time and space. *Notos*, **14**, 43-48.

Vinnikov, K.Y., and A. Robock, 2002: Analysis of seasonal cycles in climatic trends with application to satellite observations of sea ice extent. *Geophys. Phys. Res. Lett.*, **29**, No. 10, 10.1029/2001GL014481.

Wheaton, E. E., 2000: Canadian prairie drought impacts and experiences. Drought: A Global Assessment, D. Wilhite, Ed., Vol. 1, 312-330.

Wheaton, E., V. Wittrock, S. Kulshreshtha, G. Koshida, C. Grant, A. Chipanshi, and B. Bonsal, 2005: Lessons learned from the Canadian drought years of 2001 and 2002. SRC publication No. 11602-46E03. Agriculture and Agri-Food Canada.

Wilhite, D. A., 2000: Drought as a natural hazard. Drought: A Global Assessment, D. Wilhite, Ed., Vol. 1, 3-18.

Wu, H., M. J. Hayes, D. D. Wilhite and M. D. Svoboda, 2005: The effect of the length of record on the standardized precipitation index calculation. *Int. J. Climato.*, **25**, 505-520.

Zeng, N., 2003: Drought in the Sahel. *Science*, **302**, 999-1000.

Zhang, X., L. A. Vincent, W. D. Hogg, and A. Niitsoo, 2000: Temperature and precipitation trends in Canada during the 20th century. *Atmosphere-Ocean,* **38**, 395-429.

Zhang, X., W. D. Hogg, and E. Mekis, 2001: Spatial and temporal characteristics of heavy precipitation events over Canada. *J. Climate*, **14**, 1923-1936.